

REPORT DOCUMENTATION PAGE			Form Approved OMB NO. 0704-0188		
<p>The public reporting burden for this collection of information is estimated to average 1 hour per response, including the time for reviewing instructions, searching existing data sources, gathering and maintaining the data needed, and completing and reviewing the collection of information. Send comments regarding this burden estimate or any other aspect of this collection of information, including suggestions for reducing this burden, to Washington Headquarters Services, Directorate for Information Operations and Reports, 1215 Jefferson Davis Highway, Suite 1204, Arlington VA, 22202-4302. Respondents should be aware that notwithstanding any other provision of law, no person shall be subject to any penalty for failing to comply with a collection of information if it does not display a currently valid OMB control number. PLEASE DO NOT RETURN YOUR FORM TO THE ABOVE ADDRESS.</p>					
1. REPORT DATE (DD-MM-YYYY) 02-01-2020		2. REPORT TYPE Final Report		3. DATES COVERED (From - To) 10-Aug-2012 - 9-Aug-2019	
4. TITLE AND SUBTITLE Final Report: Novel Fiber Concepts for High Power Single Mode Fiber Lasers			5a. CONTRACT NUMBER W911NF-12-1-0332		
			5b. GRANT NUMBER		
			5c. PROGRAM ELEMENT NUMBER		
6. AUTHORS			5d. PROJECT NUMBER		
			5e. TASK NUMBER		
			5f. WORK UNIT NUMBER		
7. PERFORMING ORGANIZATION NAMES AND ADDRESSES Clemson University Research Foundation Office of Sponsored Programs Clemson University Research Foundation Clemson, SC 29631 -0946			8. PERFORMING ORGANIZATION REPORT NUMBER		
9. SPONSORING/MONITORING AGENCY NAME(S) AND ADDRESS (ES) U.S. Army Research Office P.O. Box 12211 Research Triangle Park, NC 27709-2211			10. SPONSOR/MONITOR'S ACRONYM(S) ARO		
			11. SPONSOR/MONITOR'S REPORT NUMBER(S) 62072-EL-HEL.54		
12. DISTRIBUTION AVAILABILITY STATEMENT Approved for public release; distribution is unlimited.					
13. SUPPLEMENTARY NOTES The views, opinions and/or findings contained in this report are those of the author(s) and should not be construed as an official Department of the Army position, policy or decision, unless so designated by other documentation.					
14. ABSTRACT					
15. SUBJECT TERMS					
16. SECURITY CLASSIFICATION OF:			17. LIMITATION OF ABSTRACT UU	15. NUMBER OF PAGES	19a. NAME OF RESPONSIBLE PERSON Liang Dong
a. REPORT UU	b. ABSTRACT UU	c. THIS PAGE UU			19b. TELEPHONE NUMBER 864-656-5915

RPPR Final Report

as of 07-Jan-2020

Agency Code:

Proposal Number: 62072ELHEL

Agreement Number: W911NF-12-1-0332

INVESTIGATOR(S):

Name: Liang Dong
Email: dong4@clemson.edu
Phone Number: 8646565915
Principal: Y

Organization: **Clemson University Research Foundation**

Address: Office of Sponsored Programs, Clemson, SC 296310946

Country: USA

DUNS Number: 159952407

EIN: 84600545

Report Date: 09-Nov-2019

Date Received: 02-Jan-2020

Final Report for Period Beginning 10-Aug-2012 and Ending 09-Aug-2019

Title: Novel Fiber Concepts for High Power Single Mode Fiber Lasers

Begin Performance Period: 10-Aug-2012

End Performance Period: 09-Aug-2019

Report Term: 0-Other

Submitted By: Liang Dong

Email: dong4@clemson.edu

Phone: (864) 656-5915

Distribution Statement: 1-Approved for public release; distribution is unlimited.

STEM Degrees: 12

STEM Participants: 10

Major Goals: The program described in this proposal consists of two thrusts. The first thrust is to investigate the feasibility of high-power single-mode hydrogen-based Raman lasers in hollow-core double-clad photonic bandgap fibers (PBF). Nonlinear thresholds are expected to be significantly improved over what are possible in solid fiber lasers due to the much lower density of gas. This concept also provides for much improved mode quality due to the unique robust single-mode regime in PBF. This novel approach is expected to enable single-mode fiber lasers with power levels well beyond current state-of-art solid fiber lasers. We will study the limits for average power scaling to 100kW with this approach. This concept works with any optically pumped gas lasers, including the very promising diode-pumped alkali vapor lasers.

The second thrust is to investigate power scaling in single-mode ytterbium-doped 100 μ m core size resonantly enhanced leakage channel fibers (reLCF) for much improved nonlinear thresholds and mode quality. The resonantly enhanced leakage channel fibers make use of naturally existing resonant couplings between higher-order modes and the leakage channel cladding in a leakage channel fiber for significant additional higher-order-mode suppression over standard leakage channel fibers (LCF). The 100 μ m core fiber provides a simple, elegant and practical all-solid solution with much enhanced mode quality suitable further power scaling to 20kW. We will investigate limits to power scaling to 20kW with this approach. This new concept can provide a critical solution for resolving the recently observed mode instability issues at high powers.

Accomplishments: In thrust I, we have made significant progress in the fabrication of hollow-core fibers. Fibers with loss of <0.05dB/m at 3 μ m has been demonstrated. In thrust II, we have made significant breakthrough in demonstrating efficient flat-top mode in active LCF with effective area of 1900 μ m² and record quantum-limited efficiency of ~95%. Systematic design study of 100 μ m-core multiple-cladding-resonance leakage channel fibers have been conducted. The 3rd iteration ytterbium-doped glass with an index of ~2.3x10⁻⁴ has enabled the demonstration ytterbium-doped 30 μ m-core LMA fiber operating near single-mode regime, proving that LMA fibers with arbitrarily low NA can be reliably made. Using 50/400 ytterbium-doped leakage channel fiber, we have systematically studied fiber lasers between 1000nm-1020nm, achieving slope efficiency >70% with respect to the launched pump power at 1018nm in 400 μ m cladding. More recently, with 50/400 all-solid photonic bandgap fiber, we have achieved single-mode power of 220W at 1018nm. A study on thermal lensing is also conducted. In this period we have made significant breakthrough in demonstrating efficiency of 63% in 976nm fiber lasers, a record for flexible fibers by using bandgap to reject Yb ASE at longer wavelength.

Training Opportunities: Nothing to Report

RPPR Final Report

as of 07-Jan-2020

Results Dissemination: (a) Papers published in peer-reviewed journals

1. G. Gu, F. Kong, T.W. Hawkins, P. Foy, K. Wei, B. Samson, and L. Dong, "Impact of fiber outer boundaries on leaky mode losses in leakage channel fibers," *Optics Express* 21, 24039-24048 (2013).
2. F. Kong, G. Gu, T.W. Hawkins, J. Parsons, M. Jones, C. Dunn, Monica T. Kalichevsky-Dong, K. Wei, B. Samson, and L. Dong, "Flat-top mode from a 50 μm -core Yb-doped leakage channel fiber," *Optics Express* 21, 32371-32376 (2013).
3. F. Kong, G. Gu, T.W. Hawkins, J. Parsons, M. Jones, C. Dunn, M. T. Kalichevsky-Dong, S.P. Palese, E. Cheung, and L. Dong, "Quantitative mode quality characterization of fibers with extremely large mode areas by matched white-light interferometry," *Optics Express* 22, 14657-14665 (2014).
4. M. Steinke, H. Tünnermann, J. Neumann, D. Kracht, B. Samson, G. Gu, L. Dong, and P. Wessels, "TEM₀₀ mode content measurements on a passive leakage channel fiber," *Optics Letters*, 40, 383-386(2015).
5. G. Gu, Z. Liu, F. Kong, H. Tam, R.K. Shori and L. Dong, "Highly efficient ytterbium-doped phosphosilicate fiber lasers operating below 1020nm," *Opt. Express* 23(14), 17693-17700 (2015).
6. F. Kong, C. Dunn, J. Parsons, M.T. Kalichevsky-Dong, T.W. Hawkins, M. Jones, and L. Dong, "Large-mode-area fibers operating near single-mode regime," *Optics Express* 24, 10295-10301 (2016).
7. L. Dong, "Thermal Lensing in Optical Fibers," *Optical Express* 24(17), 19841-19852(2016).
8. F. Kong, G. Gu, T.W. Hawkins, M. Jones, J. Parsons, M.T. Kalichevsky-Dong, S.P. Palese, E. Cheung, and L. Dong, "Efficient 240W single-mode 1018nm laser from an Ytterbium-doped 50/400 μm all-solid photonic bandgap fiber," *Optics Express* 26(3), 3138-3144 (2018).
9. T. Matniyaz, W. Li, M.T. Kalichevsky-Dong, T.W. Hawkins, J. Parsons, G. Gu, and L. Dong, "Highly efficient cladding-pumped single-mode three-level Yb all-solid photonic bandgap fiber lasers," *Optics Letters* 44, 807-810 (2019).
10. W. Li, T. Matniyaz, S. Gafsi, M.T. Kalichevsky-Dong, T.W. Hawkins, J. Parsons, G. Gu, and L. Dong, "151W monolithic diffraction-limited Yb-doped photonic bandgap fiber laser at \sim 978nm," *Optics Express*, to be published (2019).

(b) Papers published in non-peer-reviewed journals or in conference proceedings

1. Guancheng Gu, Fanting Kong, Thomas Hawkins, Liang Dong, Kanxian Wei, Bryce Samson, "Mode-dependent Losses in 50micron Core Leakage Channel Fibers," DEPS Solid State and Diode Laser Review, paper 13-SSDLTR-004, Santa Fe, June 2013.
2. Guancheng Gu, Fanting Kong, Thomas W. Hawkins, Paul Foy, Kanxian Wei, Bryce Samson, and Liang Dong, "Measurements of Mode Losses in \sim 50 μm Core Resonantly Enhanced Leakage Channel Fibers," *Advanced Solid State Lasers*, paper AM4A.04, Paris, October 2013.
3. Fanting Kong, Guancheng Gu, Thomas W. Hawkins, Joshua Parsons, Maxwell Jones, Christopher Dunn, Monica T. Kalichevsky-Dong, Kanxian Wei, Bryce Samson, and Liang Dong, "Flat-top Beam from a 50 μm -Core Yb-doped Leakage Channel Fiber," *Optical Communications Conference*, paper Tu3K.5, March 2014.
4. Fanting Kong, Guancheng Gu, Thomas Hawkins, Joshua Parsons, Maxwell Jones, Christopher Dunn, Monica Kalichevsky-Dong and Liang Dong, "50 μm -Core Yb-doped Leakage Channel Fiber with Flattened Mode," *Sixteenth Annual Directed Energy Symposium*, paper 13-Symp-064, March 2014.
5. Fanting Kong, Guancheng Gu, Thomas W. Hawkins, Joshua Parsons, Maxwell Jones, Christopher Dunn, Monica T. Kalichevsky-Dong, Kanxian Wei, Bryce Samson, and Liang Dong, "50 μm -core Yb-doped leakage channel fiber with flattened mode," *SPIE Defense and Security*. Paper 9081-14, May 2014.
6. Fanting Kong, Guancheng Gu, Thomas W. Hawkins, Joshua Parsons, Maxwell Jones, Christopher Dunn, Monica T. Kalichevsky-Dong, Kanxian Wei, Bryce Samson, and Liang Dong, "80W Flat-top Beam from an Yb-doped Leakage Channel Fiber," *International Photonics and OptoElectronics (POEM)*, paper FF3D.3 June 2014.
7. Fanting Kong, Guancheng Gu, Thomas Hawkins, Joshua Parsons, Maxwell Jones, Christopher Dunn, Monica Kalichevsky-Dong, Stephen Palese, Eric Cheung, and Liang Dong, "Quantitative Mode Quality Characterization in a Leakage Channel Fiber with 100 μm Core Diameter," *Advanced Photonics Congress*, paper SoW2B.5, August 2014.
8. Pierre Calvet, Amaud Perrin, Pierre Gouriou, Bryce N Samson, Thomas Hawkins, Fanting Kong, Liang Dong, Pascal Dupriez, and Emmanuel Hugonnot, "High-energy nanosecond-pulses from a flat-top mode 50 μm -core leakage channel fiber," *Advanced Photonics Congress*, paper SoM3B.4, August 2014.
9. L. Dong, "Control of light flow in optical fibers," 5th International Conference on Photonics, keynote speaker, September 2014, Kuala Lumpur.
10. L. Dong, F. Kong, G. Gu, T.W. Hawkins, and M.T. Kalichevsky-Dong, "Challenges and Solutions for Further

RPPR Final Report as of 07-Jan-2020

Power Scaling of Single-Mode Fiber Lasers,” 4th Photonics Global Conference, invited paper, ICMAT15-A-4343, Singapore June-July 2015.

11. L. Dong, F. Kong, G. Gu, T.W. Hawkins, M. Jones, J. Parsons, M.T. Kalichevsky-Dong, K. Saitoh, B. Pulford and I. Dajani, “Challenges for Further Power Scaling of Single-Mode Fiber Lasers,” Advanced Solid State Lasers, invited talk, Berlin, October 4-7, 2015.
12. G. Gu, Z. Liu, F. Kong, H.Y. Tam, R.K. Shori and L. Dong, “High-power Efficient Yb-doped Fiber Laser with Low Quantum Defect,” 4th Workshop on Specialty Optical Fibers, Hong Kong, paper WT4A.4, November 3-6, 2015.
13. G. Gu, Z. Liu, F. Kong, H.Y. Tam, R.K. Shori, and L. Dong, “Efficient ytterbium-doped phosphosilicate double-clad leakage-channel-fiber laser at 1008-1020nm,” PhotonicsWest, paper 9728-51, San Francisco, February 15-18, 2016.
14. F. Kong, C. Dunn, J. Parsons, M.T. Kalichevsky-Dong, T.W. Hawkins, M. Jones, and L. Dong, “30 μ m-Core Yb-Doped Step-Index Fiber Operating Near Single-Mode Regime,” Directed Energy Professional Society Annual Symposium, Albuquerque, March 7-11, 2016.
15. L. Dong, “Opportunities and challenges of power scaling of single-mode fiber lasers,” Stuttgart Laser Technology Forum, invited talk, Stuttgart, May 31st and June 1st, 2016.
16. Fanting Kong, Thomas Hawkins, Maxwell Jones, Josh Parsons, Monica Kalichevsky-Dong, Christopher Dunn, and Liang Dong, “Ytterbium-doped 30/400 LMA Fibers with a Record-low ~NA of 0.028,” Conference on Lasers and Electro Optics, SM2Q.2, San Jose, June 2016.
17. Dong, “Opportunities and challenges of power scaling of single-mode fiber lasers,” Stuttgart Laser Technology Forum, invited talk, Stuttgart, May 31st and June 1st, 2016.
18. Fanting Kong, Thomas Hawkins, Maxwell Jones, Josh Parsons, Monica Kalichevsky-Dong, Christopher Dunn, and Liang Dong, “Ytterbium-doped 30, 40/400 LMA Fibers with a Record-low ~NA of 0.028,” Advanced Photonics Congress, Vancouver, SoW2H.4, Canada, July 2016.
19. Liang Dong, Fanting Kong, Guancheng Gu, Thomas W. Hawkins, Maxwell Jones, Joshua Parsons, Monica Kalichevsky-Dong, and Christopher Dunn, “Progress and challenges in further power scaling of single-mode fiber lasers” invited talk, Asia communications and Photonics Conference, November 2-5, 2016, Wuhan, China.
20. C. Mart, B. Pulford, B. Ward, I. Dajani, L. Dong, K. Kieu, and A. Sanchez, “SBS Investigation of an All-solid Ytterbium-doped Photonic Bandgap Fiber Amplifier”, Nineteenth Annual Directed Energy Symposium, Huntsville, Alabama, 13-17 February 2017,
21. Fanting Kong, Guancheng Gu, Thomas W. Hawkins, Maxwell Jones, Joshua Parsons, Monica T. Kalichevsky-Dong, and Liang Dong, “Single-mode Ytterbium Fiber Laser with Record 220W Output Power at 1018nm,” Workshop on Specialty Optical Fibers, October 11-13, 2017, Limassol, Cyprus.
22. Fanting Kong, Guancheng Gu, Thomas W. Hawkins, Maxwell Jones, Joshua Parsons, Monica T. Kalichevsky-Dong, and Liang Dong, “Single-mode Ytterbium Fiber Laser with Record 240W Output Power at 1018nm,” PhotonicsWest, paper 10512-16 (PW18L-LA102-92), January 27 - February 1, 2018, San Francisco.
23. Liang Dong, “Advanced specialty optical fibers and their applications in high-power fiber lasers,” The 23rd Opto

Honors and Awards: Guancheng Gu, OSA Incubic Milton travel grant, 2015
Guancheng Gu, Clemson Professional Enrichment Grant Application (PEGAS) grant. 2015
Christopher Dunn, DEPS graduate student fellowship (2014, 2015)
Liang Dong, Fellow of Optical Society of America, 2014
Liang Dong, Fellow of SPIE, 2017
Liang Dong, IEEE senior fellow, 2017
Liang Dong, University Research, Scholarship, and Artistic Achievement award, 2018
Liang Dong, Dean’s Distinguished Professor Award in the Department of Electrical and Computer Engineering, 4/16/2019 to 4/15/2022
Liang Dong, IEEE fellow, 2020

Protocol Activity Status:

Technology Transfer: Nothing to Report

PARTICIPANTS:

Participant Type: PD/PI

Participant: Liang Dong 6548107

Person Months Worked: 3.00

Funding Support:

RPPR Final Report
as of 07-Jan-2020

Project Contribution:
International Collaboration:
International Travel:
National Academy Member: N
Other Collaborators:

Participant Type: Staff Scientist (doctoral level)

Participant: Monica T Kalichevsky-Dong

Person Months Worked: 6.00

Funding Support:

Project Contribution:
International Collaboration:
International Travel:
National Academy Member: N
Other Collaborators:

Participant Type: Technician

Participant: Joshua Parsons

Person Months Worked: 6.00

Funding Support:

Project Contribution:
International Collaboration:
International Travel:
National Academy Member: N
Other Collaborators:

Participant Type: Graduate Student (research assistant)

Participant: Turghun Matniyaz

Person Months Worked: 12.00

Funding Support:

Project Contribution:
International Collaboration:
International Travel:
National Academy Member: N
Other Collaborators:

Participant Type: Undergraduate Student

Participant: Grant Vegas

Person Months Worked: 1.00

Funding Support:

Project Contribution:
International Collaboration:
International Travel:
National Academy Member: N
Other Collaborators:

Participant Type: Undergraduate Student

Participant: Dylan Kensler

Person Months Worked: 1.00

Funding Support:

Project Contribution:
International Collaboration:
International Travel:
National Academy Member: N
Other Collaborators:

Participant Type: Undergraduate Student

Participant: Bailey Meehan

RPPR Final Report
as of 07-Jan-2020

Person Months Worked: 2.00

Funding Support:

Project Contribution:

International Collaboration:

International Travel:

National Academy Member: N

Other Collaborators:

Participant Type: Undergraduate Student

Participant: Bailey Meehan

Person Months Worked: 2.00

Funding Support:

Project Contribution:

International Collaboration:

International Travel:

National Academy Member: N

Other Collaborators:

ARTICLES:

Publication Type: Journal Article

Peer Reviewed: Y

Publication Status: 1-Published

Journal: Optics Express

Publication Identifier Type:

Publication Identifier:

Volume: 21

Issue: 20

First Page #: 24039

Date Submitted:

Date Published:

Publication Location:

Article Title: Impact of fiber outer boundaries on leaky mode losses in leakage channel fibers

Authors:

Keywords: (060.2280) Fiber design and fabrication; (060.2280) Fiber characterization; (060.3510) Lasers, fiber.

Abstract: In a leakage channel fiber, the desired fundamental mode (FM) has negligible waveguide loss. Higher-order modes (HOM) are designed to have much higher waveguide losses so that they are practically eliminated during propagation. Coherent reflection at the fiber outer boundary can lead to additional confinement especially for highly leaky HOM, leading to lower HOM losses than what are predicted by conventional FEM mode solver considering infinite cladding. In this work, we conducted, for the first time, careful measurements of HOM losses in two leakage channel fibers (LCF) with circular and rounded hexagonal boundary shapes respectively. Impact on HOM losses from coiling, fiber boundary shapes and coating indexes were studied in comparison to simulations. This work, for the first time, demonstrates the limit of the simulation method commonly used in the large-mode-area fiber designs and the need for an improved approach. More importantly, this work also demonstrates that a deviation from

Distribution Statement: 1-Approved for public release; distribution is unlimited.

Acknowledged Federal Support:

RPPR Final Report as of 07-Jan-2020

Publication Type: Journal Article Peer Reviewed: Y **Publication Status:** 1-Published

Journal: Optics Express

Publication Identifier Type:

Publication Identifier:

Volume: 21

Issue: 26

First Page #: 32371

Date Submitted:

Date Published:

Publication Location:

Article Title: Flat-top mode from a 50 μm -core Yb-doped leakage channel fiber

Authors:

Keywords: : (060.2280) Fiber design and fabrication; (060.2270) Fiber characterization; (060.3510) Lasers, fiber.

Abstract: We demonstrate for the first time a flat-top mode from a 50 μm -core Yb-doped leakage channel fiber (LCF). The flat intensity distribution leads to an effective mode area of $\sim 1880 \mu\text{m}^2$ in the straight fiber, an over 50% increase comparing to that of regular LCF with the same core diameter. The flat-top mode was achieved by using a uniform Yb-doped silica glass in the core center with an index of $\sim 2 \times 10^{-4}$ lower than that of the silica background. The fiber was also tested in a laser configuration, demonstrating an optical-to-optical efficiency of $\sim 77\%$ at 1026 nm with respect to the pump at 975 nm.

Distribution Statement: 1-Approved for public release; distribution is unlimited.

Acknowledged Federal Support:

Publication Type: Journal Article Peer Reviewed: Y **Publication Status:** 1-Published

Journal: Optics Express

Publication Identifier Type:

Publication Identifier:

Volume: 22

Issue: 12

First Page #: 14657

Date Submitted:

Date Published:

Publication Location:

Article Title: Quantitative mode quality characterization of fibers with extremely large mode areas by matched white-light interferometry

Authors:

Keywords: (060.2270) Fiber characterization; (060.2280) Fiber design and fabrication; (060.3510) Lasers, fiber.

Abstract: Quantitative mode characterization of fibers with cores much beyond $50 \mu\text{m}$ is difficult with existing techniques due to the combined effects of smaller intermodal group delays and dispersions. We demonstrate, for the first time, a new method using a matched white-light interferometry (MWI) to cancel fiber dispersion and achieve finer temporal resolution, demonstrating $\sim 20\text{fs}$ temporal resolution in intermodal delays, i.e. $6 \mu\text{m}$ path-length resolution. A 1m-long straight resonantly-enhanced leakage-channel fiber with $100 \mu\text{m}$ core was characterized, showing $\sim 55\text{fs/m}$ relative group delay and a $\sim 29\text{dB}$ mode discrimination between the fundamental and second-order modes.

Distribution Statement: 1-Approved for public release; distribution is unlimited.

Acknowledged Federal Support:

BOOKS:

Publication Type: Book Peer Reviewed: Y **Publication Status:** 1-Published

Publication Identifier Type: ISBN

Publication Identifier: 1498725546

Book Edition: 1

Volume:

Publication Year: 2016

Date Received:

Publication Location: Boca Raton, Longdon, New York

Publisher: CRC Press

Book Title: Fiber Lasers: Basics, Technology and Applications

Authors: Liang Dong and Bryce Samson

Editor:

Acknowledged Federal Support: Y

CONFERENCE PAPERS:

RPPR Final Report
as of 07-Jan-2020

Publication Type: Conference Paper or Presentation **Publication Status:** 1-Published
Conference Name: Advanced Solid State Lasers
Date Received: Conference Date: 27-Oct-2013 Date Published:
Conference Location:
Paper Title: Measurements of Mode Losses in ~50 μ m Core Resonantly Enhanced Leakage Channel Fibers
Authors:
Acknowledged Federal Support:

Publication Type: Conference Paper or Presentation **Publication Status:** 1-Published
Conference Name: DEPS Solid State and Diode Laser Technical Review
Date Received: 02-Aug-2018 Conference Date: 25-Jun-2013 Date Published: 25-Jun-2013
Conference Location: Santa Fe
Paper Title: Mode-dependent Losses in 50micron Core Leakage Channel Fibers
Authors: Liang Dong
Acknowledged Federal Support: **Y**

Publication Type: Conference Paper or Presentation **Publication Status:** 1-Published
Conference Name: DEPS Solid State and Diode Laser Review
Date Received: 02-Aug-2018 Conference Date: 24-Jun-2013 Date Published: 24-Jun-2014
Conference Location: Santa Fe
Paper Title: Mode-dependent Losses in 50micron Core Leakage Channel Fibers
Authors: Guancheng Gu, Fanting Kong, Thomas Hawkins, Liang Dong
Acknowledged Federal Support: **Y**

Publication Type: Conference Paper or Presentation **Publication Status:** 1-Published
Conference Name: Advanced Solid State Lasers
Date Received: Conference Date: 27-Oct-2013 Date Published:
Conference Location:
Paper Title: Measurements of Mode Losses in ~50 μ m Core Resonantly Enhanced Leakage Channel Fibers
Authors:
Acknowledged Federal Support:

Publication Type: Conference Paper or Presentation **Publication Status:** 1-Published
Conference Name: Optical Fiber Communication Conference and Exposition (OFC)
Date Received: 02-Aug-2018 Conference Date: 09-Mar-2014 Date Published: 09-Mar-2014
Conference Location: Anaheim
Paper Title: Flat-top Beam from a 50 μ m-Core Yb-doped Leakage Channel Fiber
Authors: Fanting Kong, Guancheng Gu, Thomas W. Hawkins, Joshua Parsons, Maxwell Jones, Christopher Duni
Acknowledged Federal Support: **Y**

Publication Type: Conference Paper or Presentation **Publication Status:** 1-Published
Conference Name: Sixteenth Annual Directed Energy Symposium
Date Received: 02-Aug-2018 Conference Date: 10-Mar-2014 Date Published: 10-Mar-2014
Conference Location: Santa Fe
Paper Title: 50 μ m-Core Yb-doped Leakage Channel Fiber with Flattened Mode
Authors: Fanting Kong, Guancheng Gu, Thomas Hawkins, Joshua Parsons, Maxwell Jones, Christopher Dunn, M
Acknowledged Federal Support: **Y**

RPPR Final Report
as of 07-Jan-2020

Publication Type: Conference Paper or Presentation **Publication Status:** 1-Published
Conference Name: SPIE Denfense and Security
Date Received: 02-Aug-2018 Conference Date: 05-May-2014 Date Published: 05-May-2014
Conference Location: Baltimore
Paper Title: 50 μ m-core Yb-doped leakage channel fiber with flattened mode
Authors: Fanting Kong,* Guancheng Gu, Thomas W. Hawkins, Joshua Parsons, Maxwell Jones, Christopher Du
Acknowledged Federal Support: **Y**

Publication Type: Conference Paper or Presentation **Publication Status:** 1-Published
Conference Name: International Photonics and Optoelectronics Meetings
Date Received: 02-Aug-2018 Conference Date: 18-Jun-2014 Date Published: 18-Jun-2014
Conference Location: Wuhan, China
Paper Title: 80W Flat-top Beam from an Yb-doped Leakage Channel Fiber
Authors: Fanting Kong,* Guancheng Gu, Thomas W. Hawkins, Joshua Parsons, Maxwell Jones, Christopher Dur
Acknowledged Federal Support: **Y**

Publication Type: Conference Paper or Presentation **Publication Status:** 1-Published
Conference Name: Advanced Photonics Congress
Date Received: 02-Aug-2018 Conference Date: 27-Jul-2014 Date Published: 27-Jul-2014
Conference Location: Barcelona
Paper Title: Quantitative Mode Quality Characterization in a Leakage Channel Fiber with 100 μ m Core Diameter
Authors: Fanting Kong, Guancheng Gu, Thomas W. Hawkins, Joshua Parsons, Maxwell Jones, Christopher Dun
Acknowledged Federal Support: **Y**

Publication Type: Conference Paper or Presentation **Publication Status:** 1-Published
Conference Name: Advanced Photonics Congress
Date Received: 02-Aug-2018 Conference Date: 27-Jul-2014 Date Published: 27-Jul-2014
Conference Location: Barcelona, Spain
Paper Title: High-energy nanosecond-pulses from a flat-top mode 50 μ m-core leakage channel fiber
Authors: P. Calvet, P. Gouriou, B. Samson, L. Dong, P. Dupriez and E. Hugonnot
Acknowledged Federal Support: **Y**

Publication Type: Conference Paper or Presentation **Publication Status:** 1-Published
Conference Name: SPIE PhotonicsWest, paper 9344-5, San Francisco, February 2015
Date Received: 02-Aug-2018 Conference Date: 08-Feb-2015 Date Published: 08-Feb-2015
Conference Location: San Francisco
Paper Title: Large mode area Yb-doped photonic bandgap fiber lasers
Authors: Benjamin Pulford , Iyad Dajani , Thomas Ehrenreich, Roger Holten , Christopher Vergien, Guancheng G
Acknowledged Federal Support: **Y**

Publication Type: Conference Paper or Presentation **Publication Status:** 1-Published
Conference Name: SPIE PhotonicsWest, paper 9344-2, San Francisco, February 2015.
Date Received: 02-Aug-2018 Conference Date: 08-Feb-2015 Date Published: 08-Feb-2015
Conference Location: San Francisco
Paper Title: Polarizing 50 μ m core Yb-doped photonic bandgap fiber
Authors: Fanting Kong* , Guancheng Gu , Thomas Hawkins , Joshua Parsons , Maxwell Jones , Christopher Dun
Acknowledged Federal Support: **Y**

RPPR Final Report
as of 07-Jan-2020

Publication Type: Conference Paper or Presentation **Publication Status:** 1-Published
Conference Name: SPIE PhotonicsWest, San Francisco, February 2015
Date Received: 02-Aug-2018 Conference Date: 08-Feb-2015 Date Published: 08-Feb-2015
Conference Location: San Francisco
Paper Title: Large mode area Yb-doped photonic bandgap fiber lasers
Authors: Liang Dong, Fanting Kong, Guancheng Gu, Thomas Hawkins, Joshua Parsons, Maxwell Jones, Christof
Acknowledged Federal Support: **Y**

Publication Type: Conference Paper or Presentation **Publication Status:** 1-Published
Conference Name: 7th Annual Directed Energy Symposium
Date Received: 02-Aug-2018 Conference Date: 02-Mar-2015 Date Published: 02-Mar-2015
Conference Location: Anaheim
Paper Title: High-Power All-solid Photonic Bandgap Fiber Lasers
Authors: Liang Dong , Fanting Kong, Guancheng Gu , Thomas Hawkins , Joshua Parsons, Maxwell Jones , Chris
Acknowledged Federal Support: **Y**

Publication Type: Conference Paper or Presentation **Publication Status:** 1-Published
Conference Name: Conference on Lasers and Electro-Optics
Date Received: 02-Aug-2018 Conference Date: 05-Jun-2015 Date Published: 05-Jun-2015
Conference Location: San Jose
Paper Title: Multiple Cladding-Resonance All-Solid Photonic Bandgap Fibers with Large Mode Area
Authors: Guancheng Gu, Fanting Kong, Thomas W. Hawkins, Maxwell Jones, and Liang Dong
Acknowledged Federal Support: **Y**

Publication Type: Conference Paper or Presentation **Publication Status:** 1-Published
Conference Name: Photonics Global Conference
Date Received: 02-Aug-2018 Conference Date: 28-Jun-2015 Date Published: 28-Jun-2015
Conference Location: Singapore
Paper Title: Challenges and Solutions for Further Power Scaling of Single-Mode Fiber Lasers
Authors: Liang Dong, Fanting Kong, Guancheng Gu, Thomas Hawkins, and Monica T. Kalichevsky-Dong
Acknowledged Federal Support: **Y**

Publication Type: Conference Paper or Presentation **Publication Status:** 1-Published
Conference Name: 4th Photonics Global Conference
Date Received: 02-Aug-2018 Conference Date: 28-Jun-2015 Date Published: 28-Jun-2015
Conference Location: Singapore
Paper Title: Challenges and Solutions for Further Power Scaling of Single-Mode Fiber Lasers
Authors: Liang Dong, Fanting Kong, Guancheng Gu, Thomas W. Hawkins, and Monica T. Kalichevsky-Dong
Acknowledged Federal Support: **Y**

Publication Type: Conference Paper or Presentation **Publication Status:** 1-Published
Conference Name: Advanced Solid State Lasers
Date Received: 23-Aug-2016 Conference Date: 04-Oct-2015 Date Published: 04-Oct-2015
Conference Location: Berlin, Germany
Paper Title: Challenges for Further Power Scaling of Single-Mode Fiber Lasers
Authors: L. Dong, F. Kong, G. Gu, T.W. Hawkins, M. Jones, J. Parsons, M.T. Kalichevsky-Dong, K. Saitoh, B. Pu
Acknowledged Federal Support: **Y**

RPPR Final Report
as of 07-Jan-2020

Publication Type: Conference Paper or Presentation **Publication Status:** 1-Published
Conference Name: 4th Workshop on Specialty Optical Fibers
Date Received: 23-Aug-2016 Conference Date: 03-Nov-2015 Date Published: 03-Nov-2015
Conference Location: Hong Kong
Paper Title: High-power Efficient Yb-doped Fiber Laser with Low Quantum Defect
Authors: G. Gu, Z. Liu, F. Kong, H.Y. Tam, R.K. Shori and L. Dong
Acknowledged Federal Support: **Y**

Publication Type: Conference Paper or Presentation **Publication Status:** 1-Published
Conference Name: PhotonicsWest
Date Received: 23-Aug-2016 Conference Date: 15-Feb-2016 Date Published: 15-Feb-2016
Conference Location: San Francisco
Paper Title: Efficient ytterbium-doped phPopshosilicate double-clad leakage-channel-fiber laser at 1008-1020nm
Authors: G. Gu, Z. Liu, F. Kong, H.Y. Tam, R.K. Shori, and L. Dong
Acknowledged Federal Support: **Y**

Publication Type: Conference Paper or Presentation **Publication Status:** 1-Published
Conference Name: Directed Energy Professional Society Annual Symposium
Date Received: 23-Aug-2016 Conference Date: 07-Mar-2016 Date Published: 07-Mar-2016
Conference Location: Albuquerque
Paper Title: 30 μ m-Core Yb-Doped Step-Index Fiber Operating Near Single-Mode Regime
Authors: F. Kong, C. Dunn, J. Parsons, M.T. Kalichevsky-Dong, T.W. Hawkins, M. Jones, and L. Dong
Acknowledged Federal Support: **Y**

Publication Type: Conference Paper or Presentation **Publication Status:** 1-Published
Conference Name: Stuttgart Technology Forum
Date Received: 23-Aug-2016 Conference Date: 31-May-2016 Date Published: 31-May-2016
Conference Location: Stuttgart, Germany
Paper Title: Opportunities and challenges of power scaling of single-mode fiber lasers
Authors: Liang Dong
Acknowledged Federal Support: **Y**

Publication Type: Conference Paper or Presentation **Publication Status:** 1-Published
Conference Name: Conference on Lasers and Electro-Optics
Date Received: 23-Aug-2016 Conference Date: 05-Jun-2016 Date Published: 05-Jun-2016
Conference Location: San Jose, CA
Paper Title: Ytterbium-doped 30/400 LMA Fibers with a Record-low \sim NA of 0.028
Authors: Fanting Kong, Thomas Hawkins, Maxwell Jones, Josh Parsons, Monica Kalichevsky-Dong, Christopher
Acknowledged Federal Support: **Y**

Publication Type: Conference Paper or Presentation **Publication Status:** 1-Published
Conference Name: Specialty Optical Fiber Conference
Date Received: 23-Aug-2016 Conference Date: 18-Jul-2016 Date Published: 18-Jul-2016
Conference Location: Vancouver, Canada
Paper Title: Ytterbium-doped 30, 40/400 LMA Fibers with a Record-low \sim NA of 0.028
Authors: Fanting Kong, Thomas Hawkins, Maxwell Jones, Josh Parsons, Monica Kalichevsky-Dong, Christopher
Acknowledged Federal Support: **Y**

RPPR Final Report
as of 07-Jan-2020

Publication Type: Conference Paper or Presentation **Publication Status:** 1-Published
Conference Name: Asia communications and Photonics Conference
Date Received: 02-Aug-2018 Conference Date: 02-Nov-2016 Date Published: 05-Nov-2016
Conference Location: Wuhan, China
Paper Title: Progress and challenges in further power scaling of single-mode fiber lasers
Authors: 19. Liang Dong, Fanting Kong, Guancheng Gu, Thomas W. Hawkins, Maxwell Jones, Joshua Parsons
Acknowledged Federal Support: **Y**

Publication Type: Conference Paper or Presentation **Publication Status:** 1-Published
Conference Name: Asia communications and Photonics Conference
Date Received: 02-Aug-2018 Conference Date: 02-Nov-2016 Date Published: 05-Nov-2016
Conference Location: Wuhan, China
Paper Title: Progress and challenges in further power scaling of single mode fiber lasers
Authors: Liang Dong, Fanting Kong, Guancheng Gu, Thomas W. Hawkins, Maxwell Jones, Joshua Parsons, Mor
Acknowledged Federal Support: **Y**

Publication Type: Conference Paper or Presentation **Publication Status:** 1-Published
Conference Name: Asia communications and Photonics Conference
Date Received: 02-Aug-2018 Conference Date: 02-Nov-2016 Date Published: 05-Nov-2016
Conference Location: Wuhan, China
Paper Title: Progress and challenges in further power scaling of single mode fiber lasers
Authors: Liang Dong, Fanting Kong, Guancheng Gu, Thomas W. Hawkins, Maxwell Jones, Joshua Parsons, Mor
Acknowledged Federal Support: **Y**

Publication Type: Conference Paper or Presentation **Publication Status:** 1-Published
Conference Name: Asia communications and Photonics Conference
Date Received: 02-Aug-2018 Conference Date: 02-Nov-2016 Date Published: 05-Nov-2016
Conference Location: Wuhan, China
Paper Title: Progress and challenges in further power scaling of single-mode fiber lasers
Authors: 19. Liang Dong, Fanting Kong, Guancheng Gu, Thomas W. Hawkins, Maxwell Jones, Joshua Parsons
Acknowledged Federal Support: **Y**

Publication Type: Conference Paper or Presentation **Publication Status:** 1-Published
Conference Name: Asia communications and Photonics Conference
Date Received: 02-Aug-2018 Conference Date: 02-Nov-2016 Date Published: 05-Nov-2016
Conference Location: Wuhan, China
Paper Title: Progress and challenges in further power scaling of single-mode fiber lasers
Authors: Liang Dong, Fanting Kong, Guancheng Gu, Thomas W. Hawkins, Maxwell Jones, Joshua Parsons, Mor
Acknowledged Federal Support: **Y**

Publication Type: Conference Paper or Presentation **Publication Status:** 1-Published
Conference Name: Asia communications and Photonics Conference
Date Received: 02-Aug-2018 Conference Date: 02-Nov-2016 Date Published: 05-Nov-2016
Conference Location: Wuhan, China
Paper Title: Progress and challenges in further power scaling of single-mode fiber lasers
Authors: Liang Dong, Fanting Kong, Guancheng Gu, Thomas W. Hawkins, Maxwell Jones, Joshua Parsons, Mor
Acknowledged Federal Support: **Y**

RPPR Final Report
as of 07-Jan-2020

Publication Type: Conference Paper or Presentation **Publication Status:** 1-Published
Conference Name: Workshop on Specialty Optical Fibers
Date Received: 02-Aug-2018 Conference Date: 11-Oct-2017 Date Published: 13-Oct-2017
Conference Location: Limassol, Cyprus
Paper Title: Single-mode Ytterbium Fiber Laser with Record 220W Output Power at 1018nm
Authors: Fanting Kong, Guancheng Gu, Thomas W. Hawkins, Maxwell Jones, Joshua Parsons, Monica T. Kalich
Acknowledged Federal Support: **Y**

Publication Type: Conference Paper or Presentation **Publication Status:** 1-Published
Conference Name: The 23rd OptoElectronics Communications Conference
Date Received: 02-Aug-2018 Conference Date: 02-Jul-2018 Date Published: 02-Jul-2018
Conference Location: Jeju, South Korea
Paper Title: Advanced specialty optical fibers and their applications in high-power fiber lasers
Authors: Liang Dong
Acknowledged Federal Support: **Y**

Publication Type: Conference Paper or Presentation **Publication Status:** 5-Submitted
Conference Name: OSA Laser Congress
Date Received: 02-Aug-2018 Conference Date: 04-Nov-2018 Date Published: 04-Nov-2018
Conference Location: Boston
Paper Title: Single-mode Yb-doped Double-clad All-solid Photonic Bandgap Fiber Laser Generating 27.8W at 976nm
Authors: Turghun Matniyaz, Monica T. Kalichevsky-Dong, Thomas W. Hawkins, Joshua Parsons, Guancheng Gu
Acknowledged Federal Support: **Y**

Publication Type: Conference Paper or Presentation **Publication Status:** 0-Other
Conference Name: PhotonicsWest
Date Received: 02-Aug-2018 Conference Date: 03-Feb-2019 Date Published: 04-Feb-2019
Conference Location: San Francisco
Paper Title: Diffraction-limited Yb-doped Double-clad All-solid Photonic Bandgap Fiber Laser at 976nm
Authors: 25. Turghun Matniyaz, Monica T. Kalichevsky-Dong, Thomas W. Hawkins, Joshua Parsons, Guanche
Acknowledged Federal Support: **Y**

Publication Type: Conference Paper or Presentation **Publication Status:** 1-Published
Conference Name: Conference on Lasers and Electro Optics (CLEO)
Date Received: 29-Jul-2019 Conference Date: 10-May-2019 Date Published: 10-May-2019
Conference Location: San Jose
Paper Title: A monolithic single-mode Yb three-level fiber laser at ~978nm with a record power of ~150W
Authors: Turghun Matniyaz, Wensong Li, Saddam Gafsi, Monica T. Kalichevsky-Dong, Thomas W. Hawkins, Jos
Acknowledged Federal Support: **Y**

Publication Type: Conference Paper or Presentation **Publication Status:** 1-Published
Conference Name: Conference on Lasers and Electro Optics (CLEO)
Date Received: 29-Jul-2019 Conference Date: 10-May-2019 Date Published: 10-May-2019
Conference Location: San Jose
Paper Title: Efficient High-power Single-mode Yb Three-level Cladding-pumped All-solid Photonic Bandgap Fiber Lasers at ~978nm
Authors: Turghun Matniyaz, Wensong Li, Monica T. Kalichevsky-Dong, Thomas W. Hawkins, Joshua Parsons, G
Acknowledged Federal Support: **Y**

RPPR Final Report
as of 07-Jan-2020

REPORT DOCUMENTATION PAGE*Form Approved*
OMB No. 0704-0188

Public reporting burden for this collection of information is estimated to average 1 hour per response, including the time for reviewing instructions, searching data sources, gathering and maintaining the data needed, and completing and reviewing the collection of information. Send comments regarding this burden estimate or any other aspect of this collection of information, including suggestions for reducing this burden to Washington Headquarters Service, Directorate for Information Operations and Reports, 1215 Jefferson Davis Highway, Suite 1204, Arlington, VA 22202-4302, and to the Office of Management and Budget, Paperwork Reduction Project (0704-0188) Washington, DC 20503.

PLEASE DO NOT RETURN YOUR FORM TO THE ABOVE ADDRESS.

1. REPORT DATE (DD-MM-YYYY) 10-1-2019		2. REPORT TYPE Final report		3. DATES COVERED (From - To) From 8-1-2012 to 8-9-2018	
4. TITLE AND SUBTITLE Novel Fiber Concepts for High Power Single Mode Fiber Lasers				5a. CONTRACT NUMBER	
				5b. GRANT NUMBER W911NF-12-1-0332	
				5c. PROGRAM ELEMENT NUMBER	
6. AUTHOR(S) Liang Dong, John Ballato, Roger Stolen, Alexander Gaeta, Bryce Samson, Stephen Palese, Eric Cheung				5d. PROJECT NUMBER	
				5e. TASK NUMBER	
				5f. WORK UNIT NUMBER	
7. PERFORMING ORGANIZATION NAME(S) AND ADDRESS(ES) Clemson University Office of Sponsored Programs P.O.Box 946 Clemson, SC 39631				8. PERFORMING ORGANIZATION REPORT NUMBER	
9. SPONSORING/MONITORING AGENCY NAME(S) AND ADDRESS(ES) Michael D. Gerhold Army Reseach Office P.O.Box 12211 Research Triangle Park, NC27709-2211				10. SPONSOR/MONITOR'S ACRONYM(S) 62072-EL-HEL	
				11. SPONSORING/MONITORING AGENCY REPORT NUMBER	
12. DISTRIBUTION AVAILABILITY STATEMENT					
13. SUPPLEMENTARY NOTES					
14. ABSTRACT The project is to develop double-clad hollow-core Raman gas lasers (Thrust I) and 100µm ytterbium-doped leakage channel fibers (Thrust II), both for power scaling of fiber lasers to well beyond kW. In thrust I, we have made significant progress in the fabrication of hollow-core fibers. Fibers with loss of <0.05dB/m at 3µm has been demonstrated. In thrust II, we have made significant breakthrough in demonstrating efficient flat-top mode in active LCF with effective area of 1900µm ² and record quantum-limited efficiency of ~95%. Systematic design study of 100µm-core multiple-cladding-resonance leakage channel fibers have been conducted. The 3 rd iteration ytterbium-doped glass with an index of ~2.3×10 ⁻⁴ has enabled the demonstration ytterbium-doped 30µm-core LMA fiber operating near single-mode regime, proving that LMA fibers with arbitrarily low NA can be reliably made. Using 50/400 ytterbium-doped leakage channel fiber, we have systematically studied fiber lasers between 1000nm-1020nm, achieving slope efficiency >70% with respect to the launched pump power at 1018nm in 400µm cladding. More recently, with 50/400 all-solid photonic bandgap fiber, we have achieved single-mode power of 220W at 1018nm. A study on thermal lensing is also conducted. In this period we have made significant breakthrough in demonstrating efficiency of 63% in 976nm fiber lasers, a record for flexible fibers by using bandgap to reject Yb ASE at longer wavelength.					
15. SUBJECT TERMS Specialty optical fibers, optical fiber lasers					
16. SECURITY CLASSIFICATION OF:			17. LIMITATION OF ABSTRACT	18. NUMBER OF PAGES 32	19a. NAME OF RESPONSIBLE PERSON Liang Dong
a. REPORT UNCLASSIFIED	b. ABSTRACT UNCLASSIFIED	c. THIS PAGE UNCLASSIFIED			19b. TELEPHONE NUMBER (Include area code) 864 656 5915

1. REPORT DATE. Full publication date, including day, month, if available. Must cite at least the year and be Year 2000 compliant, e.g., 30-06-1998; xx-08-1998; xx-xx-1998.

2. REPORT TYPE. State the type of report, such as final, technical, interim, memorandum, master's thesis, progress, quarterly, research, special, group study, etc.

3. DATES COVERED. Indicate the time during which the work was performed and the report was written, e.g., Jun 1997 - Jun 1998; 1-10 Jun 1996; May - Nov 1998; Nov 1998.

4. TITLE. Enter title and subtitle with volume number and part number, if applicable. On classified documents, enter the title classification in parentheses.

5a. CONTRACT NUMBER. Enter all contract numbers as they appear in the report, e.g. F33615-86-C-5169.

5b. GRANT NUMBER. Enter all grant numbers as they appear in the report, e.g. 1F665702D1257.

5c. PROGRAM ELEMENT NUMBER. Enter all program element numbers as they appear in the report, e.g. AFOSR-82-1234.

5d. PROJECT NUMBER. Enter all project numbers as they appear in the report, e.g. 1F665702D1257; ILIR.

5e. TASK NUMBER. Enter all task numbers as they appear in the report, e.g. 05; RF0330201; T4112.

5f. WORK UNIT NUMBER. Enter all work unit numbers as they appear in the report, e.g. 001; AFAPL30480105.

6. AUTHOR(S). Enter name(s) of person(s) responsible for writing the report, performing the research, or credited with the content of the report. The form of entry is the last name, first name, middle initial, and additional qualifiers separated by commas, e.g. Smith, Richard, Jr.

7. PERFORMING ORGANIZATION NAME(S) AND ADDRESS(ES). Self-explanatory.

8. PERFORMING ORGANIZATION REPORT NUMBER. Enter all unique alphanumeric report

numbers assigned by the performing organization, e.g. BRL-1234; AFWL-TR-85-4017-Vol-21-PT-2.

9. SPONSORING/MONITORS AGENCY NAME(S) AND ADDRESS(ES). Enter the name and address of the organization(s) financially responsible for and monitoring the work.

10. SPONSOR/MONITOR'S ACRONYM(S). Enter, if available, e.g. BRL, ARDEC, NADC.

11. SPONSOR/MONITOR'S REPORT NUMBER(S). Enter report number as assigned by the sponsoring/ monitoring agency, if available, e.g. BRL-TR-829; -215.

12. DISTRIBUTION/AVAILABILITY STATEMENT. Use agency-mandated availability statements to indicate the public availability or distribution limitations of the report. If additional limitations/restrictions or special markings are indicated, follow agency authorization procedures, e.g. RD/FRD, PROPIN, ITAR, etc. Include copyright information.

13. SUPPLEMENTARY NOTES. Enter information not included elsewhere such as: prepared in cooperation with; translation of; report supersedes; old edition number, etc.

14. ABSTRACT. A brief (approximately 200 words) factual summary of the most significant information.

15. SUBJECT TERMS. Key words or phrases identifying major concepts in the report.

16. SECURITY CLASSIFICATION. Enter security classification in accordance with security classification regulations, e.g. U, C, S, etc. If this form contains classified information, stamp classification level on the top and bottom of this page.

17. LIMITATION OF ABSTRACT. This block must be completed to assign a distribution limitation to the abstract. Enter UU (Unclassified Unlimited) or SAR (Same as Report). An entry in this block is necessary if the abstract is to be limited.

1. Executive Summary

1.1. Introduction

The program described in this proposal consists of two thrusts. The first thrust is to investigate the feasibility of high-power single-mode hydrogen-based Raman lasers in hollow-core double-clad photonic bandgap fibers (PBF). Nonlinear thresholds are expected to be significantly improved over what are possible in solid fiber lasers due to the much lower density of gas. This concept also provides for much improved mode quality due to the unique robust single-mode regime in PBF. This novel approach is expected to enable single-mode fiber lasers with power levels well beyond current state-of-art solid fiber lasers. We will study the limits for average power scaling to 100kW with this approach. This concept works with any optically pumped gas lasers, including the very promising diode-pumped alkali vapor lasers.

The second thrust is to investigate power scaling in single-mode ytterbium-doped 100 μ m core size resonantly enhanced leakage channel fibers (reLCF) for much improved nonlinear thresholds and mode quality. The resonantly enhanced leakage channel fibers make use of naturally existing resonant couplings between higher-order modes and the leakage channel cladding in a leakage channel fiber for significant additional higher-order-mode suppression over standard leakage channel fibers (LCF). The 100 μ m core fiber provides a simple, elegant and practical all-solid solution with much enhanced mode quality suitable further power scaling to 20kW. We will investigate limits to power scaling to 20kW with this approach. This new concept can provide a critical solution for resolving the recently observed mode instability issues at high powers.

1.2. Project Status

In thrust I, we have made significant progress in the fabrication of hollow-core fibers. Fibers with loss of <0.05dB/m at 3 μ m has been demonstrated. In thrust II, we have made significant breakthrough in demonstrating efficient flat-top mode in active LCF with effective area of 1900 μ m² and record quantum-limited efficiency of ~95%. Systematic design study of 100 μ m-core multiple-cladding-resonance leakage channel fibers have been conducted. The 3rd iteration ytterbium-doped glass with an index of $\sim 2.3 \times 10^{-4}$ has enabled the demonstration ytterbium-doped 30 μ m-core LMA fiber operating near single-mode regime, proving that LMA fibers with arbitrarily low NA can be reliably made. Using 50/400 ytterbium-doped leakage channel fiber, we have systematically studied fiber lasers between 1000nm-1020nm, achieving slope efficiency >70% with respect to the launched pump power at 1018nm in 400 μ m cladding. More recently, with 50/400 all-solid photonic bandgap fiber, we have achieved single-mode power of 220W at 1018nm. A study on thermal lensing is also conducted. In this period we have made significant breakthrough in demonstrating efficiency of 63% in 976nm fiber lasers, a record for flexible fibers by using bandgap to reject Yb ASE at longer wavelength.

1.3. List of Publications/Reports

(a) Papers published in peer-reviewed journals

1. G. Gu, F. Kong, T.W. Hawkins, P. Foy, K. Wei, B. Samson, and L. Dong, "Impact of fiber outer boundaries on leaky mode losses in leakage channel fibers," *Optics Express* 21, 24039-24048 (2013).
2. F. Kong, G. Gu, T.W. Hawkins, J. Parsons, M. Jones, C. Dunn, Monica T. Kalichevsky-Dong, K. Wei, B. Samson, and L. Dong, "Flat-top mode from a

- 50 μm -core Yb-doped leakage channel fiber," *Optics Express* 21, 32371-32376 (2013).
3. F. Kong, G. Gu, T.W. Hawkins, J. Parsons, M. Jones, C. Dunn, M. T. Kalichevsky-Dong, S.P. Palese, E. Cheung, and L. Dong, "Quantitative mode quality characterization of fibers with extremely large mode areas by matched white-light interferometry," *Optics Express* 22, 14657-14665 (2014).
 4. M. Steinke, H. Tünnermann, J. Neumann, D. Kracht, B. Samson, G. Gu, L. Dong, and P. Wessels, "TEM00 mode content measurements on a passive leakage channel fiber," *Optics Letters*, 40, 383-386(2015).
 5. G. Gu, Z. Liu, F. Kong, H. Tam, R.K. Shori and L. Dong, "Highly efficient ytterbium-doped phosphosilicate fiber lasers operating below 1020nm," *Opt. Express* 23(14), 17693-17700 (2015).
 6. F. Kong, C. Dunn, J. Parsons, M.T. Kalichevsky-Dong, T.W. Hawkins, M. Jones, and L. Dong, "Large-mode-area fibers operating near single-mode regime," *Optics Express* 24, 10295-10301 (2016).
 7. L. Dong, "Thermal Lensing in Optical Fibers," *Optical Express* 24(17), 19841-19852(2016).
 8. F. Kong, G. Gu, T.W. Hawkins, M. Jones, J. Parsons, M.T. Kalichevsky-Dong, S.P. Palese, E. Cheung, and L. Dong, "Efficient 240W single-mode 1018nm laser from an Ytterbium-doped 50/400 μm all-solid photonic bandgap fiber," *Optics Express* 26(3), 3138-3144 (2018).
 9. T. Matniyaz, W. Li, M.T. Kalichevsky-Dong, T.W. Hawkins, J. Parsons, G. Gu, and L. Dong, "Highly efficient cladding-pumped single-mode three-level Yb all-solid photonic bandgap fiber lasers," *Optics Letters* 44, 807-810 (2019).
 10. W. Li, T. Matniyaz, S. Gafsi, M.T. Kalichevsky-Dong, T.W. Hawkins, J. Parsons, G. Gu, and L. Dong, "151W monolithic diffraction-limited Yb-doped photonic bandgap fiber laser at \sim 978nm," *Optics Express*, to be published (2019).

(b) Papers published in non-peer-reviewed journals or in conference proceedings

1. Guancheng Gu, Fanting Kong, Thomas Hawkins, Liang Dong, Kanxian Wei, Bryce Samson, "Mode-dependent Losses in 50micron Core Leakage Channel Fibers," DEPS Solid State and Diode Laser Review, paper 13-SSDLTR-004, Santa Fe, June 2013.
2. Guancheng Gu, Fanting Kong, Thomas W. Hawkins, Paul Foy, Kanxian Wei, Bryce Samson, and Liang Dong, "Measurements of Mode Losses in \sim 50 μm Core Resonantly Enhanced Leakage Channel Fibers," *Advanced Solid State Lasers*, paper AM4A.04, Paris, October 2013.
3. Fanting Kong, Guancheng Gu, Thomas W. Hawkins, Joshua Parsons, Maxwell Jones, Christopher Dunn, Monica T. Kalichevsky-Dong, Kanxian Wei, Bryce Samson, and Liang Dong, "Flat-top Beam from a 50 μm -Core Yb-doped Leakage Channel Fiber," *Optical Communications Conference*, paper Tu3K.5, March 2014.
4. Fanting Kong, Guancheng Gu, Thomas Hawkins, Joshua Parsons, Maxwell Jones, Christopher Dunn, Monica Kalichevsky-Dong and Liang Dong, "50 μm -Core Yb-doped Leakage Channel Fiber with Flattened Mode," *Sixteenth Annual Directed Energy Symposium*, paper 13-Symp-064, March 2014.
5. Fanting Kong, Guancheng Gu, Thomas W. Hawkins, Joshua Parsons, Maxwell Jones, Christopher Dunn, Monica T. Kalichevsky-Dong, Kanxian Wei, Bryce Samson, and Liang Dong, "50 μm -core Yb-doped leakage channel fiber with flattened mode," *SPIE Defense and Security*. Paper 9081-14, May 2014.
6. Fanting Kong, Guancheng Gu, Thomas W. Hawkins, Joshua Parsons, Maxwell Jones, Christopher Dunn, Monica T. Kalichevsky-Dong, Kanxian Wei, Bryce Samson, and Liang Dong, "80W Flat-top Beam from an Yb-doped Leakage Channel Fiber," *International Photonics and OptoElectronics (POEM)*, paper FF3D.3 June 2014.

7. Fanting Kong, Guancheng Gu, Thomas Hawkins, Joshua Parsons, Maxwell Jones, Christopher Dunn, Monica Kalichevsky-Dong, Stephen Palese, Eric Cheung, and Liang Dong, "Quantitative Mode Quality Characterization in a Leakage Channel Fiber with 100 μm Core Diameter," Advanced Photonics Congress, paper SoW2B.5, August 2014.
8. Pierre Calvet, Amaud Perrin, Pierre Gouriou, Bryce N Samson, Thomas Hawkins, Fanting Kong, Liang Dong, Pascal Dupriez, and Emmanuel Hugonnot, "High-energy nanosecond-pulses from a flat-top mode 50 μm -core leakage channel fiber," Advanced Photonics Congress, paper SoM3B.4, August 2014.
9. L. Dong, "Control of light flow in optical fibers," 5th International Conference on Photonics, keynote speaker, September 2014, Kuala Lumpur.
10. L. Dong, F. Kong, G. Gu, T.W. Hawkins, and M.T. Kalichevsky-Dong, "Challenges and Solutions for Further Power Scaling of Single-Mode Fiber Lasers," 4th Photonics Global Conference, invited paper, ICMAT15-A-4343, Singapore June-July 2015.
11. L. Dong, F. Kong, G. Gu, T.W. Hawkins, M. Jones, J. Parsons, M.T. Kalichevsky-Dong, K. Saitoh, B. Pulford and I. Dajani, "Challenges for Further Power Scaling of Single-Mode Fiber Lasers," Advanced Solid State Lasers, invited talk, Berlin, October 4-7, 2015.
12. G. Gu, Z. Liu, F. Kong, H.Y. Tam, R.K. Shori and L. Dong, "High-power Efficient Yb-doped Fiber Laser with Low Quantum Defect," 4th Workshop on Specialty Optical Fibers, Hong Kong, paper WT4A.4, November 3-6, 2015.
13. G. Gu, Z. Liu, F. Kong, H.Y. Tam, R.K. Shori, and L. Dong, "Efficient ytterbium-doped phosphosilicate double-clad leakage-channel-fiber laser at 1008-1020nm," PhotonicsWest, paper 9728-51, San Francisco, February 15-18, 2016.
14. F. Kong, C. Dunn, J. Parsons, M.T. Kalichevsky-Dong, T.W. Hawkins, M. Jones, and L. Dong, "30 μm -Core Yb-Doped Step-Index Fiber Operating Near Single-Mode Regime," Directed Energy Professional Society Annual Symposium, Albuquerque, March 7-11, 2016.
15. L. Dong, "Opportunities and challenges of power scaling of single-mode fiber lasers," Stuttgart Laser Technology Forum, invited talk, Stuttgart, May 31st and June 1st, 2016.
16. Fanting Kong, Thomas Hawkins, Maxwell Jones, Josh Parsons, Monica Kalichevsky-Dong, Christopher Dunn, and Liang Dong, "Ytterbium-doped 30/400 LMA Fibers with a Record-low $\sim\text{NA}$ of 0.028," Conference on Lasers and Electro Optics, SM2Q.2, San Jose, June 2016.
17. Dong, "Opportunities and challenges of power scaling of single-mode fiber lasers," Stuttgart Laser Technology Forum, **invited talk**, Stuttgart, May 31st and June 1st, 2016.
18. Fanting Kong, Thomas Hawkins, Maxwell Jones, Josh Parsons, Monica Kalichevsky-Dong, Christopher Dunn, and Liang Dong, "Ytterbium-doped 30, 40/400 LMA Fibers with a Record-low $\sim\text{NA}$ of 0.028," Advanced Photonics Congress, Vancouver, SoW2H.4, Canada, July 2016.
19. Liang Dong, Fanting Kong, Guancheng Gu, Thomas W. Hawkins, Maxwell Jones, Joshua Parsons, Monica Kalichevsky-Dong, and Christopher Dunn, "Progress and challenges in further power scaling of single-mode fiber lasers" **invited talk**, Asia communications and Photonics Conference, November 2-5, 2016, Wuhan, China.
20. C. Mart, B. Pulford, B. Ward, I. Dajani, L. Dong, K. Kieu, and A. Sanchez, "SBS Investigation of an All-solid Ytterbium-doped Photonic Bandgap Fiber Amplifier", Nineteenth Annual Directed Energy Symposium, Huntsville, Alabama, 13-17 February 2017,
21. Fanting Kong, Guancheng Gu, Thomas W. Hawkins, Maxwell Jones, Joshua Parsons, Monica T. Kalichevsky-Dong, and Liang Dong, "Single-mode Ytterbium Fiber Laser with Record 220W Output Power at 1018nm," Workshop on Specialty Optical Fibers, October 11-13, 2017, Limassol, Cyprus.

22. Fanting Kong, Guancheng Gu, Thomas W. Hawkins, Maxwell Jones, Joshua Parsons, Monica T. Kalichevsky-Dong, and Liang Dong, "Single-mode Ytterbium Fiber Laser with Record 240W Output Power at 1018nm," PhotonicsWest, paper 10512-16 (PW18L-LA102-92), January 27 - February 1, 2018, San Francisco.
23. Liang Dong, "Advanced specialty optical fibers and their applications in high-power fiber lasers," The 23rd OptoElectronics and Communications Conference (OECC2018), tutorial, 2-6 July, 2018, Jeju, Korea.
24. Turghun Matniyaz, Monica T. Kalichevsky-Dong, Thomas W. Hawkins, Joshua Parsons, Guancheng Gu, Wensong Li, Max Faykus, Bradley Selee, Jonathan A. Dong, and Liang Dong, "Single-mode Yb-doped Double-clad All-solid Photonic Bandgap Fiber Laser Generating 27.8W at 976nm," OSA Laser Congress, Boston, November 4 2018.
25. Zhimeng Huang, Shankar Pidishety, Thomas Hawkins, Yujun Feng, Yutong Feng, Sheng Zhu, Liang Dong, and Johan Nilsson, "Low-birefringence 120 W Yb fiber amplifier producing linearly polarized pulses with 69-GHz linewidth at 1083 nm," OSA Laser Congress, Boston, November 4 2018.
26. Turghun Matniyaz, Monica T. Kalichevsky-Dong, Thomas W. Hawkins, Joshua Parsons, Guancheng Gu, Wensong Li, Max Faykus, Bradley Selee, Jonathan A. Dong, and Liang Dong, "Diffraction-limited Yb-doped Double-clad All-solid Photonic Bandgap Fiber Laser at 976nm," PhotonicsWest, invited talk, San Francisco, February 2 2019.
27. Liang Dong, "Challenges and potential solutions in further power scaling of single-mode fiber lasers," Oasis 7 - International Conference and Exhibition on Optics and Electro-Optics, invited talk, April 1-2, 2019, Tel Aviv, Israel.
28. Turghun Matniyaz, Wensong Li, Monica T. Kalichevsky-Dong, Thomas W. Hawkins, Joshua Parsons, Guancheng Gu, and Liang Dong, "Efficient High-power Single-mode Yb Three-level Cladding-pumped All-solid Photonic Bandgap Fiber Lasers at ~978nm," CLEO, 3160577, San Jose, May 2019.
29. Turghun Matniyaz, Wensong Li, Saddam Gafsi, Monica T. Kalichevsky-Dong, Thomas W. Hawkins, Joshua Parsons, Guancheng Gu, and Liang Dong, "A monolithic single-mode Yb three-level fiber laser at ~978nm with a record power of ~150W," CLEO, postdeadline paper, 3212958, San Jose, May 2019.

(c) Papers presented at meetings, but not published in conference proceedings

None

1.4. Scientific Personnel Supported by This Project and Honors/Awards/Degree Received

Personnel Supported by This Project:

Prof. Liang Dong, PI, Clemson University

Prof. Alexander Gaeta, Cornell University

Dr. Monica T. Kalichevsky-Dong, research associate, characterization, Clemson University

Dr. Fanting Kong, research associate, optics, Clemson University

Mr. Thomas Hawkins, associate director of fiber fabrication, Clemson University

Mr. Joshua Parsons, staff, fiber fabrication, Clemson University

Dr. Guancheng Gu, graduated PhD, Clemson University

Mr. Christopher Dunn, graduated MSc, Clemson University

Mr. Maxwell Jones, undergraduate student, fiber fabrication, Clemson University

Mr. Andrew Rennion, ECE undergraduate student, fiber taper and fiber lasers

Mr. Turghun Matniyaz, PhD student

Mr. Saddam Gafsi, PhD student

Mr. Kenneth Peters, ECE, undergraduate student, fiber fabrication

Mr. Nikhil Gandhi, ECE, undergraduate student, fiber fabrication

Mr. Jeremy Lister, ECE, fiber fabrication, fiber fabrication
Mr. Camden Griggs, MSE, glass and fiber fabrication
Mr. Jonathan Drake, MSE, glass and fiber fabrication
Mr. Bailey Meehan, ECE, glass and fiber fabrication
Mr. Max Faykus, ECE, undergraduate student, optics and lasers
Mr. Bradley Selee, ECE, undergraduate student, optics and lasers
Mr. Grant Vegas, ECE, undergraduate student, optics and lasers
Mr. Dylan Kensler, ECE, undergraduate student, optics and lasers

PhD degree received:
Guancheng Gu, ECE, August 2016

MSc degree received:
Christopher Dunn, August 2016

BSc degree received:
Mr. Devon McClane, MSE
Mr. Christopher Dunn, MSE
Mr. Tyler Hughes, MSE
Mr. Matthew Vanoverstraeten, ECE
Mr. Andrew Rennion, ECE
Mr. Maxwell Jones, MSE
Mr. Alex Gay, ECE
Mr. Camden Griggs, MSE
Mr. Jonathan Drake, MSE,
Mr. Kenneth Peters, ECE,

Honors/Awards:
Guancheng Gu, OSA Incubic Milton travel grant, 2015
Guancheng Gu, Clemson Professional Enrichment Grant Application (PEGAS) grant.
2015
Christopher Dunn, DEPS graduate student fellowship (2014, 2015)
Liang Dong, Fellow of Optical Society of America, 2014
Liang Dong, Fellow of SPIE, 2017
Liang Dong, IEEE senior fellow, 2017
Liang Dong, University Research, Scholarship, and Artistic Achievement award, 2018
Liang Dong, Dean's Distinguished Professor Award in the Department of Electrical
and Computer Engineering, 4/16/2019 to 4/15/2022

1.5. Reports of Inventions

None

1.6. Scientific Progress and Accomplishments

- i. Identifying the significance of fiber outer boundary in higher order mode suppression and ways to optimize it.
- ii. First demonstration flat-top mode in active 50 μm -core leakage channel with 50% increase of effective mode area to 1900 μm^2 .
- iii. Demonstration of record-breaking quantum-limited efficiency of 95% versus the absorbed pump power in the 50 μm -core reLCF.
- iv. Developed matched white-light interferometer for quantitative mode characterization and demonstrated quantitative mode characterization in 100 μm -core fiber for the first time.

- v. Demonstrate 100 μ m-core re-LCF with higher-order-mode contents 29dB below fundamental mode.
- vi. Fabricated negative curvature fibers with loss as low as 0.05dB/m at \sim 3 μ m
- vii. Design optimization for 100 μ m-core multiple-cladding-resonance LCF
- viii. Demonstrate ytterbium-doped LMA fibers with record low NA of 0.028.
- ix. Developed general thermal lensing normalization factor and criteria.
- x. Achieving record single-mode power of 220W at 1018nm.
- xi. 44W at 976W with record efficiency of 52.7%
- xii. Record 151W at 976nm with record efficiency of 63%

1.7. Technology Transfer, None

1.8. Copies of Technical Reports, None

2. Introduction to the Project

2.1 Statements of Objectives

The program described in this proposal consists of two thrusts. The first thrust is to investigate the feasibility of high-power single-mode hydrogen-based Raman lasers in hollow-core double-clad photonic bandgap fibers (PBF). A first photonic cladding surrounds the core and is designed to support robust single-mode operation in the hollow-core at the lasing wavelength of the first hydrogen rotational Stokes line. This is achieved by operating in the robust single-mode regime near the high frequency edge of the bandgap of the first cladding. A second cladding immediately surrounds the first cladding and provides a multimode pump guide of 100-250 μ m in diameter at the pump wavelength. This is achieved by choosing a slightly smaller mode size for the second photonic cladding so that the pump wavelength is near the low frequency edge of the bandgap of the second photonic crystal cladding. A length of a few meters is expected to be used with a hydrogen pressure in the hollow-core from a fraction to several atmospheres. Pumps can be at any wavelengths, with desired absorption length adjusted by fiber designs, using any high power multimode fiber lasers, solid state lasers, diode lasers or even gas lasers. Fiber Bragg gratings at the lasing wavelength can be spliced to two ends of the fiber to form the laser cavity for a highly efficient Raman laser. *Nonlinear thresholds are expected to be significantly improved over what are possible in solid fiber lasers due to the much lower density of gas. This concept also provides for much improved mode quality due to the unique robust single-mode regime in PBF.* This novel approach is expected to enable single-mode fiber lasers with power levels well beyond current state-of-art solid fiber lasers. We will study the limits for average power scaling to 100kW with this approach. This concept works with any optically pumped gas lasers, including the very promising diode-pumped alkali vapor lasers.

The second thrust is to investigate power scaling in single-mode ytterbium-doped 100 μ m core size resonantly enhanced leakage channel fibers (reLCF) for much improved nonlinear thresholds and mode quality. The resonantly enhanced leakage channel fibers make use of naturally existing resonant couplings between higher-order modes and the leakage channel cladding in a leakage channel fiber for significant additional higher-order-mode suppression over standard leakage channel fibers (LCF). *The 100 μ m core fiber will be designed and provides a simple, elegant and practical all-solid solution with much enhanced mode quality suitable further power scaling to 20kW.* We will investigate limits to power scaling to 20kW with this approach. This new concept can provide a critical solution for resolving the recently observed mode instability issues at high powers.

Thrust I: High Power Single-mode Hydrogen Raman Lasers in Hollow-core Double-clad Photonic Bandgap Fibers

Key objective: to investigate power scaling of single-mode hydrogen Raman lasers in hollow-core double-clad photonic bandgap fibers to well beyond current solid-state fiber lasers to average powers to 100 kW.

1. Investigate practical designs for hollow-core double-clad PBFs
2. Develop fabrication process for the hollow-core double-clad PBFs
3. Full characterizations of hollow-core double-clad PBFs at both lasing and pump wavelengths
4. Simulate and optimize designs of hydrogen Raman lasers in hollow-core double-clad PBFs
5. Demonstrate efficient hydrogen Raman lasers in hollow-core double-clad PBFs
6. Investigate thermal and other limits in power scaling of single-mode hydrogen Raman lasers in hollow-core double-clad PBFs to 100kW average powers
7. Study nonlinear effects in hollow-core PBFs
8. High power demonstration of single-mode hydrogen Raman lasers (*optional*)

Thrust II: Active 100μm Resonantly Enhanced Leakage Channel Fibers.

Key objective: to develop active 100μm Resonantly Enhanced Leakage Channel Fibers and to investigate its potential for providing sufficient mode quality for average power scaling to 20kW.

1. Optimize design for 100μm-core reLCFs
 2. Fabricate passive 100μm-core reLCFs
 3. Fully characterize fabricated passive 100μm-core reLCFs
 4. Fabricate uniform ytterbium-doped core glass with refractive within from -1.25×10^{-4} to $+2.5 \times 10^{-5}$ of silica
 5. Fabricate ytterbium-doped 100μm-core reLCFs
 6. Investigate power scaling issues with high power tests of fabricated ytterbium-doped 100μm-core reLCFs
 7. Investigate core diameter scaling to beyond 100μm (*optional*)
- Investigate tapered mode converter for splicing to 100μm core fiber (*optional*)

2.2 Work Plan

Timeline and Milestones

	Year 1	Year 2	Year 3	Year 4	Year 5
Thrust I					
Hollow-core double-clad PBF design and optimization	→	*A1			
Hollow-core double-clad PBF fabrication developments		*A2	*A3		
Hollow-core double-clad PBF characterizations				→	
Design and simulation of hydrogen Raman lasers in hollow-core double-clad PBFs			→		
Study of nonlinear effects in high power hydrogen Raman lasers (<i>at Cornell</i>)					→
Demonstration of hydrogen Raman lasers in hollow-core double-clad PBF			*A4		
Investigate power scaling in hydrogen Raman lasers in hollow-core PBF					*A5
Thrust II					
Design and optimization of reLCF	→	*B1			
Fabrication of passive 100μm reLCF		→			
Ytterbium-doped core glass developments for 100μm core reLCF				→	
Passive reLCF characterizations		*B2			
Fabrication of active 100μm reLCF			*B3		
Active reLCF characterization				→	
Amplifier and laser demonstration in 100μm reLCF			*B4		
Development of tapered mode converter for low loss splice to 100μm reLCF					*B6
High power tests and demonstration (<i>at Northrop Grumman Aerospace System</i>)			*B5		*B8
Investigate core diameter scaling beyond 100μm with reLCF					*B7
Investigate issues related to power scaling in reLCF					→

PBF=Photonic bandgap fibers, reLCF=resonantly enhanced leakage channel fibers

Milestones

Thrust I

- A1: report on design and optimization of hollow-core double-clad photonic bandgap fibers
- A2: demonstration of hollow-core photonic bandgap fibers
- A3: demonstration of hollow-core double-clad photonic bandgap fibers
- A4: demonstration of hydrogen Raman lasers in hollow-core double-clad photonic bandgap fibers
- A5: report on issues and solutions of power scaling in hollow-core photonic bandgap fibers

Thrust II

- B1: report on design and optimization of resonantly enhanced leakage channel fibers
- B2: first demonstration of passive 100 μ m resonantly enhanced leakage channel fibers
- B3: first demonstration of ytterbium-doped 100 μ m resonantly enhanced leakage channel fibers
- B4: amplifier demonstrations in ytterbium-doped 100 μ m resonantly enhanced leakage channel fibers
- B5: initial high power amplifier demonstration in ytterbium-doped 100 μ m resonantly enhanced leakage channel fibers
- B6: demonstration of mode converter for low-loss splice to 100 μ m resonantly enhanced leakage channel fibers
- B7: report on core diameter scaling beyond 100 μ m with resonantly enhanced leakage channel fibers
- B8: higher power amplifier demonstration in ytterbium-doped 100 μ m resonantly enhanced leakage channel fibers

2.3 Background of the Project

There has been significant progress made in single-mode fiber lasers in recent years, especially in single-mode and multimode CW powers. There also have been several demonstrations of single-frequency fiber lasers beyond the kW level recently. Most fiber lasers still require spectral broadening to several GHz levels in order to mitigate stimulated Brillouin scattering (SBS). For further power scaling to few tens of kilowatts single-frequency single-mode ytterbium fiber lasers, orders of magnitude improvements in nonlinear thresholds are still required. In order to achieve the necessary nonlinear thresholds, core diameter scaling to beyond 100 μ m is essential for ytterbium-doped single-mode fiber amplifiers. This, in combination with selected SBS suppression techniques demonstrated in recent years [1-5], may provide a path for over 2 orders of magnitude improvements in single-frequency single-mode power levels in the near future.

Recently it has been observed that mode instability can lead to significant deteriorations in mode quality at high power levels [6,7]. There still are debates as to the exact mechanisms though it is generally agreed that this mode instability is initiated by a small amount of higher-order mode content in current state-of-art active large-mode-area (LMA) and photonic crystal fibers (PCF). In order to overcome this, much stronger high-order-mode suppression than currently available in fiber amplifiers is required. This can only be achieved by further significant innovations in novel fiber concepts.

3. Status of the Project

Thrust I, High Power Single-mode Hydrogen Raman Lasers in Hollow-core Double-clad Photonics Bandgap Fibers

3.1.1 Fiber design

3.1.1.1 Design concepts

The concept of photonic bandgap fibers was first studied in the late seventies [11,12]. Hollow-core photonic bandgap fibers were first proposed over a decade ago. Their optical guidance is derived from anti-resonance of a 2D photonic lattice, i.e., photonic bandgap. The core is established using a hollow defect that is placed in the 2D photonic lattice. Light, once in the hollow core, is trapped and cannot escape into the surrounding cladding. The principle of the guidance is, therefore, fundamentally different from that of conventional optical fibers based on total internal reflection. It provides, for the first time, single-mode guidance in a hollow-core with losses similar to those in silica optical fibers. Understanding of the hollow-core photonic bandgap fibers along with the related fabrication and characterization technologies has progressed significantly over the past decade [13-74].

Typically a hexagonal photonic lattice is used for the cladding. The use of a hexagonal arrangement is primarily due to the relative ease of fabrication using stack-and-draw processes due to the natural stability of this geometry; though it is not an absolute necessity. Recently, the

PI has demonstrated hollow-core photonic bandgap fibers based on a square photonic lattice [74], which provide significantly improved bandgap widths. A hollow-core photonic bandgap fiber with square lattice is used for the illustration of the fundamental principle of the fiber in Figure 1. The simulated photonic bandgap was obtained by the PI from a previous study. The red area shows the bands of modes in the photonic lattice. The black area indicates an absence of any modes in the photonic lattice and is where guidance in a hollow defect core would take place. The vertical axis is the effective mode index and horizontal axis is the normalized frequency of the cladding photonic lattice given by

$$V = \frac{\pi d_1}{\lambda} \sqrt{n_{si}^2 - n_{air}^2}$$

with the silica glass index, n_{si} , the air index, n_{air} , the vacuum wavelength, λ , and the cladding node diameter, d_1 (see Figure 2). Each band of modes is derived from features in the cladding lattice. Notably, the bands reaching the top of the curve in Figure 1, i.e., of high effective mode indices, are related to modes guided in the nodes of the photonic lattice (images of the modes are shown in the insets in Figure 1). Modes in these bands typically have increasing effective indexes at higher frequencies, while the widths of the bands narrow. This is because these modes are increasingly confined to the glass nodes in the photonic lattice at higher frequencies.

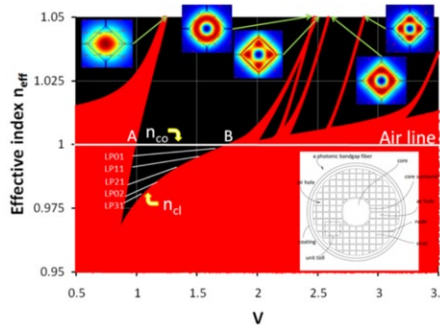


Figure 1 Simulated photonic bandgap for a square lattice for the purpose of illustrating the working principle of hollow-core photonic bandgap fibers. The horizontal axis is normalized frequency V (see text for the definition).

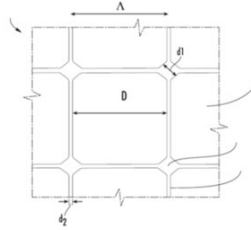


Figure 2 Unit cell and parameter definitions in a square lattice.

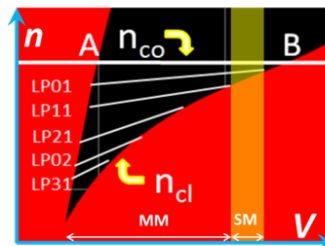


Figure 3 Multimode and single-mode regime of a hollow core photonic bandgap fiber.

The air line with a refractive index of $n_{air}=1$ is illustrated as a thick white line in Figure 1. Since light is mostly guided in air in a hollow-core photonic bandgap fiber, the equivalent core index is $n_{co}=n_{air}=1$ in this case. The guided modes have effective indices below the core index n_{co} as in conventional optical fibers [36]. Effective indices of the first 5 modes guided in a hollow-core also

are illustrated in Figure 1 and the modes are labeled as the equivalent linearly polarized (LP) modes in weakly guided optical fibers. With an increase of core diameter, more modes, with smaller modal index differences, will be guided in the bandgap. The equivalent cladding index is the boundary defining the lower edge of the photonic bandgap in Figure 1, labeled by cladding index n_{cl} . A guided mode is cut off when it meets the edge of the photonic bandgap and can no longer propagate in the hollow core.

One important feature of photonic bandgap fibers is that the equivalent cladding index, n_{cl} , is strongly dispersive. At the low frequency end, i.e., long wavelength end, of the photonic bandgap, the waveguide has high numerical aperture and supports more modes in the hollow core (see Figure 1). When moving towards higher frequency, i.e., shorter wavelength, within the photonic bandgap, waveguide gets weaker and a greater number of modes are cut off. There is a robust single-mode regime near the high-frequency end of the photonic bandgap. This effect is summarized in Figure 3, with multimode and single-mode regime clearly marked. At larger core diameters, there are more modes supported in the hollow core, with narrowing mode spacing. The single-mode regime will get smaller as the mode spacing narrows. With core diameters of 20-30 μm , robust single mode operation is possible. It is further worth noting that, in conventional optical fibers, single-mode regime is achieved by operating at low frequencies, i.e., long wavelengths, exactly the opposite as in photonic bandgap fibers.

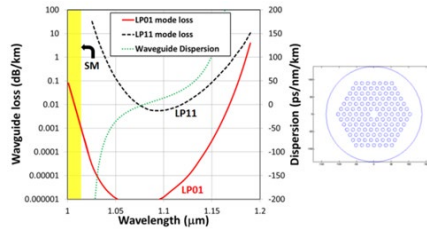


Figure 4 Simulated waveguide losses for the first two modes in an all-solid photonic bandgap fiber with 25 μm core to illustrate the single-mode regime near the high-frequency edge, i.e. shorter wavelength edge. The cross section of the fiber is also shown.

In order to further illustrate the robust single-mode regime near the high frequency edge of a photonic bandgap fiber. This team has simulated an all-solid photonic bandgap fiber with 25 μm core diameter (see inset in Figure 4 for the simulated fiber cross section). As is clearly seen in Figure 4, near the high-frequency edge, i.e., shorter-wavelength edge, the fundamental mode loss is negligible while the next higher-order mode, LP₁₁ mode, can no longer propagate. Near the low frequency edge, i.e., longer-wavelength edge, the losses of the two modes are converging, albeit higher, indicating that they are guided with similar waveguide strengths.

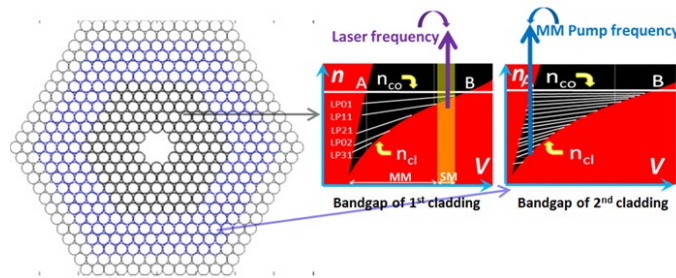


Figure 5 An illustration of the proposed hollow-core double-clad photonic bandgap fiber with corresponding photonic bandgaps for the two photonic cladding. The laser and pump frequencies are also shown.

An illustration of the proposed hollow-core double-clad photonic bandgap fiber is provided in Figure 5. The design consists of a 20-30 μm hollow core, robustly single-mode at the laser wavelength, ensured by appropriate design of the first photonic cladding in order to operate in the single-mode regime at this wavelength. The second photonic cladding is designed to provide a multimode pump guide of 100-250 μm in diameter with a 0.3 NA at the pump wavelength, by appropriate design of the second photonic cladding to operate in multimode regime at the pump wavelength. The pump guide consists of the hollow core as well as the entire

first photonic cladding. The pump wavelength is situated outside the photonic bandgap of the first photonic cladding and can freely propagate in the first photonic cladding. Apart from a small amount of silica glass in the first photonic cladding, the pump light predominantly propagates in air. The pump modes guided in the bandgap of the second photonic cladding also are illustrated in Figure 5 by white lines (see rightmost figure). The much larger pump guide supports more modes with much narrower mode spacing. The second photonic cladding is further surrounded by silica glass to enhance the mechanical strength of the fiber.

It is worth noting that the normalized frequency V determines the regime of operation of the first and second photonic claddings and can be adjusted by the node diameter, d_1 , without having to change lattice pitch, Λ . In fiber fabrication, the node diameter, d_1 , is determined by the silica rods that are placed in the interstitial space, which can be easily made to be different for the first and second photonic claddings. The pitch, Λ , of the first and second claddings, determined by the outer diameter of the capillary tubes used, can be kept constant. This allows well-developed stack-and-draw technique to be used in the fiber fabrication.

3.1.1.2 Design optimization

Initial designs have focused on large node sizes. This will create desired wider bandgaps. Large number of designs is explored. Two designs are shown in Figure 6. One criteria is feasibility of fabrication. Many parameters are correlated in the fabrication process. It is often hard to predict whether a design is feasible. Fabrication trials are sometimes required.

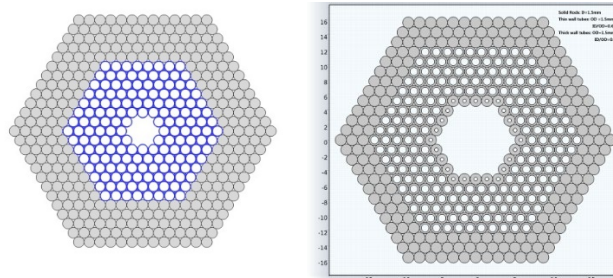


Figure 6 Design with interstitial nodes (left) and design with thick wall capillaries.

3.1.2 Fabrication of hollow-core double-clad photonic bandgap fibers

3.1.2.1 Background

The fabrication of the hollow-core photonic bandgap fibers presents some of the biggest challenges in this project. A hexagonal design is used for the hollow-core double-clad photonic bandgap fibers in this project (see Figure 5). Hexagonal designs are easier to fabricate than the corresponding square lattice designs, due to the intrinsic stability of a hexagonal stack. Square lattices do not have such intrinsic stability and keeping them from being distorted is considerably more difficult. Over the past year, we have developed many of the required procedures for the fabrication of hollow-core photonic bandgap fibers at Clemson University.

A stack-and-draw process is used to fabricate the hollow-core double-clad photonic bandgap fibers. A stack first is formed on a specially-designed stacking station with capillaries of appropriate dimensions. Preform canes, typically a few millimeters in diameter, much larger than fibers, are drawn from the stack. A vacuum is applied in the interstitial space to allow controlled collapse of this area during the caning phase. In the fabricated cane, the holes of each capillaries expanded to take up the space formerly occupied by the interstitial gaps. The cane is further sleeved with a larger tube and drawn into fibers with separate core and cladding pressures. A digital pressure controller capable of precisely supplying three different pressures and a vacuum simultaneously is available on our draw tower at Clemson.

The pressures within the core and cladding holes must be controlled separately during the fiber drawing process, due to their different dimensions. Consequently, different internal pressures are required to counter the different surface tensions during the fiber draw. Separate pressure connectors are made to the core and the cladding.

3.1.2.2 Fabrication trials

The first design tested has very large node. The nodes are equivalent size of the rods in the stack. Canning is successful, but fiber drawing proves to be highly challenging. The node size needs to be reduced to sub-micron size in dimension. This leads to large reduction ratio during fiber drawing, which proved to be impossible to maintain this structure in the fiber.

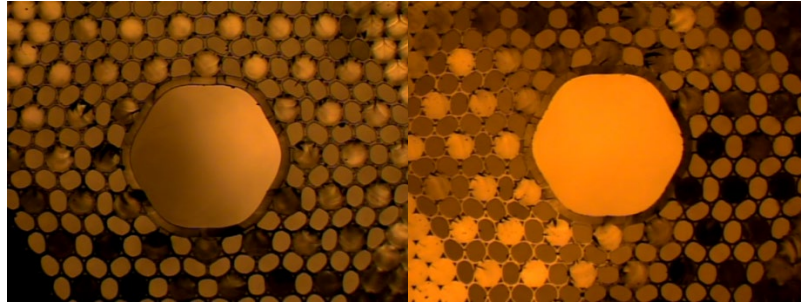


Figure 7 Hollow-core photonic bandgap fiber with large cladding nodes.

The second design iteration is based on a design with thick wall capillaries (see Figure 6). Canning was successful (see Figure 8). Fiber drawing was not possible. The third design incorporate an additional inner tube (see middle figure of figure 8). Fiber draw was successful (see right figure of figure 8).

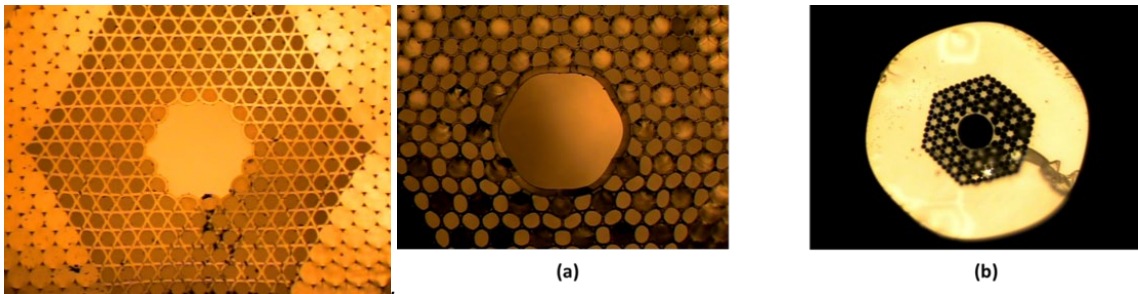


Figure 8 Hollow-core photonic bandgap fiber with thick wall capillaries.

3.1.3 Hollow-core fibers with negative-curvature core surround.

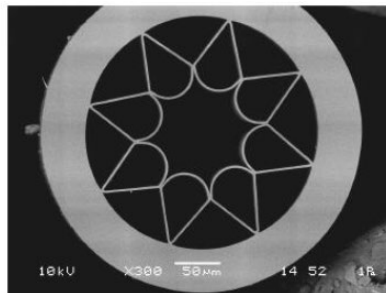


Figure 9 Hollow-core fiber with negative curvature core surround.

It has been recently reported that low-loss hollow-core fibers are possible with a simple design consisting of a negative-curvature core surround (Figure 9). The fiber in Figure 9 has a core of $94\mu\text{m}$. It is shown to have 34dB/km loss at $3.05\mu\text{m}$, where silica absorption is extremely high. It is found that the negative curvature in the core surround can significantly reduce mode interaction with the silica glass in this case, leading to low loss at wavelength where absorption in silica is very high. This is a significant discovery which can impact our design choice. We have decided to investigate this further as part of design efforts.

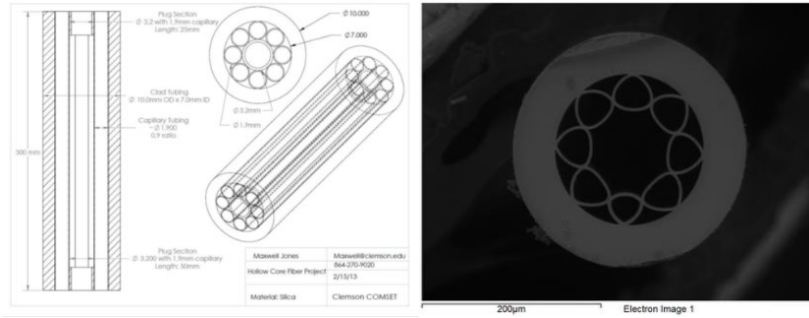


Figure 10 Hollow-core fiber with negative curvature core surround fabricated at Clemson University.

We have been able to fabricate fibers with very similar geometry (Figure 10). A simultaneous simulation efforts has developed the capability to simulate these fibers at Clemson (see Figure 11). Our simulation is benchmarked to results in published literature with high accuracy.

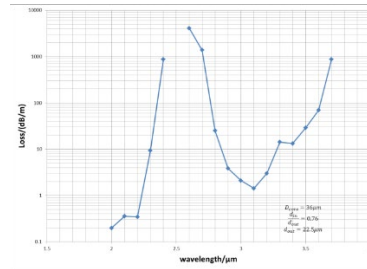


Figure 11 Simulation of hollow-core fiber with negative curvature core surround fabricated at Clemson University.

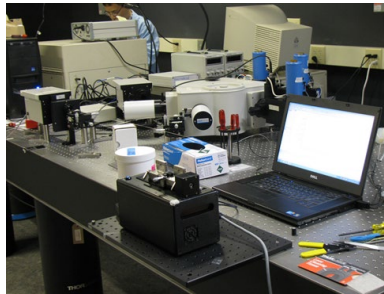


Figure 12 Horiba iHR spectrometer system for spectral loss measurement over $0.4\text{--}14\mu\text{m}$.

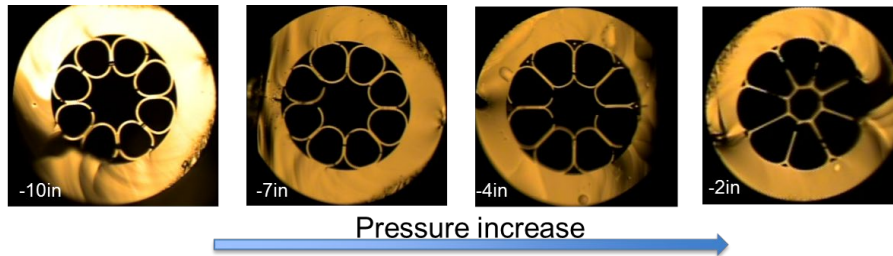


Figure 13. Effect of pressurization during fiber draw.

To study these fibers, we need a loss measurement system covering a wide range of spectrum. A Horiba iHR spectrometer system is set up, covering wavelength from 0.4-14 μm with tungsten halogen lamp and Globar in combination with a range of detectors: TE-cooled silicon detector (0.2-1.1 μm), liquid nitrogen cooled extended InGaAs (0.9-2.1 μm), liquid nitrogen cooled solid-state Indium Antimonide detector (2-5.5 μm), and liquid nitrogen cooled solid-state Mercury Cadmium Telluride detector (2-14 μm). A monochromator with multiple gratings and inter-changeable filters are used for wavelength selection. This setup is shown in Figure 12.

In this period, we have made significant progress in the fabrication process of hollow-core fibers at Clemson. Figure 13 illustrates a test of the effect of pressurization during the fiber drawing. Figure 14 illustrates a summary of our more recent hollow-core fibers.

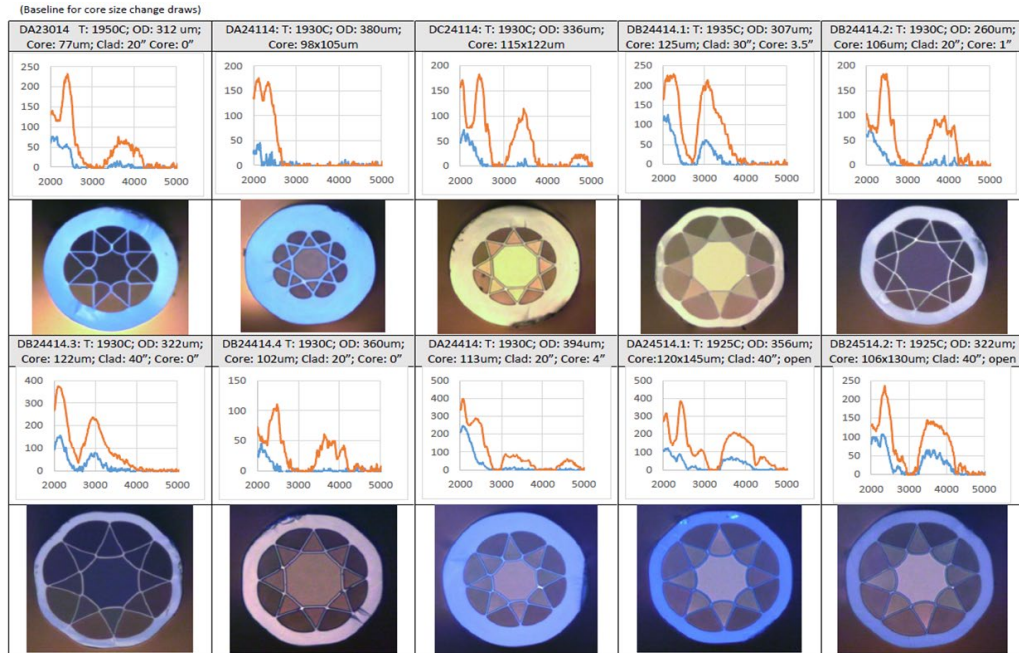


Figure 14 Hollow-core fibers fabricated recently at Clemson.

The cross section of one of our latest fiber and its transmission between 2-5 μm are shown in Figure 15. We observed transmission close to 5 μm over 5m of fiber. This is significant as material loss of silica is close 10000 dB/m at 5 μm (see Figure 16). The loss in the fiber is 4 orders of magnitude below that of the silica glass of which the fiber is made of. Transmission spectra for various fiber lengths are shown in the left figure in Figure 17. It can be clearly seen that the most significant drop in transmission happens in the first 8m. This is due to the higher loss of higher-order modes propagating mostly at the beginning of the fiber. The cut-back measurements for various lengths of the reference measurement (the length of the short fiber) are shown in the right figure in Figure 17. As expected, a longer length of the reference measurement generates the lowest loss. This loss is $\sim 0.05\text{dB/m}$ at 3 μm when the cut-back length is over 8m.

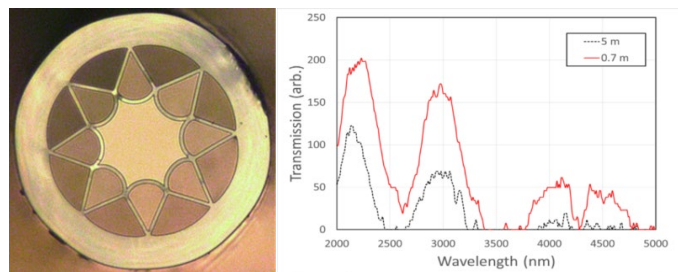


Figure 15 Cross section of one of latest fiber (left) and transmission over 5m and 0.7m of the fiber (right).

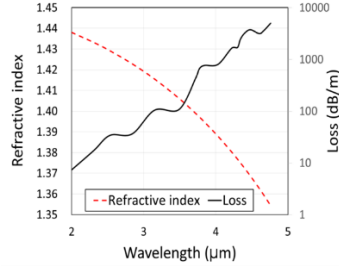


Figure 16 Refractive index and material loss of silica.

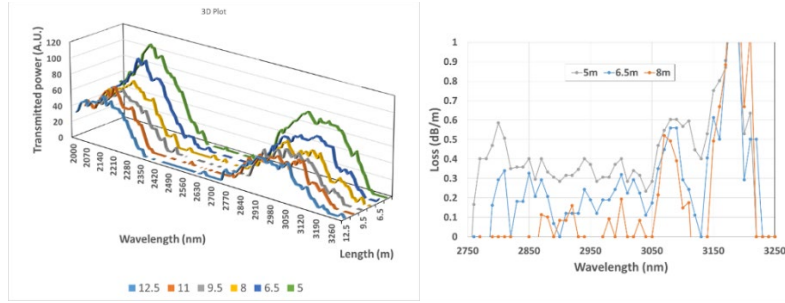


Figure 17 Transmission for various fiber lengths (left) and cut-back measurements at $\sim 3\mu\text{m}$ for various lengths of the reference measurement.

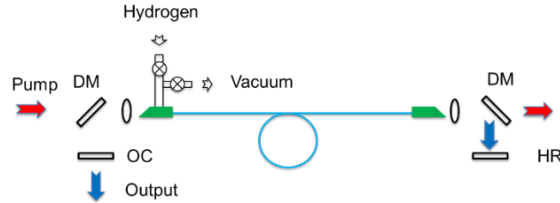


Figure 18 Hydrogen gas Raman fiber laser.

With loss at this level, i.e. $<50\text{dB/km}$, we can use as long as 20m of the fiber in our Raman lasers. We are currently planning for the hydrogen Raman laser experiment. Initial pump will be ytterbium fiber laser at $\sim 1030\text{nm}$ and we are also hope to use Tm fiber laser at $2\mu\text{m}$ as pump in the future for high-power mid-IR sources. The planned setup is shown in Figure 18. The first Stokes of hydrogen vibrational Raman energy is 4155cm^{-1} , and rotational Raman energy is 586.9cm^{-1} . Pumping at 1030nm , the first vibrational Raman will be at $\sim 1801\text{nm}$ and the first rotational Raman will be at $\sim 1096\text{nm}$. Pumping at $2\mu\text{m}$, the first vibrational Raman will be at $\sim 11.8\mu\text{m}$ and the first rotational Raman will be at $\sim 2.27\mu\text{m}$. Rotational hydrogen Raman gain coefficient: $g_R=4 \times 10^{-12} \text{ m/W}$ at 300K and 1Bar, proportional to signal frequency and pressure. Stokes gain can be calculated as, $\exp(g_R L P/A_{\text{eff}})$. Assuming $L=30\text{m}$, $A_{\text{eff}} = 2000\mu\text{m}^2 = 2 \times 10^{-9} \text{ m}^2$, and cavity loss of $\alpha_L=10\text{dB}$, $P_{\text{th}}=\alpha_L (\text{dB}) * A_{\text{eff}} / (4.34 g_R L) \sim 40\text{W}$.

Thrust II, Active $100\mu\text{m}$ Resonantly Enhanced Leakage Channel Fibers

3.2.1 Background

Figure 19 illustrates the concept of resonantly enhanced leakage channel fibers. In contrast to standard leakage channel fibers, the two layers of features are no longer the same. In this illustration, we allow the first layer of features to be the same with a refractive index $n_1=n_b-0.0013$, where background index $n_b=1.444$. The second layer of features are identical with a refractive index $n_2=n_b-0.0155$. The core diameter is $2\rho=50\mu\text{m}$ and the simulation is performed at $1.05\mu\text{m}$.

In the first instance, d_1/Λ (relative diameter of the first cladding layer features) is fixed and d_2/Λ (relative diameter of the second cladding layer features) is allowed to vary while the waveguide losses of the first and second modes are considered. Other higher-order modes always have much higher losses (at least one additional order of magnitude) and are not considered here. Three sets of curves, in red, black, and green, represent simulations for fixed d_1/Λ of 0.6, 0.7, and 0.8 respectively. A resonance peak is clearly observed in all three second order mode losses, leading to at least one order of magnitude further increase in differential mode loss at the peak. The differential mode loss is close to four orders of magnitude at the resonance peak, representing a significant increase in higher-order mode suppression over standard leakage channel fibers. At points A, B, and C on the second order mode curve for $d_1/\Lambda=0.7$ (black curves), the mode distributions are shown at the bottom of Figure 19. At point C where the curve behaves as normal, the second mode is well confined to the core of the LCF. At point B at the loss peak, this mode significantly spread into the cladding. At point A, the extent of spreading into cladding is reduced relative to that at point B. These mode images clearly demonstrate the resonance of the second order mode with the cladding at $d_2/\Lambda=0.425$ at point B.

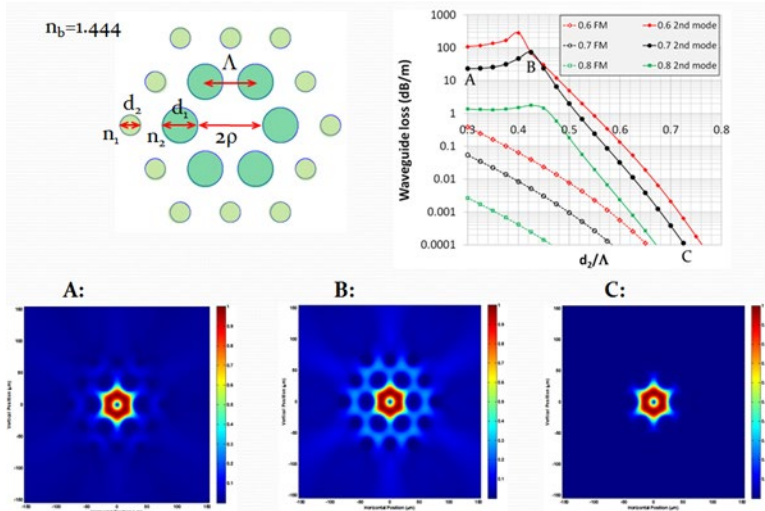


Figure 19 Demonstration of resonantly enhanced leakage channel fibers. The default parameters are $2p=50\mu\text{m}$, operating wavelength $\lambda=1.05\mu\text{m}$, $n_b=1.444$, $n_1=n_b-0.0013$ and $n_2=n_b-0.0155$. In these LCFs, d_1/Λ is fixed while d_2/Λ is scanned. The plotted curves are respective waveguide losses for the fundamental mode (dotted lines) and second order mode (solid lines) for i) $d_1/\Lambda=0.6$, red, ii) $d_1/\Lambda=0.7$, black, and iii) $d_1/\Lambda=0.8$, green.

3.2.2 Optimization of fiber outer boundary

Higher-order-mode losses are very important design parameters for the performance of fibers with large effective mode areas. They have, however, never been accurately measured in actual optical fibers. Using S^2 technique, higher-order-mode content at the output of an optical fiber can be measured accurately. This is typically done in a way that is hard to separate the contributions to higher-order-mode content at the output from many possible contributors such as launching conditions, fiber layout configurations, and fiber designs.

Design simulations are often based on the assumption of infinite cladding. This is a good assumption for well guided modes where light is mostly in the core. It is no longer a good assumption for highly leaky modes where a significant amount of light is radiated away from the core into the cladding. In this case, the reflection from any material interface, e.g. glass/coating boundary, in the fiber can provide additional confinement of the mode, leading to lower waveguide losses for the modes. The effect of circular glass/coating boundary on waveguide losses has been theoretically studied previously, showing that the waveguide

losses of modes are strongly dependent on the fiber diameter. This is not surprising, considering the coherent nature of reflection.

Another important question is regarding the impact of refractive index of coating on the waveguide losses of modes. Double-clad fibers used in fiber lasers are often coated with a low-index polymer coating in order to provide a multimode pump guide. Total internal reflection can take place at such boundary, completely trapping optical power in the guided modes of the highly multimode pump guide. The radiated power from modes guided mostly in the core region is expected to satisfy the total internal reflection condition at such boundary. Does this mean waveguide losses of core modes will vanish? It was speculated in that the leaky core modes will still lose power to modes in the multimode pump waveguide in this case. This is, however, never proven.

For the further progress of mode area scaling of optical fibers, it is very important to accurately know the losses of higher-order modes in optical fibers and how they relate to designs. It is also very important to understand how factors such as coiling, fiber shapes and index of coating impact the waveguide losses in relation to designs. All these factors change the nature of reflection at material interfaces in fibers.

In an effort to answer some of these questions, we have accurately measured waveguide losses of modes using a cut-back technique in combination with a S^2 technique and a fully spliced configuration to ensure constant launch conditions. The measured waveguide losses were then compared to simulations based on infinite cladding. The test was conducted for a variety of coil diameters to identify any impact from coiling. Two Re-LCFs with $\sim 50\mu\text{m}$ core diameter were tested. The first fiber has a circular glass/coating boundary and is coated with standard coating with higher refractive index. The second fiber has a rounded hexagonal glass/coating boundary and is coated with low-index acrylic coating with a refractive index of 1.375.

The results confirm that the design based on infinite cladding is accurate for well confined modes with low waveguide losses. For the highly leaky modes, the measured losses can be significantly lower than the design at large coil diameters for the circular LCF. The measured loss, however, start to approach the design at smaller coil diameters. The measured losses of the highly leak modes in the hexagonal LCF, on the other hand, is consistent with design even at large coil diameters.

The results show that tight coiling can mitigate the effect of coherent reflection at the material interfaces in fibers. The effect of coherent reflection on waveguide losses can be reduced by the curved cylindrical glass/coating boundary in a coiled fiber, possibly due to phase walk-off from the coiled cylindrical surface. The results from the rounded hexagonal fiber are even more startling. It suggests that a deviation from circular boundary can be very effective in mitigating the impact of the coherent reflection from material interfaces in fibers. The low-index polymer coating on this fiber does not seem to matter much, indicating that the radiated powers are reflected into guided modes in the multimode pump waveguide in this case. This is a strong proof that the design concept of exploiting strong leakage losses of higher-order modes works even in double-clad fibers with suitable design of fiber boundary.

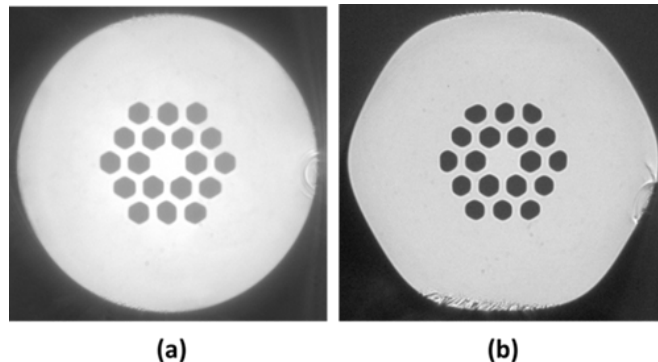


Figure 20 Cross-section images of Re-LCFs used in this work, (a) circular Re-LCF and (b) hexagonal Re-LCF.

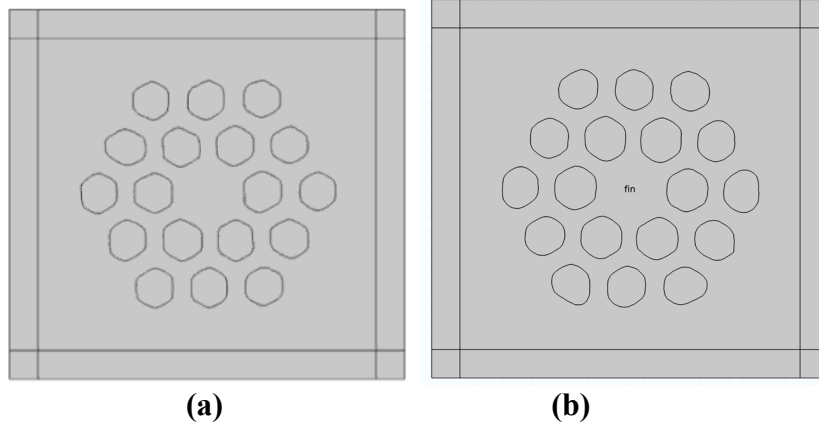


Figure 21 Designs used for the simulation, (a) circular and (b) hexagonal Re-LCF. The designs are acquired from feature boundaries in the cross-section images.

The cross-section images of the two fibers used in this work are shown in Figure 20. The dimensions of features for each of the cladding layers are slightly different for optimized higher-order-mode losses at the operating coiling condition and around the wavelength of 1050nm. The fibers were designed to operate at a coil diameter of ~ 40 cm. For the circular Re-LCF, the core is $48\mu\text{m}$ at its smallest dimension (flat-to-flat) and $49.3\mu\text{m}$ at its largest dimension (corner-to-corner). The diameter of the circular Re-LCF is $392.7\mu\text{m}$. For the hexagonal Re-LCF, the core is $50.9\mu\text{m}$ at its smallest dimension and $51.3\mu\text{m}$ at its largest dimension. The cladding is $426.1\mu\text{m}$ at its smallest dimension (flat-to-flat) and $449.3\mu\text{m}$ at its largest dimension (corner-to-corner). The refractive index of the features for both fibers is 0.0155 below silica. The circular Re-LCF is coated with a standard high index coating and was fabricated at Nufern. The hexagonal Re-LCF was drawn at Clemson with features fabricated at Nufern and is coated with low-index acrylic coating ($n=1.375$). This fiber was drawn at a slightly lower temperature in order to maintain the hexagonal shape of the stack.

The feature boundaries were acquired from the cross-section images and were used in the simulations. A perfect matched layer (PML) is used to simulate the infinite cladding. The designs used in the FEM mode solvers are shown in Figure 21 (a) and (b) for the circular and hexagonal Re-LCFs respectively.

In order to ensure launch stability during the measurements, the Re-LCF was spliced to a SM980nm fiber through a tapered mode adaptor, which was fabricated by tapering the Re-LCF down to a core diameter of $\sim 8\mu\text{m}$ over a length of ~ 6 cm. The fiber was laid in a circular groove fabricated into an aluminum plate. The part of the fibers which was outside the circular groove is made to be as straight as possible. Circular grooves with various diameters are fabricated into the same aluminum plate so that dependence on coil diameters can be tested.

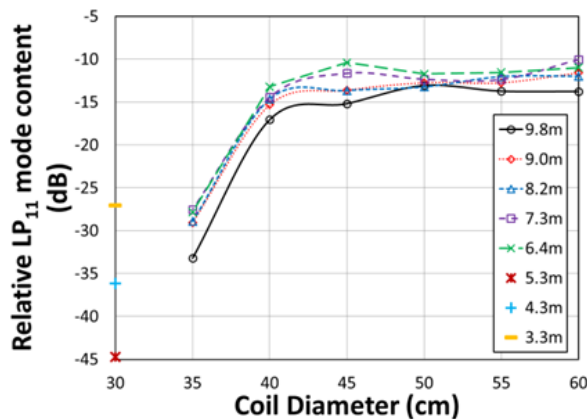


Figure 22 Measured relative LP₁₁ mode content at various coil diameters for the circular Re-LCF.

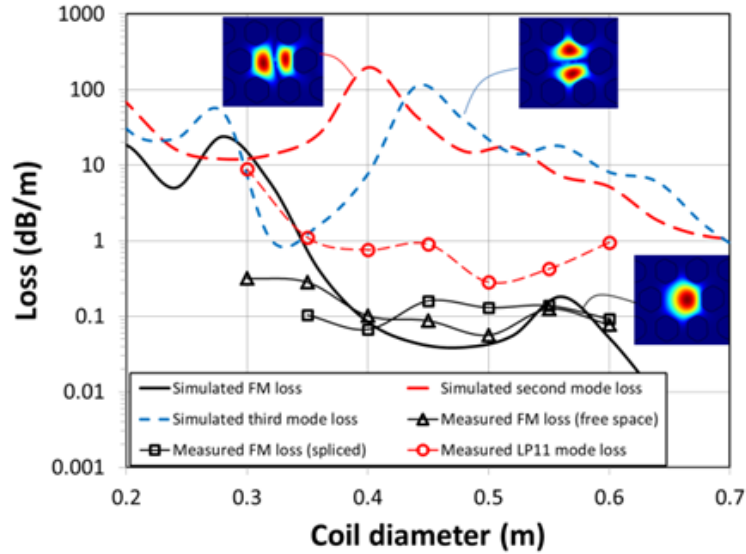


Figure 23 Simulated and measured mode losses in the circular Re-LCF.

Our S^2 setup has a ~ 40 dB detection limit in ratio of higher-order-mode power to fundamental mode power. In all of our experiments, only LP11 mode was observed in the two Re-LCFs. The normal scan range was from 1026nm to 1076nm with a center wavelength of 1051nm. After power ratio of LP11 mode to LP01 mode was determined at varying coil diameters, the fiber was cut by approximately 1m. The measurements were repeated for varying coil diameters. The fibers were cut back several times during the measurements. Eventually, the measured LP11 mode contents were plotted against the lengths of coiled fibers for each coil diameter and a straight line was fitted. The slope of the straight line was regarded as the loss of the LP11 mode. Since the measured LP11 mode in the S^2 measurements always show a well-defined narrow peak in delay, we have assumed that the coupling between LP01 and LP11 modes is minimal in our fibers. The fundamental mode loss is assumed to be negligible in arriving at the LP11 mode loss. This is largely true for the range of coil diameters used in the measurements (see Figures 22 and 23). The fundamental mode loss was measured separately at fixed wavelength of 1050nm using a cut-back technique while ensuring fundamental mode at the output.

The measured LP11 mode content, i.e. power ratio of LP11 and LP01 mode, is summarized in Figure 22 for the circular Re-LCF. The coil lengths for each fiber length are different depending on coil diameters (see Table 1). The LP11 mode content at the output is largely determined by the launch condition and LP11 mode loss over the coiled section of the fiber. The LP11 mode losses are determined, as described earlier, by the slope of linear fit to the measured LP11 mode content versus coil length data for each coil diameter. Due to the very high LP11 mode loss at 30cm coil diameter, much shorter fiber length had to be used in this case (see Figure 22).

The simulated loss for the fundamental mode, second mode and third mode are shown in Figure 23. The second mode and third mode are two different orientations of the LP11 mode (see insets in Figure 23). The measured fundamental mode loss is also shown along with the measured LP11 mode loss. Two sets of measurement are shown, one with free space launch and one with spliced input. The fiber was designed for operation at a coil diameter of 40cm. At smaller coil diameters, the fundamental mode loss can be very high (see Figure 23 for diameters less than 0.35m). As it can be seen, the measured fundamental mode losses fit well with the simulation in the low loss regime. This is consistent with what we expected. The mode is well confined to the core region in the low loss regime. There is very little impact from what is going on far beyond the core. The measured fundamental mode losses are, however, lower than the simulation in the high loss regime when coil diameter is below 35cm. The measured LP11 mode losses are much lower than the simulation at large

coil diameters. The difference between the measured LP11 mode losses and the simulation are, however, converge at small coil diameters when coil diameter is below 0.35m. The LP11 mode is designed to have high waveguide loss and consequently, is expected to experience larger impact from the coherent reflection at the fiber glass/coating boundary. The lower measured losses of both the fundamental and LP11 modes in the high loss regime are expected from the effect of coherent reflection from the fiber glass/coating boundary. The convergence of the measured LP11 mode losses and the simulation at smaller coil diameters is interesting. This may be an indication that phase walk-off in the reflection from the curved cylindrical boundary of the coiled fiber can mitigate the impact of coherent reflection at small coil diameters. It is worth noting that, since we could not distinguish the LP11 mode with the two different orientations illustrated in the insets in Figure 23, our measured data represent an average of the two orientations. Our tunable light was slightly polarized and there was no polarization control in the measurement.

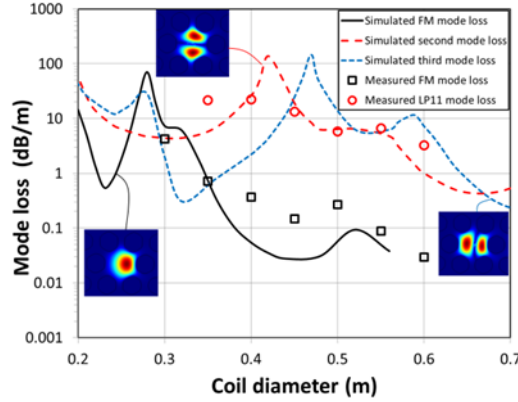


Figure 24 Simulated and measured mode loss in the hexagonal Re-LCF.

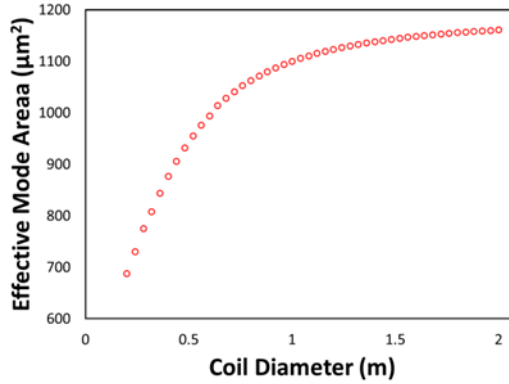


Figure 25 Simulated effective mode area in the hexagonal Re-LCF.

To investigate further on how to mitigate the effect of the coherent reflection from fiber boundary, we studied the hexagonal Re-LCF. This fiber is coated with low-index polymer coating ($n=1.375$) to simulate the effect of double-clad fiber. In a double-clad fiber, optical powers can be trapped within the pump guide due to the total internal reflection at the interface between pump core and cladding, leading potentially to lower mode losses than those with high index coating. Since this is the situation where most large mode area fibers are used, it is very important to understand the impact of pump cladding on the higher-order-mode losses. The simulated mode losses for the fundamental mode, second mode and the third mode for this fiber are shown in Figure 24. The curves present similar loss pattern as the previous ones do in Figure 23. The minor differences of the loss curves between the circular and hexagonal Re-LCF are mainly caused by slightly different dimensions of the features. This fiber was also designed for operating at ~ 40 cm coil diameter. The measured LP11 mode loss is also shown in the figure. It is interesting to see the LP11 mode losses fit reasonably well with the simulation even at large coil diameters. Since the radiated optical

powers from the core modes are expected to be trapped by the pump cladding, it is reasonable to assume that the loss of LP11 mode power is through reflection into modes of the multimode pump guide at the pump core and cladding interface. Since low index coating represents the worst case scenario, we expect similar effect from fibers with standard high index coating. The result is a strong indication that non-circular pump cladding can be very effective in mitigation of the coherent reflection at the pump core and cladding interface. This is significant. It confirms the validity of all design approaches based on high leakage loss of higher-order modes for the suppression of higher-order-mode propagation in order to scale the effective mode area of the fundamental mode. The measured fundamental mode losses also fit reasonably well to the simulation (see Figure 24).

Effective mode area was also simulated for the hexagonal Re-LCF for various coil diameters. The results are shown in Figure 25. The effective mode area is $\sim 900\mu\text{m}^2$ at 40cm coil diameter.

The wavelength dependence of LP11 mode content can be measured by dividing the wavelength scan used in the S^2 measurement into a number of smaller sub-scans with equal wavelength span. This was done in Figure 25 for the LP11 mode content in the 4m hexagonal Re-LCF coiled in 35cm diameter coil. The sub-scan has a wavelength range of 10nm. Wavelengths at the center of each sub-scan are used for the plot. The flat wavelength dependence over this wavelength range is expected and consistent with the simulation. It is worth noting that $\sim 40\text{dB}$ higher-order-mode suppression can be achieved over such a short fiber length, especially considering the short length of the coiled section of $\sim 1.4\text{m}$.

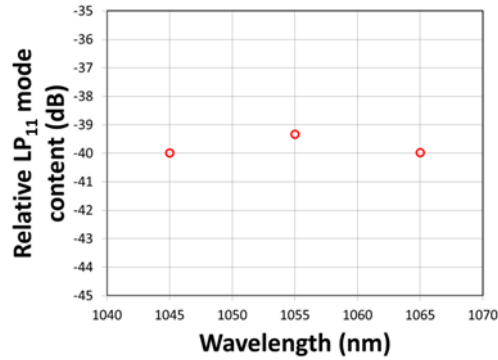


Figure 26 Wavelength dependence of the measured LP11 mode content in the 4m hexagonal Re-LCF in 35cm coil. Coiled length is 1.37m.

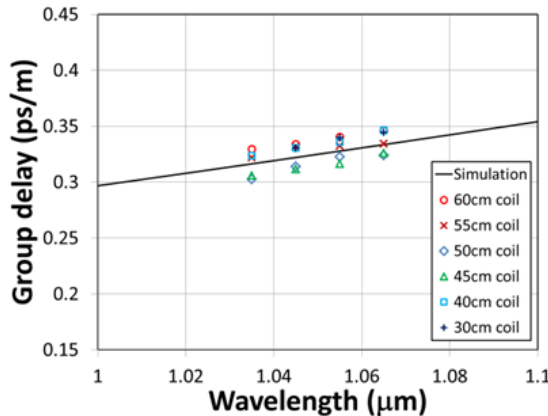


Figure 27 Simulated and measured differential group delay between LP01 and LP11 modes in the circular Re-LCF. The simulation was done for a straight fiber. The measurements were performed at a range of coil diameters.

Differential group delay between the LP01 and LP11 modes can also be measured by dividing the total wavelength scan in the S^2 measurement into a number of sub-scans of

equal wavelength span. The differential group delays were obtained from the S^2 measurement of the circular Re-LCF and are plotted against the center wavelengths of each of the sub-scans in Figure 27. The differential group delay was also simulated by a multipole mode solver using approximate circular features and is also plotted in Figure 27. There is an excellent agreement between the measured differential GVD and the simulation.

3.2.3 Active 50 μm LCF

Using ytterbium-doped core glass from our other MRI program, we have fabricated an active 50 μm core LCF. The cross section is shown in Figure 28. The fiber core is 52 μm at its smallest dimension (flat-to-flat) and 60 μm at its largest dimension (corner-to-corner). The doped area (the dim area in the center of Figure) is 30 μm in diameter and is made of a highly uniform Yb-doped glass with an index very slightly below that of silica glass by 2×10^{-4} . The two-layers of features in the cladding are made from fluorine-doped silica glass with a refractive index of 0.0155 below that of silica. The cladding diameter is ~ 420 μm and is coated with a low-index polymer coating ($n=1.375$) to guide the pump light with a NA of 0.46. Pump absorption at 975 nm was measured to be 1.05 dB/m.

The first optical characterization of this fiber was to determine the refractive index difference between the Yb-doped active glass and silica background glass ($\Delta n = n_{\text{background}} - n_{\text{core}}$). White light, after going through a long pass filter with a cut-off at 1 μm , was launched into the fiber core of a short fiber. The measured mode image and intensity distribution across the core (see the white line in the mode image) are shown in Figure 29(a). Meanwhile, the guided fundamental mode was simulated for the fiber at 1050 nm with various Δn from 0.25×10^{-4} to 3×10^{-4} with increments of 0.25×10^{-4} . The mode is not strongly dependent on wavelength for this LCF. The boundaries used in simulation were extracted from the measured fiber cross-sectional image and represent the geometry of the real fiber. Figure 29(b) shows the mode pattern at $\Delta n = 2 \times 10^{-4}$ with intensity distributions for all the simulated index differences. The asymmetry in the mode is from the slight asymmetry in the fabricated fiber. By comparing these intensity plots, the index difference between active glass and background silica glass is estimated to be $\sim 2 \times 10^{-4}$.

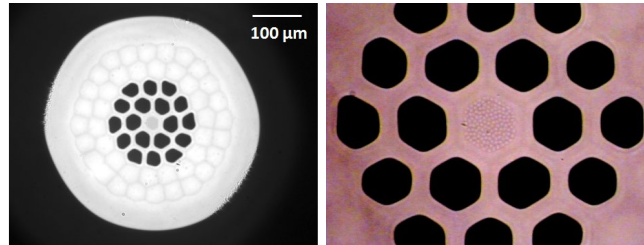


Figure 28 Cross-section image of the fabricated 50 μm -core Yb-doped LCF fiber.

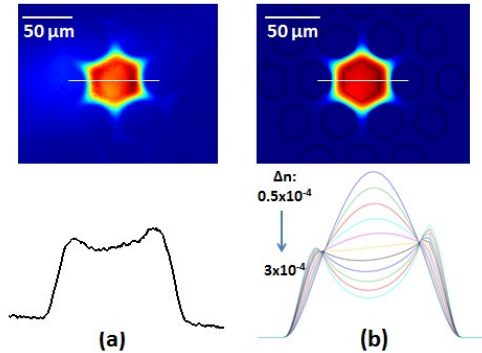


Figure 29 Mode pattern and intensity distribution (across the white line in the mode image) from (a) experiment, and (b) simulations for various Δn with 0.25×10^{-4} increment.

To investigate the impact of index difference Δn to the effective mode area, we simulated the effective mode area of the fundamental mode in a straight fiber for various Δn from zero to 4×10^{-4} , as shown in Figure 30. The effective mode area is increased to $\sim 1880 \mu\text{m}^2$ at Δn of 2×10^{-4} , thanks to the uniform intensity distribution of the mode. This is $\sim 50\%$ increase compared to the $1200 \mu\text{m}^2$ of the Gaussian-like mode with the same core size at zero index difference. From Figure 29(b), we also found that the beam profile has the best flatness at the index difference Δn of 1.75×10^{-4} with a slightly decreased effective mode area as shown in Figure 30. However, obtaining index accuracy on the order of 0.25×10^{-4} in fabrication is very difficult. The wavelength used in the simulation is 1050 nm .

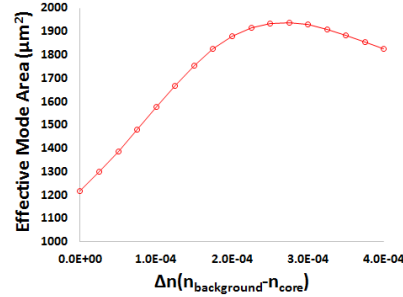


Figure 30 Simulated effective mode area versus Δn in straight fiber.

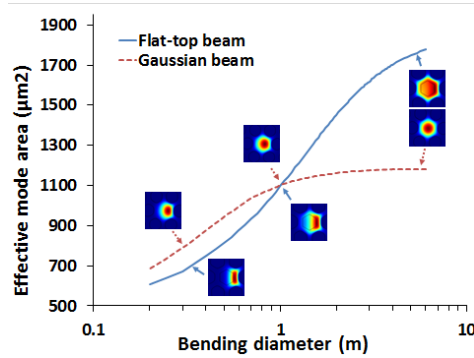


Figure 31 Simulated effective mode area versus various bending diameter for both Flat-top and Gaussian beam with the same core size.

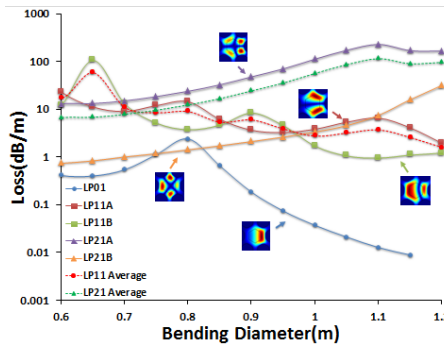


Figure 32 Simulated mode losses in the core index depressed LCF.

We also simulated and compared the effective mode area of the flat-top mode and the Gaussian-like mode in the regular LCF under various coiling conditions, as shown in Figure 31. The solid line represents the effective mode area of the flat-top mode in the active LCF fiber with the depressed refractive index active glass ($\Delta n = 2 \times 10^{-4}$) and the dashed line represents that of the Gaussian-like mode in the LCF fiber with uniform core index. As shown in the figure, the effective mode area of the flat-top mode reaches $1750 \mu\text{m}^2$ at 5 m bending diameter, while the Gaussian-like mode reaches its maximum of $1190 \mu\text{m}^2$. In a straight fiber, the flat-top mode has an effective mode area of $\sim 50\%$ larger than the Gaussian-like mode of

regular LCF. However, the effective mode area of the flat-top mode decreases very quickly with a reduction of coil diameter, and is smaller than Gaussian-like mode below 1m bending diameter. This strong bending sensitivity of the flat-top mode is a result of intensity concentration in the area just outside the doped glass with a relatively higher index in the coiled fiber (see inset in Figure 31). Thus, the flat-top fiber is more suitable to be used in a straight configuration to benefit from large effective mode area. One possible approach is to leave a long straight section at the end of an amplifier, where the core-guided optical power is near the maximum and the effective mode area is also the largest. Thus the optical power density can be kept below the nonlinear threshold. Another possibility is to use a short straight length of fiber with high rare earth dopant concentration, in which bending of fiber is avoided.

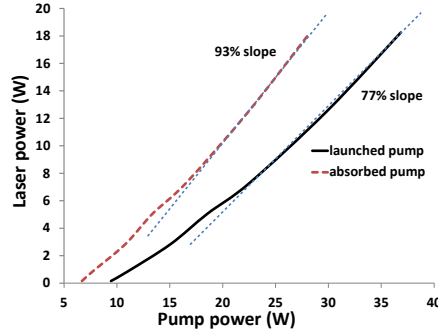


Figure 33 Lasing slope efficiency measurements.

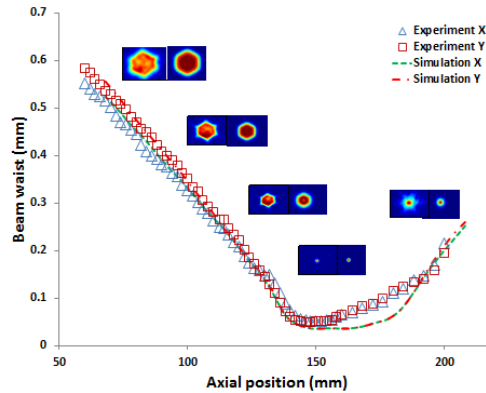


Figure 34 Propagation of flat-top mode in free space.

Simulation was also performed on the waveguide confinement loss in this fiber for bending diameters from 0.6 m to 1.2 m, as shown in Figure 32. The wavelength used in the simulation is 1050 nm and Δn is 2×10^{-4} . The line with circular dots represents the fundamental mode LP_{01} . The loss is below 0.01 dB/m when the bending diameter is above 1.15 m with the tendency of decreasing at larger coil size. The two lines with square symbols represent the next set of high-order modes LP_{11} . The losses are slightly above 1 dB/meter at 1.2 m bending diameter with remaining around 1 dB/m at larger coil sizes. The two lines with triangle symbols represent the second set of high-order modes LP_{21} . The losses are above 10 dB/meter at 1.2 m bending diameter and larger at larger coil size. The two dashed lines represent the set average for two sets of high-order modes. The high-order suppressions in this flat-top-mode LCF are much lower comparing to regular LCF of the same core diameter.

We also tested the lasing efficiency for this core-index depressed active LCF fiber. A 6 meter long fiber was right-angle cleaved on both ends to create a 4%- and 4%-reflection laser cavity. The fiber was coiled at 1 meter diameter during the test. A multimode diode laser emitting at 975 nm with a 250 μm delivery fiber was used as pump source. Laser at 1026 nm was achieved and emitted from both ends of the fiber which were measured for calculation of the slope efficiency. The lasing slope efficiency with respect to the launched pump power was measured to be $\sim 77\%$, as shown in Figure 33. By subtracting the residual pump, the lasing

slope efficiency with respect to the absorbed pump power for this fiber is ~93%, very close to the theoretical limit of 95% for the laser at 1026 nm with pump at 975 nm, obtained by considering only the quantum defect.

The output laser beam quality was also examined by tracing a focused beam propagation over 15 cm-long distance and comparing with the simulation. The output laser beam was first collimated by an aspheric lens and then focused by a spherical lens with 15 cm focal length. After the focusing lens, the beam profile was captured with a CCD camera in 2 mm steps along the propagation direction and analyzed for dimensions, as shown in Figure 34. The triangle and square dot lines represent the measured beam waist in horizontal X and vertical Y directions. The results also show that the laser beam keeps a hexagonal shape with a nearly flat top over 6 cm-long distance down to 300 μm in diameter and then continues to contract as a Gaussian beam down to 100 μm in diameter. We also simulated the flat-top mode with the multi-Gaussian method which uses a sum of coherent Gaussian beams to create a flat-top mode. The simulated flat-top beam propagation is also plotted in Figure 34 in the dashed lines, which fits reasonably well with the experimental result. The difference around the beam waist is due to the fine details of the mode around its edge, which is hard to accurately represent in the simulation. The mode images in Figure 34 were taken along the propagation from experiment (left) and simulation (right), which also show that the experimental result is consistent with theoretical analysis of a coherent flat-top beam.

3.2.4 Quantitative mode quality characterization

In order to verify HOM suppression, precisely quantitative mode characterization of a fiber is required. Several methods have been demonstrated recently, including spatially and spectrally resolved (S^2) imaging [103] and cross-correlated (C^2) imaging [104], which have demonstrated mode characterization of large-mode-area fibers with up to 50 μm core diameter. As the core diameter becomes much larger, modes become increasingly more densely packed in effective mode refractive index. When the mode spacing is too close, such as in a 100 μm core fiber, the intermodal group delay is much less than the spread in time of the various frequency components due to fiber dispersion. This spread due to chromatic dispersion is ~30fs/m/nm at ~1050nm in silica, comparing to the LP01-LP11 intermodal delay of ~50fs/m in the 100 μm -core Re-LCF used in this work. Temporal spread from chromatic dispersion of a 2nm wide source would be larger than the intermodal delay, making the modes inseparable. The C^2 method can no longer resolve modes in this case. The S^2 method would also require a very wide-bandwidth optical source to be able to cover multiple periods of the widely spaced frequency beating.

We demonstrated quantitative mode characterization in a 1m long straight passive Re-LCF with 100 μm core diameter using a matched white-light interferometer (MWI) in order to cancel out the effect of fiber dispersion. This is the first quantitative mode characterization in a 100 μm -core fiber to our knowledge. The Re-LCF has two non-identical layers in the cladding, optimized for a simulated HOM loss of 60dB/m (Figure 35 and 36). The measured relative group delay between the FM and the second-order mode is 55fs/m, very close to the expected 56fs/m. The LP11 mode content after the straight 1m-long Re-LCF with low-index coating was measured to be ~-29dB relative to that of the FM. A separate M2 measurement was also performed on the same fiber, giving a $M^2 = 1.01$.

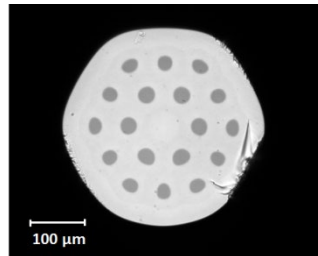


Figure 35 Fabricated Re-LCF with 100 μm core diameter.

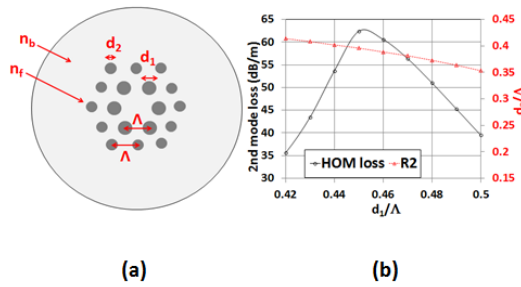


Figure 36 (a) Re-LCF design with non-identical cladding layer structure, (b) simulated 2nd HOM loss versus variable node-pitch ratio. $R2=d_2/\Lambda$.

The Re-LCF fiber shown in Figure 35 was fabricated according to the design. The nodes in the cladding lattice are made from fluorine-doped silica which has a slightly lower refractive index than the silica background glass by 8×10^{-4} . The sizes of the nodes in the outer and inner layers are $33.2 \mu\text{m}$ and $29.6 \mu\text{m}$ respectively with the same pitch $\Lambda=70 \mu\text{m}$. The diameter of the core in the center is $\sim 100 \mu\text{m}$. The shape of the fiber is intentionally kept non-circular to reduce the coherent reflection from the outer boundary, which lowers HOM. This passive fiber is coated with low-index coating to mimic a double-clad fiber.

White light is generally considered as incoherent and it is only temporally coherent over femtoseconds. This unique property enables white light to have a very fine temporal resolution, which is exploited in optical coherence tomography (OCT) for a fine spatial resolution. White-light interferometry composed of a white light source and a Michelson interferometer has been reported previously to perform dispersion measurements on thin optical samples. The same capability, in principle, can also be used to resolve modes in large-core optical fibers with very small intermodal group delays.

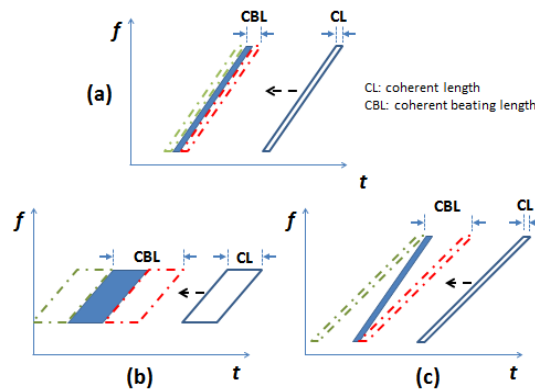


Figure 37. Illustration of interferometry resolution: (a) broad spectrum and balanced dispersion; (b) narrow spectrum and balanced dispersion; (c) broad spectrum and un-balanced dispersion. Filled and open parallelogram represents coherent light from measurement and reference arms respectively.

This high temporal resolution of MWI is a result of the short coherent length (CL) of the broad-spectrum source and the balanced arms of the interferometer, as illustrated in Figure 37(a). The filled and open parallelograms represent coherent lights at the detector from the measurement and reference arms respectively. As the length of the reference arm is adjusted, coherent beating can only be observed over a short distance of translation, i.e. coherent beating length (CBL). Figure 37(b) illustrates an interferometry with a narrow-spectrum source and two balanced arms, showing the poor temporal resolution due to the long coherent length of the source. The interferometer with two un-balanced arms shown in Figure 37(c) also leads to a deterioration of temporal resolution due the spread of coherent

light over arrival time at the detector. The broader the light spectrum, the more critical it is to balance the arms in order to obtain high temporal resolution. A MWI is demonstrated here to perform the quantitative mode characterization in our Re-LCF fiber. The principle is displayed in Figure 38.

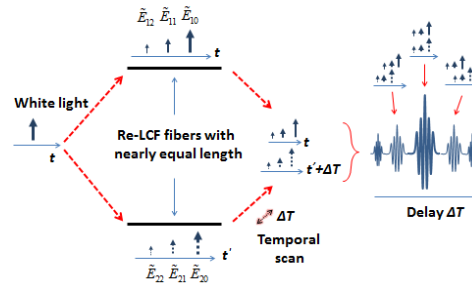


Figure 38 Principle of mode characterization in optical fiber with matched white-light interferometry (MWI).

The experimental setup for the matched white-light interferometry is shown in Figure 39. A Bentham white light source WLS100 with quartz halogen lamp emitting from 350nm to 2500nm was spectrally filtered with a 780nm long pass filter, split into two beams and coupled into two identical straight fibers which were placed in an aluminum V-groove to keep them straight. From the simulation in the fiber design, the second-order mode in this fiber has a loss of ~62dB/m and a relative group delay of ~56fs/m to the FM. The length of the fiber used in the test was 1m. The beam out of one fiber was sent to a motorized scanning stage with 1 μ m accuracy and 100 mm travel. The beam from the other fiber was sent to a piezo-controlled scanning stage with 5nm accuracy and 20 μ m travel. After the two arms were roughly balanced by the motorized stage, the piezo stage was used to perform the fine interferometry scanning with a 50nm incremental step up to the 20 μ m maximum travel. Effectively, the path length was scanned with a 0.1 μ m incremental step up to 40 μ m maximum travel due to the double passed configuration. Meanwhile, a high speed silicon camera was used to record the two-beam interference pattern after each incremental step during the scan, which does not respond to the wavelengths larger than 1.1 μ m. In order to reduce the random noise on the camera, each 4 adjacent pixels in the original image are added together to reconstruct one pixel in the final image. The intensity oscillation on one pixel versus the delay time ΔT is the function mentioned above.

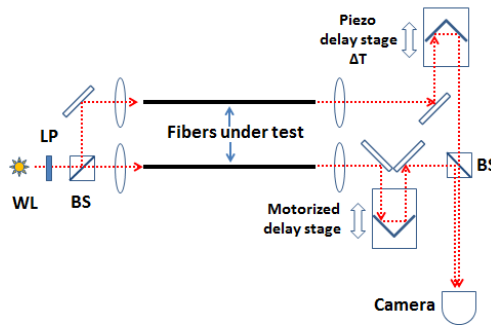


Figure 39 Schematic diagram of the matched white-light interferometry.

Figure 40 shows the intensity oscillation throughout the scanning process on one pixel of the image, which is located at the lobe center of the reconstructed mode image corresponding to peak B. There are two horizontal axes in the figure. The lower one is the temporal delay in femtoseconds and the top one is the corresponding path length delay in micrometers. Five peaks are found in the plot. The major one marked as A comes from the

coherent beating between the two FMs with the maximum amplitude of E_0^2 . Peaks B, D arises from beating between a FM and a second-order mode, with roughly the same maximum amplitude of E_1E_0 . The measured intermodal group delays between peaks A, B and A, D are 50fs and 59fs respectively, with an average of ~ 55 fs which is very close to the calculated value of 56fs from the fiber design. The group delays between peaks A, C and A, E are measured to be 77.7fs and 78.9fs respectively. Figure 1 shows the reconstructed mode patterns and phases corresponding to the oscillation peaks from A to E found in Figure 40. The mode pattern for peak A is a Gaussian-like beam with a flat phase pattern, which indicates it is the LP01 mode. The mode patterns for peaks B and C show two lobes with a π phase shift between them, which indicates they are LP11 modes. These two LP11 modes have different orientations and there is a 28fs time delay between them. The MPI values for these two LP11 modes are -29dB and -37dB for peaks B and C respectively. The modes for peaks D and E are similar to the ones for peaks B and C. Their MPI values are -33dB and -37dB respectively. The measured lower HOMs losses than the simulation could be due to some coherent reflection from the fiber outer boundary. The linewidths of the envelopes of the coherent beating between FM and HOMs corresponding to peaks B, C, D and E are not broadened, as shown in Figure 40, which indicates that there is insignificant mode coupling during the propagation in the fiber. The minimum intensity detection capability for this interferometry was tested by measuring the MPI value of the flat DC region without any coherent beating, which is determined to be -43dB.

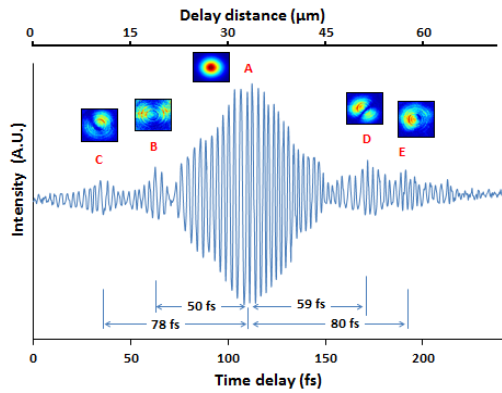


Figure 40 Intensity oscillation during the interferometry scanning at the pixel at the lobe center of the reconstructed image B.

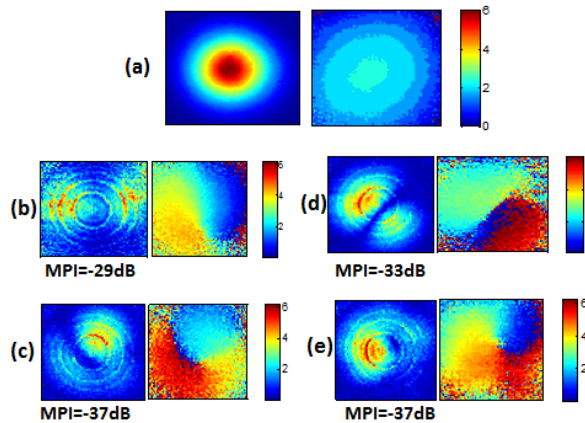


Figure 41 Reconstructed mode patterns and phases corresponding to the peaks from A to E found in Figure 37 with calculated MPI value for HOMs.

The mode quality guided in this Re-LCF fiber was also tested qualitatively. The light from a LED source emitting from 890nm to 1090nm was collimated into the 1m-long straight

Re-LCF. The mode pattern of the output beam was recorded while the launching beam at the input end was moved across the fiber core with the intention to excite HOMs. The mode pattern did not change at all while the launching beam was moved. The only thing that changed is the mode intensity which is due to the change in launching efficiency. M^2 of the mode was also measured when the LED light was carefully coupled into the fiber. The result is shown in Figure 42, giving $M^2=1.01$.

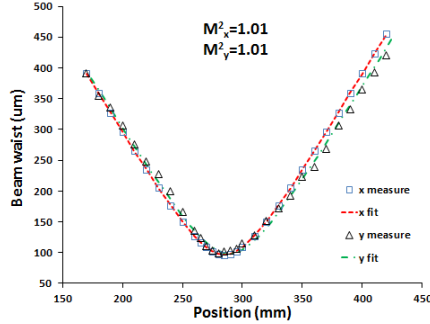


Figure 42 M^2 measurement of the output beam from the Re-LCF fiber in x, y directions.

3.2.5 Multiple-cladding-resonance (MCR) fiber

Further higher-order-mode (HOM) suppression is required for the suppression of mode instability and further mode area scaling. Multiple-cladding-resonance (MCR) fiber (see Figure 43) is a promising approach. In this design the cores in the cladding is coupled with a higher-order mode in the central core. Using few cores in the cladding to suppression HOM is not new. MCR, however, uses strongly coupled multiple cores which significantly enhance the coupling to HOM and enable broad coupling resonance. Previous approaches have very narrow resonance which is hard to hit. MCR, on the other hand, significantly broadens the resonance and is much more practical to fabricate. The open cladding of LCF also lends itself for the coupling.

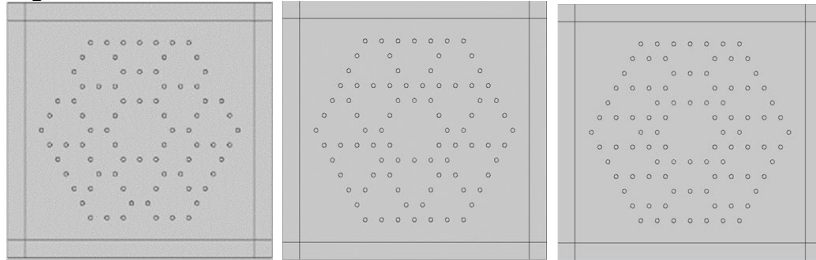


Figure 43 Multiple-cladding-resonance designs: mixed cell (right), three cell (middle) and two cell (left).

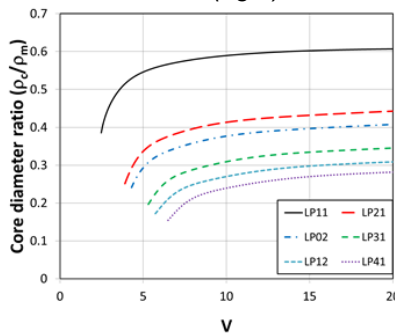


Figure 44 Required core diameter ratio (ρ_d/ρ_m) for maximum resonant coupling between the fundamental mode of the cladding core and one of the higher-order modes of the main core versus normalized frequency (V value) of the main core.

Additional smaller cores can be easily created in the cladding of photonic bandgap fibers by missing several nodes. The smaller cores share the same cladding as the main core. If the cladding cores are well isolated, the resonant conditions between the fundamental mode in the cladding cores and various higher-order modes of the main core can be easily calculated. Using step-index fiber analogue, the propagation constant of modes in the main core can be written as

$$\beta_m^2 = k^2 n_b^2 - \frac{U_m^2}{\rho_m^2} \quad (1)$$

where k is the vacuum wavenumber; n_b is the refractive index of the background glass; ρ_m is the main core radius; and main core parameter U_m is as normally defined for optical fibers. It needs to be noted that the refractive index of all the cores is the same as that of the background glass n_b in this case. Similarly, the propagation constant of modes in the cladding cores can be written as

$$\beta_c^2 = k^2 n_b^2 - \frac{U_c^2}{\rho_c^2} \quad (2)$$

The cladding core parameter U_c is defined similarly as U_m . The resonant condition for maximum coupling of a mode in the main core and a mode in the cladding core is $\beta_m = \beta_c$. Using the relations obtained thus far in Eq.1 and Eq.2, the resonant condition can be written as

$$\frac{U_m}{\rho_m} = \frac{U_c}{\rho_c} \quad (3)$$

Since the refractive index of core and cladding are the same for both main and cladding cores. The resonant condition can be rewritten using the normalized frequency, i.e. V value, V_m and V_c for the main and cladding cores respectively.

$$\frac{U_m}{V_m} = \frac{U_c}{V_c} \quad (4)$$

This can be easily calculated for the fundamental mode of the cores in the cladding and various higher-order modes in the main core (see Figure 44).

The horizontal axis is the V value of the main core. For weakly coupled cladding cores, Fig.1 provides a reasonable approximations for a straight fiber. In the multimode regime with $V > 10$, for coupling with LP11 and LP21 modes in the main core, $\rho_c/\rho_m \approx 0.6$ and 0.44 respectively. This multimode regime is what is used for large-core designs. The flat response in Figure 44 indicates very weak wavelength dependence.

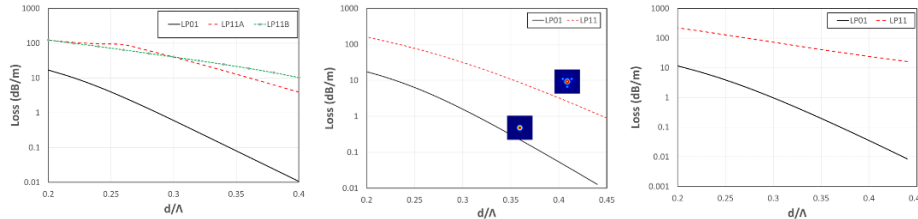


Figure 45 Simulated loss for straight 100 μ m-core LCF with mixed-cell design (left), three-cell design (middle) and two-cell design (right).

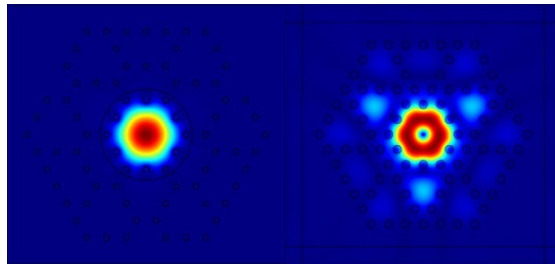


Figure 46 The first and second mode in the three-cell design.

Fiber Type	Wavelength (nm)	Minimum FM loss (dB/m)	Corresponding HOM loss (dB/m)	Loss ratio
Mixed-cell	1050	0.1	16	135
Three-cell	1050	0.1	5	49
Two-cell	1050	0.1	32	264

Table 1 Performance comparison of the three designs.

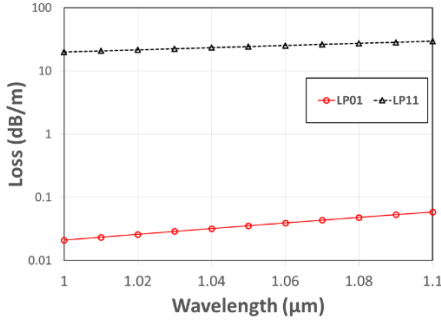


Figure 47 The wavelength dependence of the two-cell design ($\Delta n = -8 \times 10^{-4}$, $d/\Lambda = 0.4$).

Simulations for the mixed-cell, three-cell and two-cell designs shown in Figure 43 are shown in Figure 45. The significance loss difference between the fundamental LP01 mode and next HOM is clearly seen. Mixed-cell and two-cell provide better performance in this case. First two modes in the three-cell design are shown in Figure 46. The fundamental mode is well guided and the HOM is significantly de-localized into the cladding due to the weakened guidance. The performance of the three designs is summarized in Table 1. The wavelength dependence of the two-cell design is shown in Figure 47, showing the significant flat response over the simulated wavelength range. This will make this MCR design much easier and consistent to fabricate.

3.2.6 Efficient ytterbium-doped fiber lasers operating below 1020nm

Multimode high-power fiber lasers operating below 1020nm can be used in a tandem pumping scheme as pumps to reduce quantum defect heating and provide high pump brightness in ytterbium-doped fiber lasers operating at ~ 10 kW. In this high-power regime, single-mode operation becomes much more challenging due to mode instability driven by quantum defect heating. Thermal management also becomes much more challenging due to the much higher heat load. Multimode 1018nm fiber lasers are key components in the tandem pumping scheme to provide high brightness pumps and much lower quantum defects in IPG 10kW fiber lasers. Single-mode fiber lasers of >1 kW level at these wavelengths have very low quantum defect and can be much more power scalable than operating at longer wavelength. Ytterbium fiber laser operating at 1018nm have quantum defect of only 4.1%.

However, it is difficult to realize stable and efficient 1000-1018nm ytterbium-doped fiber lasers in conventional ytterbium-doped aluminosilicate host as it requires a large population inversion to reach gain threshold. Stable operation can only be realized by shortening the fiber, which leads to poor pump absorption. The first key factor for high efficiency for a given launched pump power is low inversion required for reaching the lasing threshold. A second key factor is a small cladding-to-core ratio. This effectively lowers signal intensity in a relatively larger core if the cladding is kept the same, allowing a lower pump intensity to maintain a given inversion. Addressing these two factors effectively can further minimize pump power exiting the fiber.

Phosphosilicate host is known for reaching gain threshold at lower inversion than that required for conventional aluminosilicate host for lasing wavelengths below 1020nm due to its high emission cross section at shorter wavelength. Our 50/400 phosphosilicate leakage channel fiber is an ideal fiber for this application.

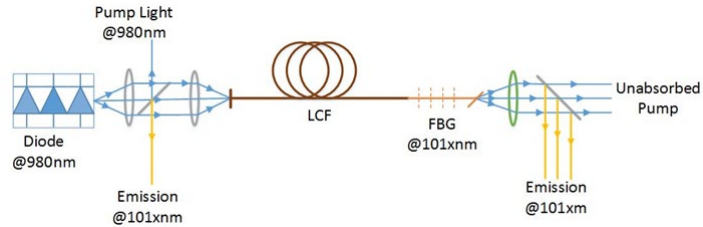


Figure 48 Schematic Experimental Setup.

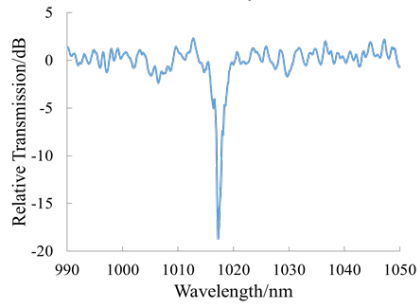


Figure 49 Transmission spectrum of a 1018nm FBG.

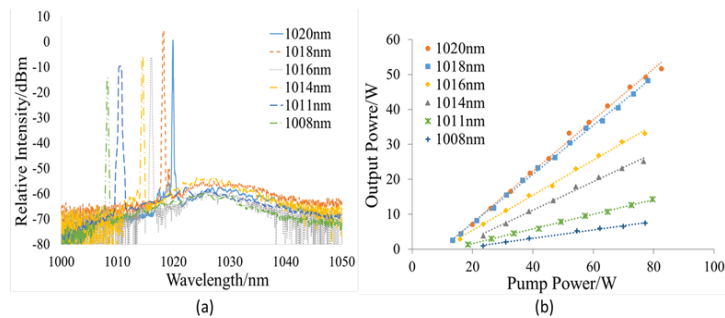


Figure 50 (a) Optical spectra at the laser output, wavelengths ranges from 1008nm to 1020nm. (b) Output powers versus the launched pump powers at various lasing wavelengths.

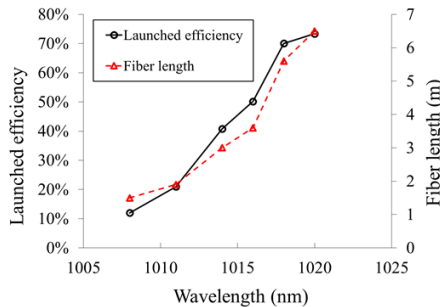


Figure 51 Launched efficiency (black circle) and fiber length (red triangle) as a function of wavelength.

The configuration of the fiber laser system shown in the Figure 48 consists of a section of Yb-doped phosphosilicate LCF and a FBG with high reflectivity. The photosensitive fiber for the fiber Bragg gratings was specially made at Clemson and has a similar core/cladding dimension of $50\mu\text{m}/400\mu\text{m}$ as the LCF to minimize splicing loss. A series of FBGs with different reflecting wavelengths were written using an interferometer and a frequency-quadrupled YAG laser in our laboratory at Clemson. It is worth mentioning that the fabrication process is kept constant to ensure the reflectivity for various wavelengths is similar. Due to the inherent nature of the multimode photosensitive fiber, one cannot

accurately obtain the reflectivity of the FBG. Figure 49 shows the relative transmission spectrum of a 1018nm FBG. Nearly 20dB of relative transmission loss is achieved at peak of the reflectivity. This measurement is strongly dependent on the excitation of modes in this multimode fiber. It indicates >99% reflectivity for a subset of modes. One end of the FBG is angle cleaved to suppress the ASE while the other end is spliced to the Yb-doped LCF. The Yb-doped LCF is coiled at diameter of 80cm and pumped by 976nm laser diode. Emitted laser lights are recorded at both ends of the fiber.

To begin with, a 8m Yb-doped LCF and 1018nm FBG is used. However, the ASE is very strong and ultimately lead to spurious oscillation at 1030nm when the pump power exceeds the threshold even though the FBG was angle cleaved. The fiber was then gradually cut back by 30-40cm each time so that the net gain at 1018nm can ultimately exceed the net gain near 1030nm. Once the fiber laser is operating stably at the desired wavelength and the efficiency is recorded. The FBG is then replaced with a slightly shorter wavelength FBG and the cut-back process was repeated. Figure 50(a) shows the spectra of the output of all the fiber lasers tested. The laser wavelength ranges from 1008nm to 1020nm. All the spectra are captured at the highest pump power. Over 50dB of difference between signal peak and ASE peak has been achieved for all the wavelengths tested. In particular, as for the 1018nm fiber laser, the laser peak is over 60dB higher than the ASE peak. Figure 50(b) shows the output power of the corresponding fiber lasers versus the launched pump power. The slope efficiency then start to decrease as lasing wavelength becomes shorter.

The efficiency of the fiber lasers with respect to the launched pump power and the ytterbium-doped fiber lengths used are shown in Figure 51. It can be seen clearly that the slope efficiency decreases sharply when the operating wavelength is below 1018nm. The decrease of the slope efficiency at shorter lasing wavelengths correlates well with the shorter fiber lengths used at various wavelength. Based on the results in Figure 51 alone, we cannot be sure if the poorer efficiency at the shorter lasing wavelength is due to inadequate pump absorption as a result of the shorter fiber length used or some up-conversion processes at higher inversions or a combination of both.

To further understand the mechanisms responsible for the poorer efficiency at shorter lasing wavelengths, we need to characterize slope efficiency with respect to both launched and absorbed pump powers at various inversion levels. It is hard to get an accurate measurement of the unabsorbed pump powers in order to determine the slope efficiency with respect to the absorbed pump powers in the case where a FBG is spliced to the Yb-doped fibers. We therefore decided to do the cut-back measurement in a free-running fiber laser without the FBG. Another ~6m Yb-doped LCF was used for the 1030nm fiber laser measurement. Two facets of the fiber were perpendicularly cleaved to serve as two reflectors at ~4% reflectivity thus the laser would naturally emit at ~1030nm. The fiber was repeatedly cut back 40-50cm every time followed by laser efficiency test at each fiber length.

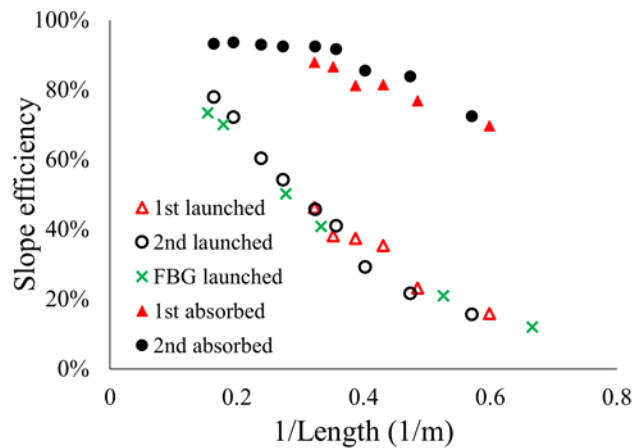


Figure 52 Slope efficiency versus the inverse of the fiber length.

The slope efficiency with respect both to the launched and absorbed power of the 1030nm fiber laser versus the inverse of fiber length is plotted in Figure 52. The free-running fiber laser measurements were done twice and both results are shown as the 1st measurement and the 2nd measurement. The inverse of fiber length serves as a good surrogate for the average inversion in case of constant round-trip loss. For comparison, the efficiency with respect to the launched pump power of the LCF-FBG fiber lasers is also presented. It can be clearly seen that the efficiency with respect to the launched pump power overlaps fairly well in all cases including the free-running fiber laser and the LCF-FBG fiber laser. The LCF-FBG fiber laser has a lower round-trip loss due to the much higher reflectivity of the FBG. The free-running fiber laser therefore operates at a much higher threshold gain and therefore a much higher average inversion for the same fiber length. Despite the difference in inversion levels among the two types of fiber lasers, their efficiency with respect to the launched pump power versus inverse fiber length overlaps very well. This is a strong indication that the launched efficiency is primarily limited the poor pump absorption as a result of the shorter fiber length and is not related to the higher inversion. A further evidence is that the slope efficiency versus the absorbed pump power for the free-running laser at fiber length longer than 3m, i.e. $1/L < 0.33$, is between 92.4% to 93.5%, very close to the quantum limit of 94.7%. The average inversion of the free-running fiber laser with 3m-long fiber is estimated to be ~40% based on the run-trip loss and absorption/emission cross sections. This is higher than the average inversion of any of the fiber lasers with FBGs. The highest of which is ~40% for the LCF-FBG fiber laser with a lasing wavelength of 1008nm.

Another detail worth noting is that the absorbed efficiency of the free-running 1030nm fiber laser starts to decrease when the fiber is cut back to shorter than 3m, i.e. $1/L > 0.33$. This suggests that other loss mechanism is introduced at higher population inversion. This additional loss mechanism may be related to the cooperative luminescence as the characteristic green fluorescence indeed becomes more visible at shorter fiber length. The difference between the measured absorbed efficiency and the quantum limited efficiency is plotted in Figure 53 versus the estimated average inversion. A quadratic fit is expected if the cooperative up-conversion process is expected to be responsible for the deviation from the quantum limit. The data at higher inversion can indeed be reasonably fitted with a quadratic curve. At lower inversion, the measured data deviates from a quadratic fit. This poor fit at lower inversion may be due to the fact that other losses such as fiber background loss and measurement errors play a more significant role in this regime.

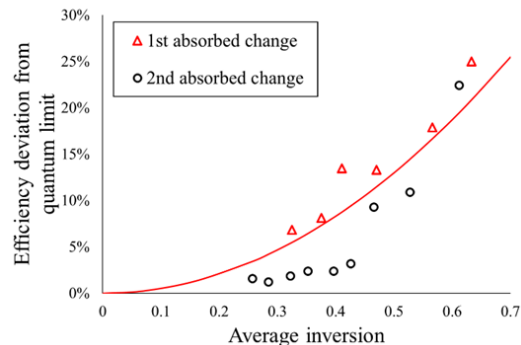


Figure 53 Deviation of measured absorbed efficiency from quantum efficiency as a function of average inversion. Solid red line is the quadratic fit for the measured data.

We have demonstrated that ytterbium-doped phosphosilicate host is much superior for efficient lasing operation at wavelengths between 1008-1020nm. Highly efficient 1018nm fiber laser with 70% efficiency with respect to the launched pump power is demonstrated in a 50 μ m-core Yb-doped LCF with 420 μ m cladding diameter, demonstrating the low brightness pump required for such efficiency. This large cladding diameter will allow the use of much higher power, lower brightness pump diodes, which is essential for tandem pumping of single-mode fiber lasers at higher powers. Single-mode operation is also possible with more optimized fibers. These fiber lasers have a very low quantum defect of 4.1% when pumped at

976nm, providing a path for the mitigation of thermal effects without the complexity of tandem pumping for multi-kilowatt fiber lasers.

3.2.7 Large-mode-area fibers operating near single-mode regime

In recent years, it has been recognized that transverse mode instability (TMI) imposes a significant limit on average powers of single-mode fiber lasers. One very effective method is to operate as close to the single-mode regime as possible, because TMI does not exist in the single-mode regime. This has driven kW fiber lasers to use smaller core diameters of 25 μm and 20 μm in recent years. Further reduction of NA can move fibers even closer to the single-mode regime while maintaining acceptable core diameters. Currently fabrication tolerance has limited commercial LMA fiber NA to 0.06 ($\Delta N \sim 1.2 \times 10^{-3}$).

Using a technique involving first fabrication of a large number of ytterbium-doped preforms on a Modified Chemical Vapor Deposition (MCVD) system, then extraction of the doped core glass and a repeated stack-and-draw process to homogenize the glass, we have been able to controllably make a large volume of ytterbium-doped glass with refractive index very close to that of silica. Optimized ytterbium-doped phosphosilicate glass is used with additional boron doping to lower the refractive index, enabling high doping levels and low photo-darkening. Glass made using a similar process was previously used to make ytterbium-doped leakage channel fibers and photonic bandgap fibers.

We have demonstrated ytterbium-doped double-clad LMA fibers with a low NA of 0.028, i.e. $\Delta N = 2.7 \times 10^{-4}$, using ytterbium-doped phosphosilicate glass made at Clemson. Two double-clad fibers were made. The first fiber has a geometry close to 30/400. It has an estimated second-order-mode cut-off at $\sim 1.2\mu\text{m}$ and is nearly single mode for ytterbium fiber lasers. The second fiber has a geometry close to 40/400. The second-order-mode cut-off is estimated to be at $\sim 1.55\mu\text{m}$ and is double-mode for ytterbium fiber lasers. High laser efficiency was demonstrated in both fibers. $M^2=1$ was measured in the 30/400 fiber and $M^2=1.06$ for the 40/400 fiber. We have studied bend loss limits and issues related further optimization. The new fabrication technique effectively eliminates the current NA limits imposed by the fabrication tolerance, opening up many new possibilities for LMA fiber designs.

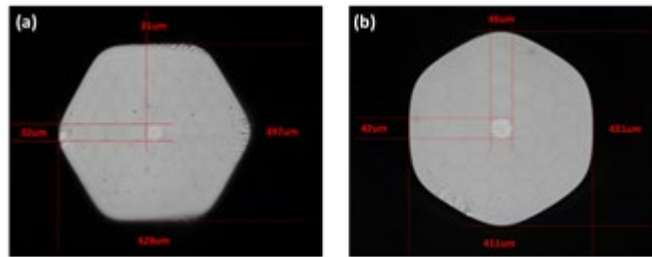


Figure 54 The cross section photos of the (a) 30/400 and (b) 40/400 LMA fibers.

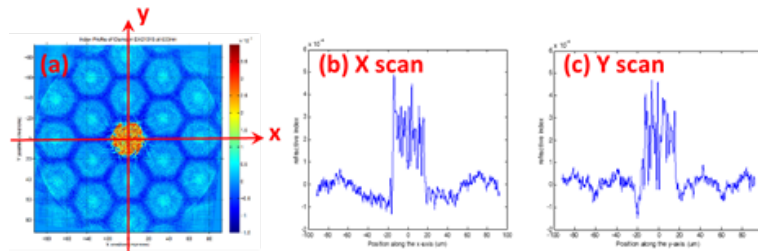


Figure 55 (a) 2D refractive index of the 30/400 fiber, (b) refractive index scan along X axis and (c) Y axis.

The two fibers are coated with low-index acrylic coating to provide a pump NA of 0.46. The 30/400 fiber has a hexagonal core which is 31 μm flat-to-flat and 34 μm corner-to-corner. The pump guide also has a hexagonal shape, measuring 397 μm flat-to-flat and 428 μm corner-to-corner. The measured pump absorption is $\sim 3\text{dB}$ at 976nm. The 40/400 fiber has a hexagonal core which is 42 μm flat-to-flat and 46 μm corner-to-corner. The pump guide has a hexagonal shape with 411 μm flat-to-flat and 431 μm corner-to-corner. The measured pump absorption is $\sim 4.5\text{dB}$ at 976nm. The fiber cross sections of the fibers are shown in Figure 54. The measured refractive index profile of the 30/400 fiber was given in Figure 55. The pixilated structure of the doped core is clearly visible, but the individual pixels are small compared to the laser wavelength. They are not expected to be a problem.

The bend loss of the 30/400 fiber was measured for bend diameters of 0.8m, 0.9m and 1m. It is shown in Figure 56 (a). The missing data is due to the ytterbium absorption. The simulated bend loss using the bend loss formulas in was obtained using $\text{NA}=0.0281$, i.e. $\Delta N=2.7\times 10^{-4}$, and a core diameter equaling the average of the flat-to-flat and corner-to-corner core dimensions. The simulated loss fits well with the measured loss. The estimated second-order-mode cut-off wavelength is $\sim 1.2\mu\text{m}$ and third-order-mode cut-off wavelength is $\sim 750\text{nm}$. The measured third-order-mode cut-off wavelength can be found at the loss peak at $\sim 700\text{nm}$ (see Figure 56), which is associated with its estimated cut-off, to be $\sim 750\text{nm}$. This is consistent with the result obtained from loss simulation. This 30/400 fiber is therefore very close to the single-mode regime at the wavelengths of ytterbium fiber lasers. A coil diameter of $>1\text{m}$ needs to be used to minimize bend loss.

The bend loss of the 40/400 fiber was measured for bend diameters of 0.9m, 1m and 1.1m which is shown in Figure 56 (b). The simulated bend loss was obtained using $\text{NA}=0.027$, i.e. $\Delta N=2.51\times 10^{-4}$, and a core diameter equaling the average of the flat-to-flat and corner-to-corner core dimensions. The simulated loss fits well with the measured loss. The estimated second-order-mode cut-off wavelength is $\sim 1.55\mu\text{m}$ and third-order-mode cut-off wavelength is $\sim 973\text{nm}$.

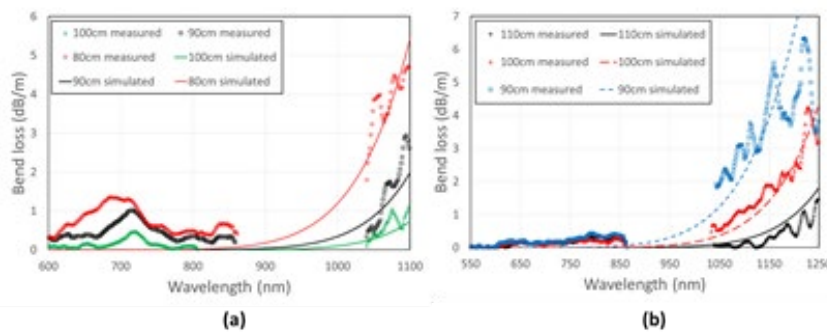


Figure 56 (a) The measured loss of the 30/400 fiber with simulated bend loss using $\text{NA}=0.285$ and core radius of 32.5 μm and (b) The measured loss of the 40/400 fiber with simulated bend loss using $\text{NA}=0.27$ and core radius of 44 μm .

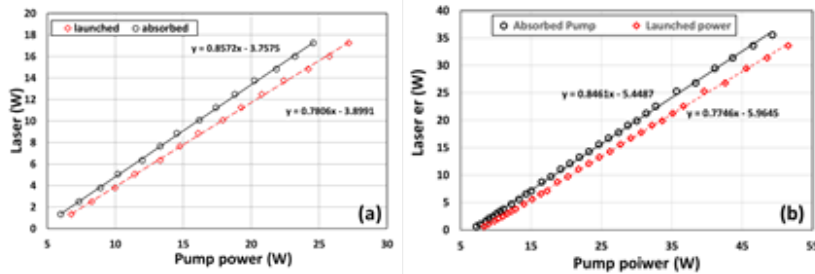


Figure 57 Measured efficiencies of fiber lasers made with (a) 4m of the 30/400 fiber coiled at 1.9m in diameter and (b) 2.5m of the 40/400 fiber coiled at 1m.

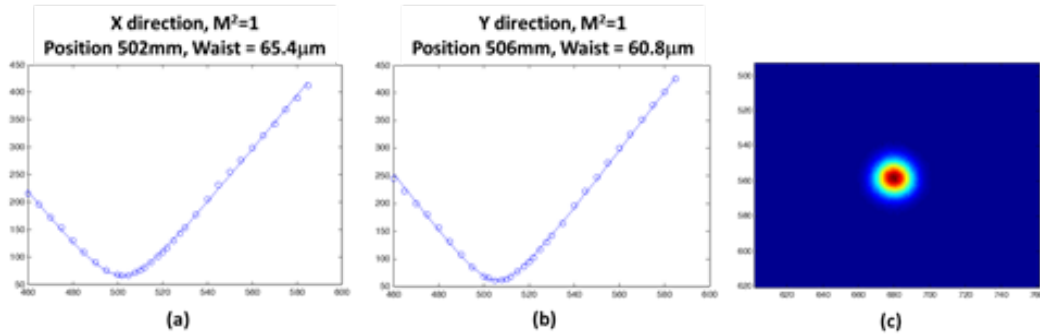


Figure 58 Measured beam quality of the fiber laser made from the 4m 30/400 fiber coiled at 1.9m in diameter.

A fiber laser at ~1030nm was constructed with 4m of the 30/400 fiber with two straight cleaved ends. The fiber was coiled at 1.9m diameter. At bend diameters below 1.5m, some leaked laser light in the cladding can be seen. The measured lasing slope efficiencies are 78% and 86% versus launched and absorbed pump powers respectively (Figure 57 (a)). The M^2 was measured to be 1 (Figure 58), reflecting a perfect Gaussian mode at the output.

A fiber laser at ~1035.5nm was also constructed with 2.5m of the 40/400 fiber with two straight cleaved ends. The fiber was coiled at 1m diameter. The measured lasing slope efficiencies are 77% and 85% versus launched and absorbed pump powers respectively (Figure 57 (b)). The M^2 was measured to be 1.06 (Figure 59). The output beam appears to be a really good Gaussian mode (see Figure 59 (c)). The ability to coil the 40/400 fiber to a smaller diameter of 1m is due to its larger core diameter.

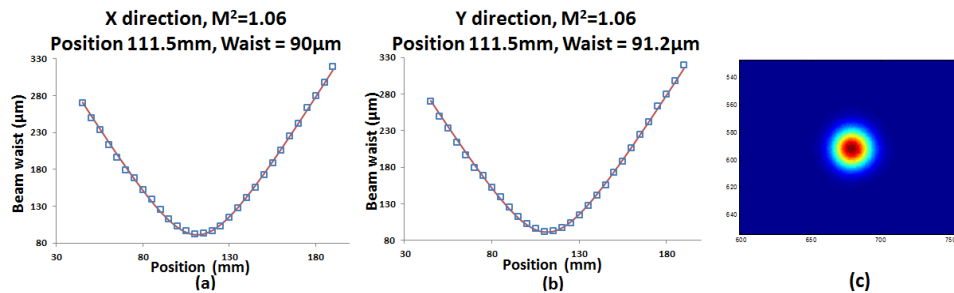


Figure 59 Measured beam quality of the fiber laser made from the 2.5m 40/400 fiber coiled at 1m in diameter.

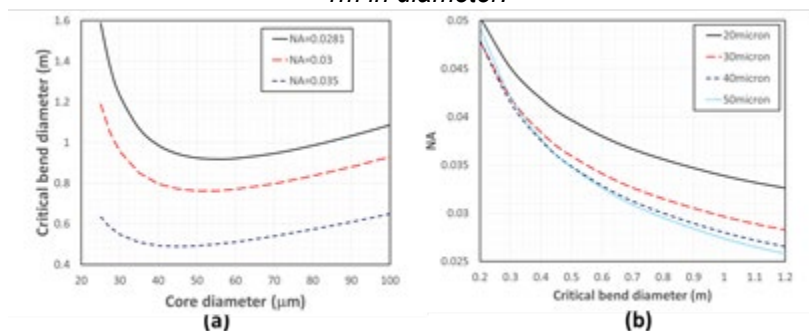


Figure 60 (a) Simulated critical bend diameter versus core diameter for $NA=0.0281$, 0.03 and 0.035 , and (b) simulated NA versus critical bend diameter for core diameters of $20\mu\text{m}$, $30\mu\text{m}$, $40\mu\text{m}$ and $50\mu\text{m}$.

The lower NA may result in more robust single-mode operation; but it also causes significantly increased bend loss. It is therefore important to understand the tradeoffs. The critical bend diameter, defined as when the bend loss is 0.1dB/m , was simulated for various

core diameters for NA=0.0281 (see Figure 60 (a)). A slightly smaller critical bend diameter of $\sim 0.92\text{m}$ can be obtained at $\sim 55\mu\text{m}$ core diameter for this NA. This is consistent with what was measured for the 40/400 fiber. The critical bend diameter is actually larger for larger core diameters. This is due to the dependence of bend loss on both V value and core diameter. The critical bend diameter versus core diameter was also simulated for larger NAs of 0.03 and 0.035. A much smaller critical bend diameter of $< 0.5\text{m}$ can be obtained for NA=0.035, which has a minimum of 0.49m at $\sim 45\mu\text{m}$ core diameter. It needs to be noted that this smaller critical bend diameter comes at the cost of operating much further away from the single-mode regime. Thus a much lower TMI threshold is expected [9].

We have also simulated the dependence of NA on the critical bend diameter for various core diameters (see Figure 60 (b)). For critical bend diameter of 0.5m , the minimum NAs are 0.0396, 0.0359, 0.0349, and 0.0348 for core diameters of $20\mu\text{m}$, $30\mu\text{m}$, $40\mu\text{m}$, and $50\mu\text{m}$ respectively.

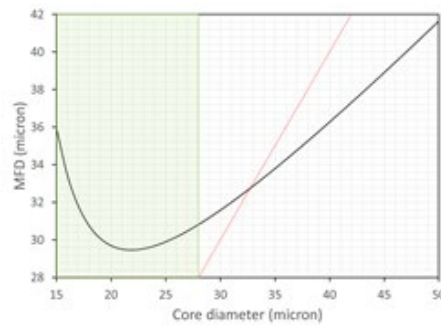


Figure 61 Simulated mode field diameter (MFD) at 1030nm of a LMA fiber with NA=0.0281 versus core diameter. The shaded area is single-mode regime. The dotted line is when MFD=core diameter.

We have also calculated the mode field diameter (MFD) at 1030nm versus core diameter for the LMA fibers with NA=0.0281 (Figure 61). The shaded area is the single-mode regime and the dotted line is when MFD equals core diameter. The MFD reached a minimum when the core diameter was $\sim 22\mu\text{m}$. The MFD increases at smaller core diameter due to a loss of core guidance. It is worth noting that the MFD is much larger than the core diameter in the single-mode regime. This is a well-known feature of the single-mode regime, where there is significant amount of power outside the core. For the 30/400 fiber, the MFD is close to the core diameter, indicating there is still a significant amount of power outside the core. Far into the multimode regime, the MFD is much smaller than the core diameter and most of the optical power is in the core. In cases where only the core is doped, the doped area has much better overlap with the fundamental mode than with the next higher-order modes near the single-mode regime. This helps to improve single-mode operation and to raise the TMI threshold.

Using a specially developed fabrication process, we have shown that ytterbium-doped fiber with NA as low as ~ 0.028 can be realized in a controlled fashion. This allows us to make an ytterbium-doped 30/400 fiber operating very close to the single-mode regime. A M^2 of 1 was measured, indicating a perfect Gaussian mode as would be expected from operating near the single-mode regime. Good M^2 of 1.06 was also measured in an ytterbium-doped 40/400 fiber which operated deeper in the two-moded regime, but demonstrated a smaller coiled diameter of $\sim 1\text{m}$, consistent with our simulation. Both fibers demonstrated excellent lasing efficiency. This fabrication technique will enable new LMA designs with significantly improved TMI threshold. The potential tradeoff between TMI threshold and the critical bend diameter was also studied.

3.2.8 Thermal lensing in optical fibers

Average powers from fiber lasers have reached the point that a quantitative understanding of thermal lensing and its impact on transverse mode instability is becoming

critical. Although thermal lensing is well known qualitatively, there is a general lack of a simple method for quantitative analysis. We first conduct a study of thermal lensing in optical fibers based on a perturbation technique. The perturbation technique becomes increasingly inaccurate as thermal lensing gets stronger. It, however, provides a basis for determining a normalization factor to use in a more accurate numerical study. A simple thermal lensing threshold condition is developed. The impact of thermal lensing on transverse mode instability is also studied.

The thermal-optic effect is introduced by

$$n(r)=n_0(r)+k_T\Delta T(r) \quad (1)$$

where refractive index profile n , initial refractive index profile n_0 and change in temperature ΔT are expressed in cylindrical coordinates, and $k_T=1.1\times 10^{-5} \text{ K}^{-1}$ is the thermal-optic coefficient for silica. Under the influence of heat load, the guided mode is expected to shrink down to a new equilibrium where it would be stable. This is very similar to what happens under nonlinear self-focus. The only difference is in the time taken to reach this new equilibrium. It is expected to be much slower and determined by the thermal diffusion rate perpendicular to the propagation direction. Under very strong thermal lensing, the optical mode can be focused down to a very small size over a distance in the order of the Rayleigh range, similar to that in nonlinear self-focus.

The temperature profile is approximated by the parabolic solution for uniform heating in the core with a heat load of Q_0 (w/m) and we have ignored the temperature change outside the core by setting $\Delta T=0$ for $r>\rho$, where ρ is the core radius. This is reasonable for multimode fibers commonly found in fiber lasers as the optical power is mostly in the core in these cases. It is however not a good approximation for single-mode fibers where there is significant optical power outside the core.

$$\Delta T(r)=\frac{Q_0}{4\pi\kappa\rho^2}(\rho^2-r^2) \quad (2)$$

where $\kappa=1.38 \text{ w/m/K}$ is the thermal conductivity. Details of the perturbation analysis are given in appendix A. It is based on finding a relationship between modes in the fiber perturbed by the heat load and the original unperturbed fiber. With the assumption of a Gaussian mode (see equation A11 in appendix A), we can obtain an equation for the relative mode size $\gamma=w/w_0$, where w is the spot size of the mode in the perturbed fiber and w_0 in the unperturbed fiber. Spot size is half of the MFD for a Gaussian mode (see equation A11 in appendix A for a detailed definition).

$$\frac{1}{2}\xi Q_0 w_0^2 \gamma^6 + \left(U^2 + 3\xi Q_0 \rho^2 + \frac{9}{2}\xi Q_0 w_0^2 \right) \gamma^4 + 3\xi Q_0 \rho^2 \gamma^2 - U^2 = 0 \quad (3)$$

where U is the core parameter as normally defined for optical fiber, and

$$\xi = \frac{k_T k_0^2 n_{co}^2}{4\pi\kappa} \quad (4)$$

where k_0 is the vacuum wave number and n_{co} is the core refractive index. Equation (3) can be solved numerically and the result is shown in Figure 62 for $V=3-8$.

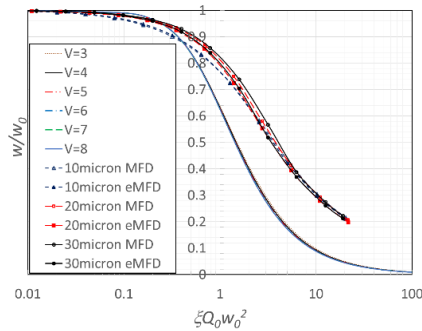


Figure 62 Mode collapse under the influence of thermal lensing. Equation (3) is evaluated for normalized frequency $V=3-8$. A numerical simulation is also performed for comparison for fibers with core diameters of $10\mu\text{m}$, $20\mu\text{m}$ and $30\mu\text{m}$ and NA of 0.06. The results are plotted as MFD for near-field MFD and eMFD for effective MFD, i.e. $2(A_{\text{eff}}/\pi)^{1/2}$.

The relative mode size is plotted against the normalized thermal lensing parameter $\xi Q_0 w_0^2$ in figure 62. It can be seen that the rate of change in the relative mode size is slow at small $\xi Q_0 w_0^2$, but accelerates at larger $\xi Q_0 w_0^2$. There is very little difference in the curves for different V values. The relative mode size can collapse to small values at high heat load and the rate of change slows down when $\xi Q_0 w_0^2 > 2$. The most interesting observation is the fact that the effect of thermal lensing is fully characterized by the normalized thermal lensing parameter $\xi Q_0 w_0^2$, where ξ is fully determined by material properties and laser wavelength. This normalized thermal lensing parameter scales linearly with heat load Q_0 and also scales quadratically with MFD. Since the total effect of thermal lensing is determined by the integrated effect seen by the entire mode, it is reasonable to expect it to scale with the mode area, i.e. w_0^2 .

For a more accurate study of the impact of thermal lensing, we need to conduct a numerical study. We will focus on the regime where the fundamental mode dominates and ignore any mode distortion due to bending. Since we are only dealing with optical modes with a cylindrical symmetry in this case, we will use an optical mode solver for an arbitrary refractive index profile with a cylindrical symmetry. We already have established such a vector optical mode solver for an earlier work.

We also need to deal with the temperature profile resulting from the heat load from an optical mode with cylindrical symmetry. In our analysis, we have assumed that heat load is proportional to the local mode intensity; consequently we have ignored the effect of gain saturation. Gain saturation will lead to a flattening out of heat load in the center of the core and therefore slightly weaken the effect of thermal lensing.

Since a simple parabolic solution exists for the temperature profile in the case of a spatially uniform heat load in a cylinder, it has been used in many previous thermal analysis of fiber lasers. We need to have a more accurate numerical model for the temperature profile in a cylinder given an arbitrary cylindrical heat load profile. We start by dividing the area with the heat source into many fine layers so that we can assume each layer has a uniform heat load and we can then use the parabolic solution over each layer. This approach, however, does not have enough free parameters to ensure the solution has both continuity and continuity in the 1st order derivative at the boundary between layers, both required for a rigorous solution. We subsequently devised a scheme where we first divide the area with the heat load into many fine layers with equal thickness. We then divide each layer into two sub-layers, one sub-layer with the total heat load for the layer and one sub-layer without source. We can then use the known parabolic solution over the sub-layer with the source and the known logarithmic solution for the sub-layer without source. The relative thickness of the sub-layers can be determined by the continuity condition at the boundary between layers. This new scheme allows us to find an accurate solution while ensuring necessary continuities at all the boundaries. A detailed derivation is provided in appendix B. In the simulations in this work, the region with the heat load is typically divided into 100-200 layers. This is found to be sufficient for a stable solution.

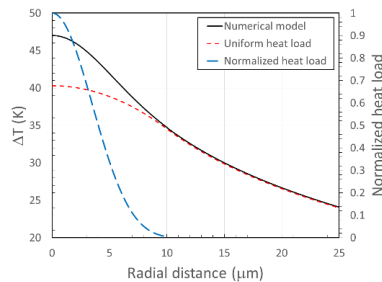


Figure 63 Comparison of the temperature profile from the numerical method used in this work and the parabolic solution for a uniform heat load. ΔT is set to be 0K at the cladding boundary. Core diameter is $20\mu\text{m}$; cladding diameter is $400\mu\text{m}$ and NA is 0.06. The total heat load is 64w/m in both cases. The laser wavelength is at $1.03\mu\text{m}$. The normalized heat load profile, i.e. normalized mode intensity profile, is also shown.

A comparison of the temperature profiles from the numerical model used in this study and the uniform heat load is shown in figure 63. The fiber has a NA of 0.06 and a core diameter of $20\mu\text{m}$, operated at $1.03\mu\text{m}$. We use a cladding diameter of $400\mu\text{m}$ throughout this study. The total heat load in the core is 64w/m in both cases and there is no heat load outside the core. The normalized heat load profile, i.e. the normalized mode intensity profile, is also shown. The numerical model used an iteration process described in the next paragraph to find the optical mode under heat load. It can be seen clearly that the solution in the cladding is the same for both cases and the uniform heat load model underestimates the temperature in the core. This is due to the fact that more heat is deposited near the core center than that accounted in the uniform heat load model.

In the following analysis of thermal lensing in an optical fiber, we first find the fundamental optical mode in the fiber without any heat load. We then apply one M^{th} of the heat load with a heat load profile equaling the fundamental optical mode intensity. The temperature profile is then calculated, which is then used to calculate the refractive index profile of the new fiber. The fundamental mode is then found for this new fiber. Two M^{th} of the heat load is then used with a heat load profile equaling the new fundamental mode intensity for the next iteration. This is repeated until total heat load is applied. This slow increase of heat load over many iterations is essential to keep the change in optical mode profile to a minimal for each iteration. Otherwise it can lead to numerical instabilities especially at large heat loads. We found $M=30$ to be adequate to ensure stability and convergence for our analysis. This is used throughout this study.

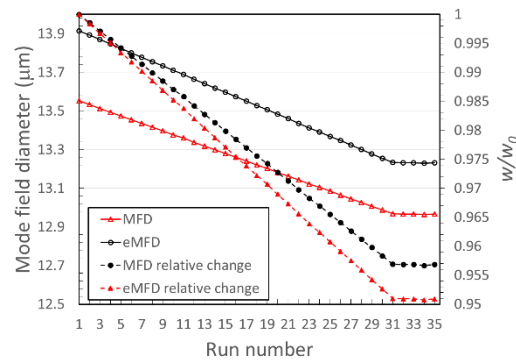


Figure 64 Typical run for the case in Fig. 2. Core diameter is $20\mu\text{m}$ and NA is 0.06. The total heat load is 64w/m . The laser wavelength is at $1.03\mu\text{m}$. Relative changes are shown on the vertical axis on the right. The heat load is gradually increased over 30 steps.

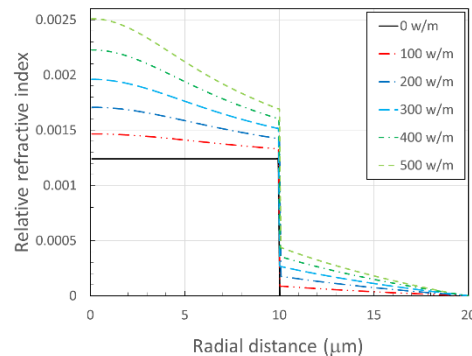


Figure 65 Refractive index profiles under various heat loads. Core diameter is $20\mu\text{m}$ and NA is 0.06. The laser wavelength is at $1.03\mu\text{m}$.

The evolution of MFD (near-field MFD) and eMFD (effective MFD obtained from effective mode area) over the gradual increase of heat load for the case in figure 63 is shown in figure 64. The relative change in MFD and eMFD is shown on the right vertical axis. The

reduction of mode size due to thermal lensing when heat load is gradually increased can be clearly seen. Also can be seen is that the mode size stabilizes at a constant value after the 31st run when the heat load is no longer increased. This demonstrates the convergence of the solution and stability of the numerical process.

The refractive index profiles obtained by the numerical model for the 20 μm -core fiber are shown in figure 65 for various total heat loads. The refractive index profile is truncated at a radius 20 μm , i.e. twice the core radius in this case. In our following analysis of optical mode, we are only concerned with the part of the waveguide seen by the optical mode of interest. We typically truncate the refractive index profile to 2 to 5 times of the core radius depending on guiding strength of the waveguide. Using an unnecessarily large cladding radius in the analysis can lead to poor numerical stability in the optical mode solver in addition to longer computation time. Care is taken in each case to ensure that the truncation does not compromise accuracy.

We then proceed to study the impact of thermal lensing on mode size for three fibers with core diameters of 10 μm , 20 μm and 30 μm . All fibers have a NA of 0.06 and a cladding diameter of 400 μm . This study is conducted for a wavelength of 1.06 μm . The respective V values are 1.778, 3.557, and 5.335. The 10 μm -core fiber is in the single-mode regime and the other two fibers are in the multimode regime. The results are shown in Fig. 1 for both MFD and eMFD (see figure caption for detailed definition). It can be seen that the results from the perturbation method are reasonable for a small normalized thermal lensing parameter, but overestimate the effect of thermal lensing when $\xi Q_0 w_0^2 > 0.1$. The results for the three fibers at $\xi Q_0 w_0^2 > 2$ are very close. In this regime, wave guidance is almost entirely from the effect of thermal lensing and the original waveguide plays a very small part. At smaller $\xi Q_0 w_0^2$, the single-mode fiber suffers slightly more mode size reduction. The mode is much larger than the core in the single-mode regime and this enhances the impact of thermal lensing on mode size. MFD and eMFD follows each other fairly closely. A convenient place to set the thermal lensing threshold is $\xi Q_0 w_0^2 = 0.5$, where the mode size is reduced by ~10% and the effective mode area by ~20%.

There is a strong interest in understanding the impact of thermal lensing on TMI. TMI can be quantified by the TMI nonlinear coefficient χ . TMI threshold is inverse proportional to χ and also dependent on input higher-order-mode power and amplifier configuration. Since we can easily evaluate the refractive index profile of the fiber under thermal loading, we just need to find the fundamental and higher-order modes to evaluate χ under the influence of thermal lensing. We have assumed that the fundamental mode is dominating in this case and conducted this study for the LP₁₁ mode. Our cylindrical optical vector cannot directly find the LP₁₁ mode, but can find its constituent TE₀₁ and HE₂₁ modes. These modes have the same radial intensity profile as LP₁₁. We therefore found the radial mode intensity profile for the HE₂₁ mode and used this for our study.

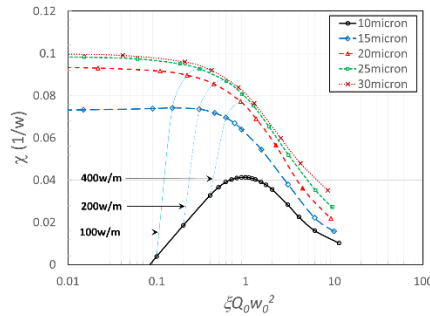


Figure 66 Simulated TMI nonlinear coupling coefficient for fibers with core diameters of 10 μm , 15 μm , 20 μm , 25 μm and 30 μm respectively. The fiber NA is 0.06 and cladding diameter is 400 μm . This study is conducted at a wavelength of 1.06 μm . Contour lines indicate constant thermal load.

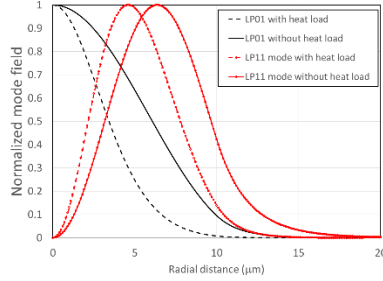


Figure 67 The LP_{01} and LP_{11} modes at $1.06\mu\text{m}$ in a fiber with a NA of 0.06 and a core diameter of $20\mu\text{m}$ without heat load and with a heat load of 1000w/m , i.e. $\xi Q_0 w_0^2 = 2.19$. The cladding diameter is $400\mu\text{m}$.

We studied 5 fibers with core diameters of $10\mu\text{m}$, $15\mu\text{m}$, $20\mu\text{m}$, $25\mu\text{m}$ and $30\mu\text{m}$ respectively. The fiber NA is 0.06 and cladding diameter is $400\mu\text{m}$. This study is conducted at a wavelength $1.06\mu\text{m}$. The V values are respectively 1.778, 2.667, 3.557, 4.446, and 5.335. The results are shown in figure 66. The $10\mu\text{m}$ -core fiber is single mode at low heat load, but the LP_{11} mode is guided when $\xi Q_0 w_0^2 > 0.084$. Its TMI nonlinear coupling coefficient χ increases until $\xi Q_0 w_0^2 \sim 1$ as the LP_{11} mode is increasingly guided. When $\xi Q_0 w_0^2 > 1$, thermal lensing becomes significant and χ starts to decrease. Thermal lensing pulls all modes to the core center, but this is more significant for the fundamental mode (see figure 67). This lowers the overlap between the LP_{01} and LP_{11} modes, consequently leading to a reduction in χ . A similar trend can be seen for the $15\mu\text{m}$ -core fiber. Since the LP_{11} is already well guided in this fiber with heat load, the initial increase in χ at low heat load is less pronounced. χ starts to decrease when $\xi Q_0 w_0^2 > 0.3$. The remaining fibers have similar χ at low heat load; this is due to that fact that χ changes very slowly at large V [6]. For these fibers, χ starts to decrease significantly when $\xi Q_0 w_0^2 > 0.3$. Similar studies were conducted for LP_{02} mode and similar trends were obtained. This reduction of TMI at high thermal load is, however, of limited practical use as the effect of thermal lensing is significant at this point. For most practical fibers, the TMI threshold is also well below this thermal load.

We have studied thermal lensing effects in optical fibers with both a perturbation method and numerical method and have developed a normalized thermal lensing parameter. A simple thermal lensing threshold condition is also developed. We have further studied the impact of thermal lensing on TMI and found that strong thermal lensing leads to a reduction in TMI.

3.2.9 $100\mu\text{m}$ -core leakage channel fibers

The 4th iteration ytterbium-doped glass was measured to have an index of $\sim 4 \times 10^{-4}$ with respect to that of silica glass, much higher than expected. There is clear evidence that the fabrication process and residual thermal stress play a role in determining the refractive index at this level. The 4th iteration ytterbium-doped glass was made by mixing the 2nd iteration (index $\sim -2.25 \times 10^{-4}$) and 3rd iteration (index $\sim 2.3 \times 10^{-4}$) with a ratio of 1:1.

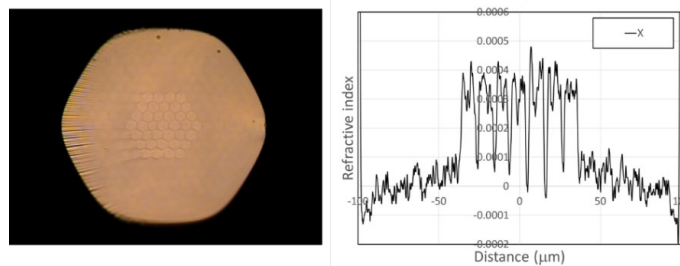


Figure 68 The cross section and refractive index of the step-index fiber based on the 4th iteration ytterbium-doped glass.

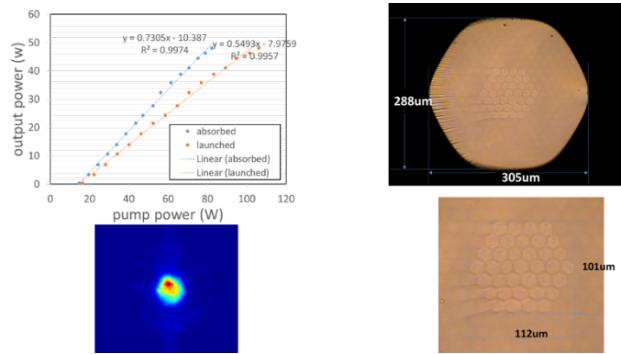


Figure 69 Laser efficiency, mode and cross section of the 100/300 ytterbium-doped step-index fiber based on the 4th iteration ytterbium-doped glass.

Initially 7-cell 100µm-core LCF was made. It showed clear guidance over each of the 7 ytterbium-doped core rods. It is therefore decided to reduce the dimension of the dimension of each of the core rods by using a 37-cell design. Step-index fibers with 80µm and 100µm core was made using 37 4th iteration ytterbium-doped glass rods. The cross section of the 80µm-core fiber and its refractive index profile are shown in figure 68. The 100/300 fiber (see figure 69 for detailed dimensions) was tested for lasing action using two cleaved fiber ends. The pump absorption was measured to be ~10dB/m at ~976nm. The efficiency is ~55% and ~73%, with respect to the launched and absorbed pump powers respectively. The output is reasonably single mode.

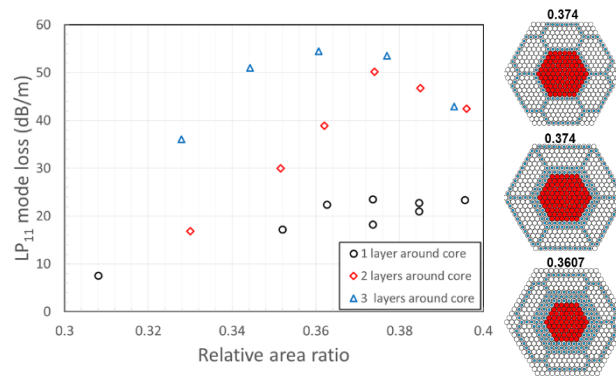


Figure 70 LP_{11} mode loss versus relative area ratio of the cladding core to the central core for fundamental mode loss of 0.1dB/m (61-cell-core design).

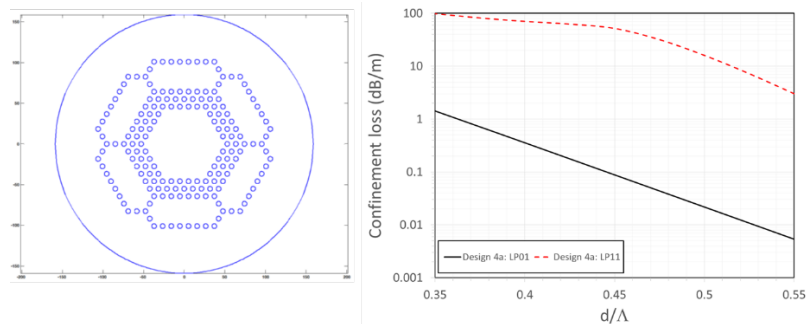


Figure 71 The three-layer and 61-cell-core design and its LP_{11} and LP_{01} mode losses versus d/λ .

LCF design studies were conducted for 61-cell-core design. The design is summarized in figure 70 by plotting the LP_{11} mode loss when the fundamental mode loss is

0.1dB/m versus relative area ratio of the cladding core and the central core. Some designs are also shown in figure 70. Impressive HOM loss of ~ 55 dB/m can be achieved for a fundamental loss of 0.1dB/m. Such design also has reasonable tolerance to geometrical errors (see the tolerance in the area ratio for achieving HOM loss in excess of 50dB/m in figure 70). The best design is achieved with three layers of low-index nodes (index of 8×10^{-4} below that of silica) around the central core. The optimum design is achieved at $d/\Lambda = 0.445$ where the fundamental mode loss is 0.1dB/m (see figure 71). The design also has weak wavelength dependence (see figure 72). The second mode TE_{01} clearly shows resonance with cladding cores (see figure 72). The fabrication plan is illustrated in figure 73. The cross section of the fabricated fiber is shown in figure 74 along with its key dimensions listed.

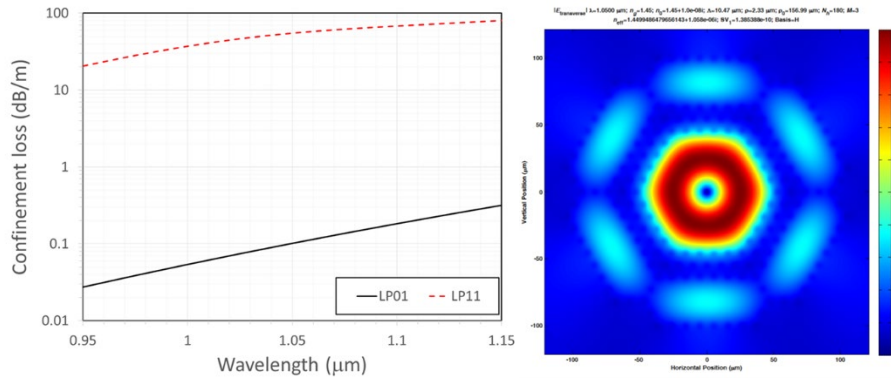


Figure 72 The wavelength dependence of the optimum design and its TE_{01} mode.

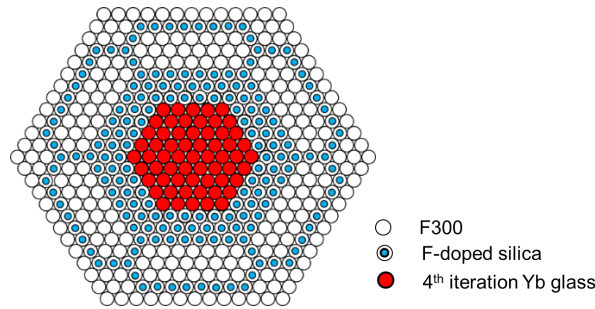


Figure 73 Fabrication plan for the optimized 61-cell-core LCF.

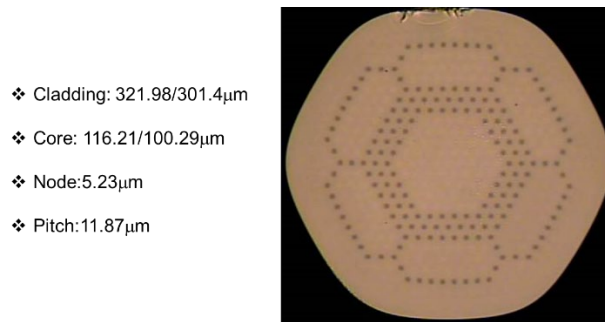


Figure 74 Fabricated LCF and its key dimensions.

The laser was constructed with two cleaved ends and its efficiency was characterized along with output mode when fiber was straight (see figure 75). The measured efficiency is $\sim 74\%$ and $\sim 92\%$ with respect to the launched and absorbed pump powers respectively. The mode shows clear multi-mode output. The high index of the ytterbium-doped core glass significantly detuned the HOM coupling and consequently degraded HOM suppression of the original design.

The mode pattern did not show much improvement when the fiber was coiled in various configurations. In an amplifier arrangement, the improved output mode was achieved (see figure 76), but the output mode starts to degrade when pump power is increased.

To prove the degraded output mode is due to the high refractive index of the ytterbium-doped glass in the core, we fabricated and tested a passive LCF made with silica rods in the core instead of the ytterbium-doped rods. The passive LCF has the same dimensions as the active LCF. The output mode is shown in figure 77, clearly demonstrated the expected fundamental mode.

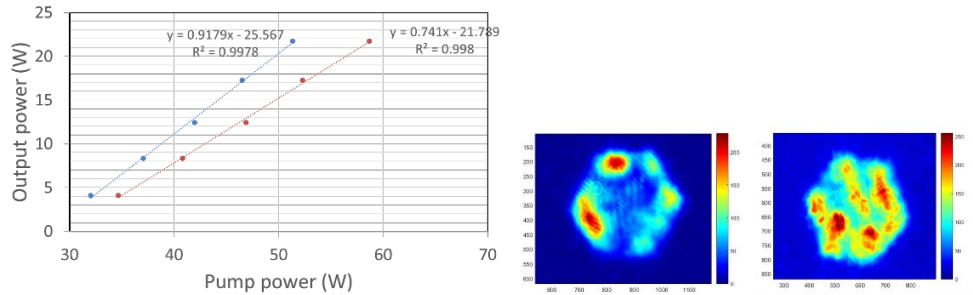


Figure 75 Measured laser efficiency and modes when fiber is straight.

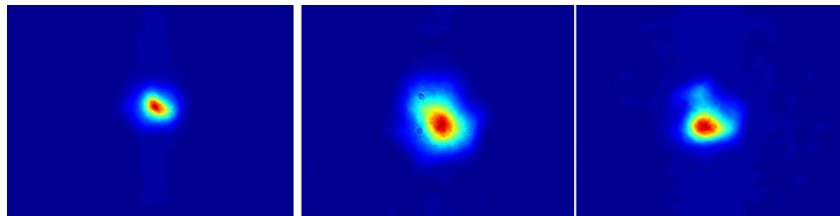


Figure 76 Output mode in an amplifier configuration when pump was off.

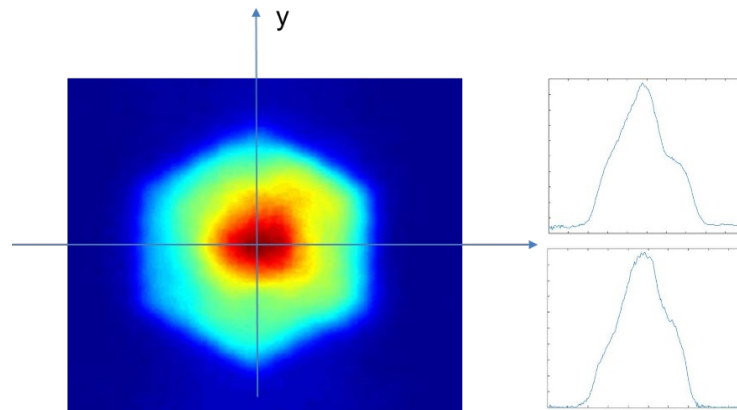


Figure 77 Output mode measured from a passive LCF.

Long taper at the input end in an amplifier configuration can improve mode quality at the output of the ytterbium-doped LCF. In the long run, improved ytterbium-doped glass is required to make 100 μm -core LCF to work robustly.

3.2.10 Ytterbium fiber laser at 980nm.

The three-level system of Yb fiber lasers at $\sim 976\text{nm}$ has attracted much attention in the past two decades. The initial interests in the late nineties were largely driven by the need for higher pump powers for the increasing power-demand of erbium-doped fiber amplifiers in dense wavelength-division-multiplexing optical communication systems. The recent interests are mostly

in pumping ultrafast solid-state and fiber lasers. Such lasers are critical for rapidly emerging micro-machining applications. Peak powers in these lasers are limited by optical nonlinearities, which can be overcome by using shorter lasers. Solid-state lasers and core-pumped fiber lasers are powerful approaches to mitigate optical nonlinearities. Diffraction-limited pump powers at $\sim 976\text{nm}$ of at least a few tens of watts are required for these applications. In addition, 976nm fiber lasers can also be frequency-doubled to 488nm for many other applications including pumping Ti: Sapphire lasers near its peak absorption and underwater communications and sensing.

To achieve the required power of over a few tens of watts, cladding-pumping is necessary. The major limit to the efficient operation of cladding-pumped three-level Yb fiber lasers is the competing four-level systems operating at longer wavelengths and the necessary high inversions. The four-level system has much higher gain at low inversions. To suppress its operation, higher inversion is required and has to be maintained throughout the fiber, causing a large amount of the pump to leave the fiber. It has long been recognized that a large core-to-cladding ratio is the key to efficient three-level fiber lasers. A given inversion is maintained largely due to the competing effects of pumping and stimulated emission rates, which are determined by the pump and signal intensities once absorption and emission cross sections are fixed. A relatively smaller pump waveguide leads to lower pump power leaving the fiber for a given pump intensity. Since single-mode operation sets an upper limit on core diameter, large core-to-cladding ratio therefore sets an upper limit on cladding size and consequently available pump powers.

We report the use of all-solid photonic bandgap fibers for efficient three-level cladding-pumped Yb fiber lasers. The all-solid photonic bandgap fibers provide two major benefits. Firstly, they allow robust single-mode operation of coiled fibers at large core diameters and therefore enable large core-to-cladding ratio. Secondly, they also provide efficient suppression of the four-level system by distributed loss arising from placing these lasing wavelengths to be outside the bandgap. In addition, these flexible all-solid photonic bandgap fibers can be readily integrated into all-fiber monolithic fiber lasers, unlike rod-type photonic crystal fibers

3.2.10.1 All-solid photonic bandgap fibers for Yb three-level fiber lasers with free-space optics

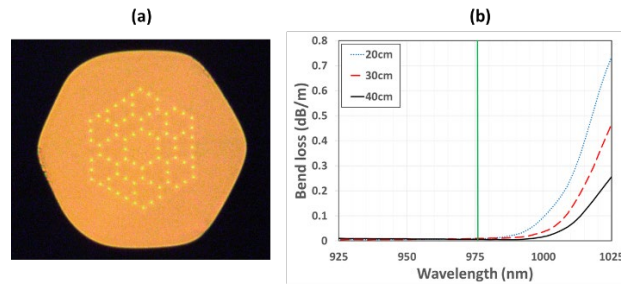


Figure 78. (a) Cross section of the Yb-doped multiple-cladding-resonance all-solid photonic bandgap fiber and (b) bend loss measured from a passive all-solid photonic bandgap fiber of identical design (coil diameters are shown in the legend).

The cross section of the Yb all-solid photonic bandgap fiber is shown in Figure 78 (a). The fiber has a core with corner-to-corner distance of $24\mu\text{m}$ and side-to-side distance of $21\mu\text{m}$. The cladding has a corner-to-corner distance of $131\mu\text{m}$ and side-to-side distance of $124\mu\text{m}$. The fiber is coated with low index acrylate to provide a pump NA of ~ 0.46 . The pump absorption was measured to be $\sim 1.76\text{dB/m}$ at 915nm . A passive fiber of identical design was drawn first and its bandgap position was measured in order to determine the target dimension for the active fiber. The background loss for core propagation in the passive fiber was measured to be around 20dB/km at $\sim 976\text{nm}$. Bend loss was also measured on the passive fiber for bend diameters of 20cm , 30cm and 40cm . This is given in Figure 78 (b), showing negligible bend loss for coil diameters of 20cm at the lasing wavelength of $\sim 976\text{nm}$. The high bend loss at the longer wavelengths is related to the long wavelength edge of the bandgap, which is optimally positioned

for the suppression of the Yb four-level system without incurring loss on the three-level system at $\sim 976\text{nm}$. The low-loss window was measured to be around 400nm wide in a passive fiber and the lower wavelength edge of the bandgap is just below 600nm for the active fiber, not shown in Figure 78 (b).

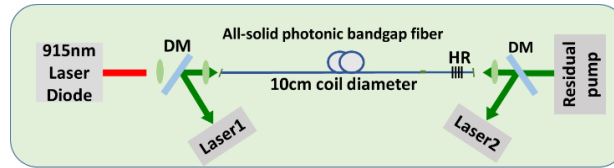


Figure 79. A laser configuration used in the experiment (DM: dichroic mirror, HR: FBG high reflector, $>99.5\%$). A few other alternative arrangements were also used. 4%+4%: straight cleaves at both fiber ends, 4%+HR: straight cleave at the pump end and HR at the other end, 1%+HR: 1% FBG output coupler at the pump end and HR at the other end, angle+HR: angled cleave at the pump end and HR at the other end, angle+angle: angled cleaves at both ends.

The basic laser arrangement is a counter-pumped configuration shown in Figure 79. A number of alternative laser configurations were also used, including 4%+4%, 4%+HR, 1%+HR, angle+HR, angle+angle. The details are explained in the caption of Figure 79. FBGs were written in-house using a frequency-quadrupled YAG laser at 266nm . A matching 25/125 photosensitive fiber was made in-house for the HR FBGs. The all-solid photonic bandgap fiber can be easily spliced like conventional fibers. For some arrangements, several different fiber lengths were also tested. This was done by repeatedly cutting back the same fiber. The coil diameter was 10cm in all cases. We tested several coil sizes down to 10cm and found very little efficiency degradation at 10cm . Outputs at both fiber ends were monitored along with residual pump. The pump was delivered in a 0.22NA 105/125 fiber. We started with a 100W 915nm pump diode.

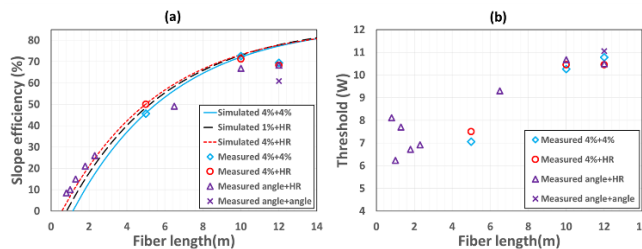


Figure 80. (a) Simulated efficiency at 976nm versus coupled pump powers at 915nm (signal loss: 0.02dB/m , pump loss: 0.02dB/m) and measured efficiencies versus fiber length for a number of laser arrangements and (b) measured thresholds.

The efficiency of the laser was simulated using a homemade Matlab code taking account of local pump, signal, and ASE powers in both directions as well as local inversion. All the optical powers were initially propagated forward numerically with appropriate boundary conditions at the fiber input and guessed values were used for all other parameters which could not be determined. Once the propagation reached the fiber end, only the appropriate parameters at the output end were reset by the required boundary conditions and all the optical powers propagated numerically backward. Once the input was reached, only the appropriate parameters at the input were reset by the required boundary conditions. This was repeated until numerical convergence was achieved. The simulation was performed for 4%+4%, 4%+HR, and 1%+HR, shown in Figure 80 (a). Both outputs were considered for the efficiency calculations. The efficiencies are very close in these three cases. There is a only small difference especially for shorter fibers. This is mostly due to the different total cavity losses, with lower total cavity loss leading to slightly higher efficiency.

The efficiency was measured in a number of configurations. Laser outputs from both ends were added for the calculation of the efficiency. This is also summarized in Figure 80 (a). We started with 4%+4%, since this was the easiest one to test. An efficiency of $\sim 72.6\%$ was achieved with 10m fiber. Maximum output for laser 1 (pump end) was 19.9W and laser 2 was 31.5W in this case. The M^2 for the laser 1 (pump end) was measured to be ~ 1.3 .

Several other configurations were also tested. This included 4%+HR, angle+HR, and angle+angle. The high cavity gain is sufficient to enable lasing for schemes with not only one angled cleave but two angled cleaves, albeit with a slight efficiency reduction. The efficiency decreases beyond 10m. This is expected when inversion falls too low far from the pump end, also evidenced by an increase in threshold with longer fibers shown in Figure 80 (b).

We also sought to maximize the ratio of output powers of laser 1 to laser 2 for counter-pumping schemes (Figure 81 (a)) and the ratio of output powers of laser 2 to laser 1 for co-pumping schemes (Figure 81 (b)). There are a few interesting observations. Using HR FBG with a reflectivity >99% typically over ~2nm in wavelength, we still observed output passing through the FBG HR (laser 2). A typical laser output spectrum has a 3dB bandwidth of 1-2nm and 10dB bandwidth of ~4nm. The ratio of outputs of laser 1 to laser 2 is maximized with angle+HR scheme for the counter-pumping case shown in Figure 81 (a). These indicate a strong ASE nature of the fiber lasers, where a higher reflection at the pump end increases laser 2 output, vice versa for laser 1 output. The ratio also decreases for long fiber lengths. We have also observed a significant amount of light at the laser wavelength in the cladding for lasers 2 for long fibers in the counter-pumping cases shown in Figure 81 (a). For the co-pumping schemes in Figure 81 (b), the ratio of output of laser 2 to laser 1 is maximized for HR+angle scheme, i.e. HR at the pump end.

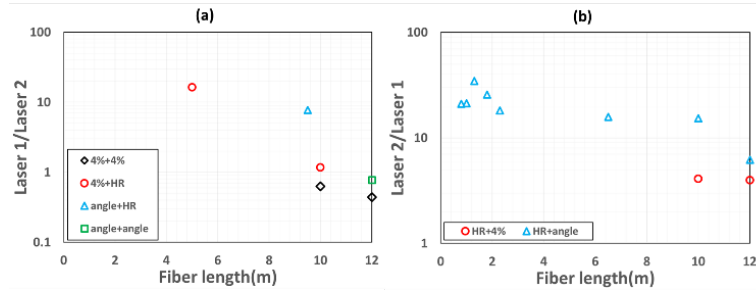


Figure 81. (a) Ratio of output powers of laser 1 to laser 2 for various counter-pumping schemes, and (b) ratio of output powers of laser 2 to laser 1 for various co-pumping schemes.

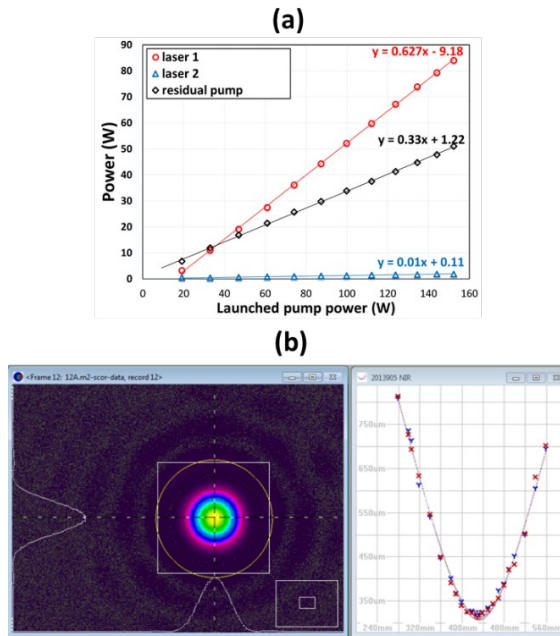


Figure 82. (a) Output powers of laser 1 and Laser 2 and residual pump versus coupled pump power and (b) M^2 measurement, $M^2=1.11$ and 1.12 respectively for x and y axis at 80W for laser 1. The laser is in angle+HR configuration with 9m fiber.

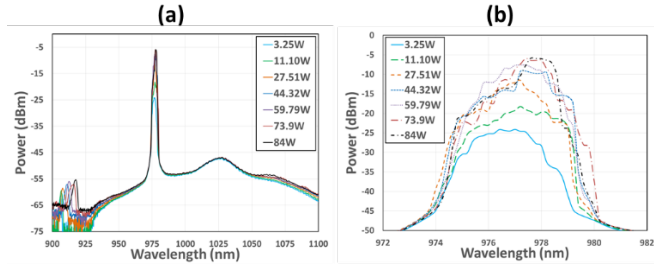


Figure 83. Spectra of laser 1 at various powers of the laser detailed in Fig. 5, (a) wide spectral range and (b) close-in at the lasing wavelength.

For angle+HR configuration with 9m fiber length with a 200W 915nm pump diode, the output powers of laser 1 and 2 along with residual pump power are plotted in Figure 82 (a). In this case M^2 was measured to be 1.11 and 1.12 respectively for the two axes at 80W for laser 1 (Figure 82 (b)). M^2 was also measured at several other powers throughout the output power range and was found to change very little. The efficiency with regard to the coupled pump power is 62.7% for just laser 1 output. The efficiency of the combined output powers of laser 1 and laser 2 with regard to the absorbed pump power is ~94%, at the quantum limit. For most of the lasers tested even involving fibers which have been repeatedly used over many month, the efficiency of the combined output powers with regard to the absorbed pump power is mostly very close to the quantum-limited efficiency, a testament to the low excess loss and photo-darkening of the fiber. The ASE at ~1026nm was well suppressed with signal-to-noise ratio >40dB (Figure 83 (a)).

We are currently planning for testing in monolithic fiber laser configurations as next phase of the program. More quantitate lifetime test is planned in a monolithic arrangement, as many longtime instabilities of the current setup can be eliminated then. Test of pump recirculation is also planned in the next phase.

One interesting observation of the Yb three-level fiber laser is its broad spectral bandwidth, almost ASE like (see Figure 83 (b)). The saturation intensity of Yb fiber lasers at ~976nm is expected to be low due to the relatively high absorption and emission cross sections. This alone would have not caused the broad laser spectrum if the spectral linewidth of the gain were homogeneously broadened. If spectral linewidth of the gain is dominated by inhomogeneous broadening, then gain saturation can lead to a broad laser spectrum.

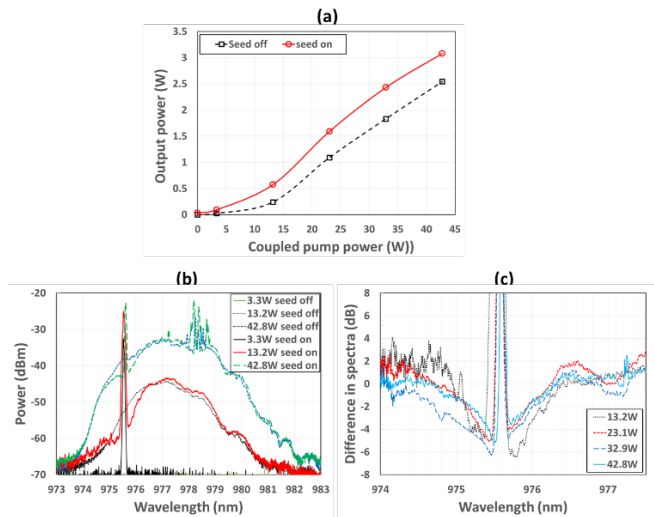


Figure 84. (a) Output powers for seed on and off versus coupled pump powers at ~915nm, (b) spectra for seed on and off at various pump powers, and (c) the differential spectra for various pump powers.

For erbium-doped glass, the emission at $\sim 1550\text{nm}$ was found to be mostly a homogeneously broadened line at room temperature. This is due to the small Stark splitting of in the order of $20\text{-}80\text{cm}^{-1}$, leading to rapid redistribution among adjacent Stark Levels at room temperature on the order of ps. Spectral hole burning can be used to characterize homogeneous linewidth in a inhomogeneously broadened system. This was expected to be hard to see at room temperature in an erbium-doped fiber due to its homogeneously broadened nature. It was however observed to have a spectral width of $4\text{-}8\text{nm}$ dependent on wavelength. As expected for a largely homogeneously broadened system, the maximum spectral hole depth was only measured to be $\sim 0.3\text{dB}$ in this case.

On another hand, Stark splitting of ${}^2F_{5/2}$ and ${}^2F_{7/2}$ levels in a ytterbium-doped fiber is in the order of $500\text{-}700\text{cm}^{-1}$, an order of magnitude larger than that for the erbium transition at $\sim 1550\text{nm}$, and the transition at $\sim 976\text{nm}$ is originated from a single transition between the lowest Stark lines of ${}^2F_{5/2}$ and ${}^2F_{7/2}$ levels. In this system, redistribution among adjacent Stark levels at room temperature is much slower and consequently is expected to play a much lesser role.

In order to measure the homogenous linewidth of the transition at $\sim 976\text{nm}$, we attempted to measure spectral hole burning. A counter-pumped amplifier was set up using 3.5m fiber with both ends angle-cleaved. A single-mode diode at $\sim 976\text{nm}$ was used as the seed laser. 519mW was launched into the fiber after passing a fiber-coupled isolator. The spectral linewidth of the seed laser cannot be fully resolved by our OSA with 20pm resolution. For each pump power, two spectra were collected, one with the seed off and one with the seed on. The respective powers at the output were also measured after the pump was rejected by a dichroic mirror.

The output powers for both seed on and seed off are plotted in Figure 84 (a) versus coupled pump powers. The spectra for seed on and seed off for three pump powers at 3.3W , 13.2W and 42.8W are given in Figure 84 (b). The OSA spectral resolution is 20pm for all spectra collected. At the low pump power of 3.3W , the seed laser spectrum can be clearly see to be resolution limited without any side bands. At pump powers of 13.2W and 42.8W , spectral hole burning can be clearly seen by comparing the spectra for seed on and off. At the pump power of 42.8W , lasing can be seen at $\sim 978.2\text{nm}$. The spectral difference between seed on and off are plotted in Figure 84 (c) for various pump powers in order to see the spectral hole burning clearly. The FWHM of the spectral hole is $\sim 1\text{nm}$. It is worth noting the significant depth of the spectral hole of up to 6dB in this case, indicating the emission at $\sim 976\text{nm}$ is mostly inhomogeneously broadened. The low saturation intensity and inhomogeneous nature of the emission can easily explained our observed broad laser linewidth. This also implies the difficulty of achieving narrow linewidth and high power from this system using either an oscillator or amplifier configuration. To our knowledge, this is the first time that spectral hole burning is observed in a ytterbium-doped fiber.

In summary, we have demonstrated efficient Yb three-level fiber lasers operating at $\sim 976\text{nm}$ using Yb-doped all-solid photonic bandgap fibers with free-space optics. Single-mode operation with a record 62.7% efficiency with regard to the coupled pump power was demonstrated for the Yb-three-level cladding-pumped fiber lasers with single-pass pump. The highest single-mode output power was 84W at $\sim 978\text{nm}$, only limited by the pump power. Efficiency with regard to the absorbed pump power was $\sim 94\%$, reaching quantum limit. In addition, we find that the Yb three-level system is mostly inhomogeneously broadened with a homogenous FWHM bandwidth of $\sim 1\text{nm}$.

3.2.10.2 Monolithic all-solid photonic bandgap fibers for Yb three-level fiber lasers

We have demonstrated an all-fiber monolithic fiber laser operating at $\sim 978\text{nm}$ which was built using in-house fabricated Yb-doped double-clad all-solid photonic bandgap fiber. We have achieved continuous wave output power of 151.4W with laser slope efficiency of 63% . Compared to our previous report using bulk optics for pump and output coupling, we have increased maximum output power by a factor of ~ 2 while maintaining the high laser efficiency in an all-fiber monolithic laser scheme. Furthermore, we have conducted long term power stability test.

The cross section of the all-solid photonic bandgap fiber used in this work is shown in Figure 85 along with the measured bend loss showing the carefully engineered bandgap of the active fiber for the suppression of the Yb 4-level system. The fiber can be coiled down to below

20cm diameter without significant in-band bend loss and show strong loss above ~980nm due to a loss of core guidance. This fiber was designed and fabricated in-house by the optical fiber fabrication facility at Clemson University. It is the same active fiber as the one used in our previous work. The fiber has a core with a corner-to-corner distance of 24 μ m and side-to-side distance of 21 μ m. The cladding has a corner-to-corner distance of 131 μ m and side-to-side distance of 124 μ m. The fiber is coated with low index acrylate to provide a pump NA of ~0.46, and the cladding pump absorption was measured to be ~1.76dB/m at 915nm.

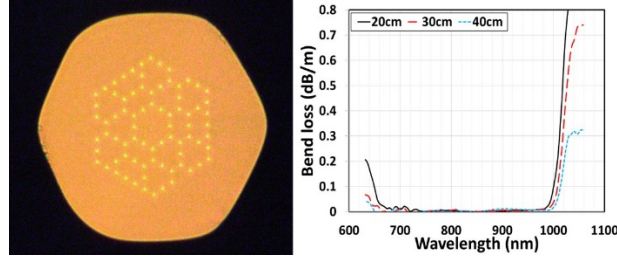


Figure 85. The 2D all-solid photonic bandgap fiber cross section and measured bend loss at 20cm, 30cm and 40 cm coil diameters in a passive fiber which has the same bandgap structure as the active fiber.

The basic laser arrangement is a counter-pumped monolithic configuration shown in Figure 86 with two pump diodes at ~915nm (200W, 0.22NA 105/125 μ m) spliced to a 2+1 pump combiner. Three meters of 20/105 μ m Er-doped fiber with a highly Er doped core (7wt% Er) coiled at 5cm in diameter was used in each pump path to absorb any backward propagating leakage light at the lasing wavelength at ~978nm. Pump loss at ~915nm was measured to be ~0.1dB for the 3m Er fiber and ~0.46dB for the pump combiner. The high-reflectivity fiber Bragg grating (FBG) was written in-house using a frequency-quadrupled YAG laser at 266nm in a 24/125 μ m photosensitive fiber which was also made in-house. The FBG has a reflectivity of >99% and a bandwidth of 2nm. The output is angle cleaved. This configuration was previously found to minimize output at the FBG end, i.e. laser 2 in Figure 86, without compromising the laser efficiency.

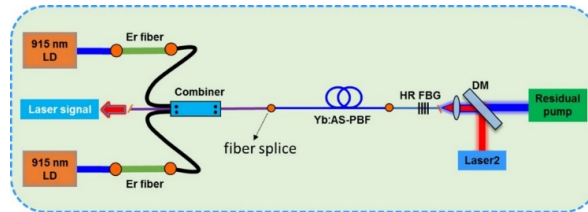


Figure 86. Configuration of the Yb 3-level-system monolithic fiber laser.

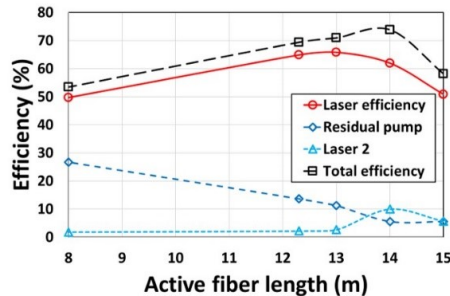


Figure 87. Laser performance versus active fiber length. **Laser efficiency**: accounting for just output power from the pump combiner with respect to the launched pump, **total efficiency**: accounting for both laser output powers with respect to the launched pump, **residual pump**: with respect to the launched pump power, and **laser 2**: with respect to the launched pump.

The length of the bandgap fiber was optimized first by progressively cutting back the bandgap fiber while fully characterizing the laser performance. The bandgap fiber was coiled to 15cm diameter, and the residual pump light as well as the light at the lasing wavelength (laser 2) were monitored at the far end.

Laser efficiency, total efficiency, residual pump as percentage of the launched pump power, and laser 2 as percentage of the launched pump power are shown versus the photonic bandgap fiber length in Figure 87. The optimized fiber length is ~13m, and 12.3m fiber was used in the last experiment. The reason we ended up using only 12.3m long active fiber in the final test is that we had been using the same piece of active fiber for several measurements. Eventually, the active fiber got shortened during this process due to cut-back measurements and fiber cleaving. But, we did not replace the active fiber with a new piece because of limited amount of active fiber left in the lab.

Output powers with a single pump and double pump are shown in Figure 88, with the spectra at various powers. This output power does not include the output power at laser 2. A maximum output power of 90.9W at the output was achieved with a single pump and 151.4W with double pumping, limited by available pump powers in each case. The corresponding output for the double pumping at laser 2 is 7W, i.e. 4.4% of total power of 158.4W. With double pumping, the efficiency was ~63% and ~75.4% with regards to the launched pump power after the combiner and absorbed pump power respectively. The efficiency of ~63% is at the same level as the efficiency of 62.7% that we achieved in a free-space bulk optics laser configuration. However, the novelty in this work is that we were able to achieve much higher output power using a practical monolithic configuration. The ASE from the 4-level system was well suppressed to below 40dB at highest laser output power.

The M^2 at ~150W was 1.25/1.24 (Figure 89), which was also found to be almost constant across the whole power range. The M^2 at ~3W was 1.20/1.21.

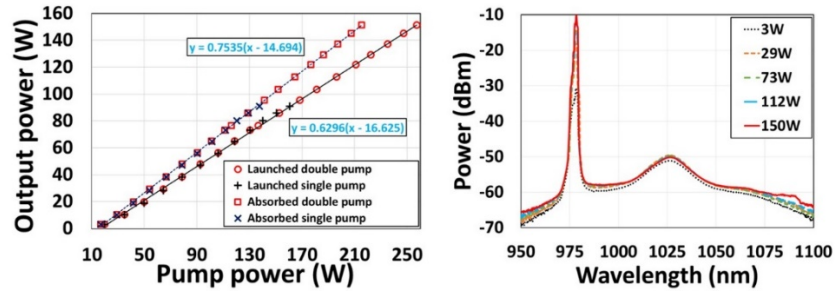


Figure 88. **Left:** measured output versus pump power for both with respect to the launched pump power and absorbed pump power; **Right:** measured output spectrum for double pump case under various output power.

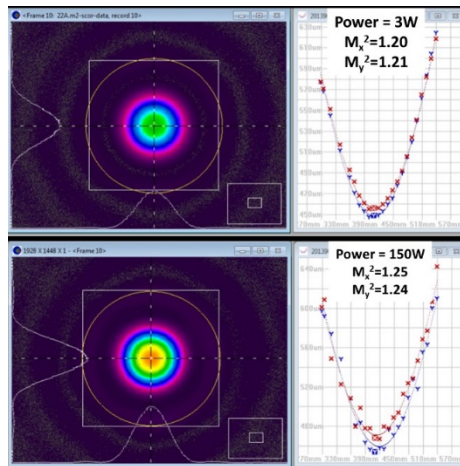


Figure 89. M^2 measurement at output of 3W and 150W.

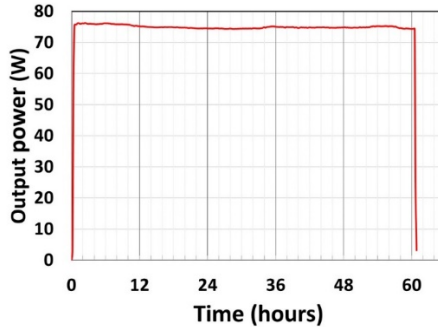


Figure 90. Laser stability test at 75W. Laser was turned off at $t=60.8$ hrs.

Photo-darkening increases significantly with inversion levels in Yb fiber lasers and is expected to be a severe problem for the Yb 3-level system due to its high inversion. The Yb phosphosilicate core glass used in our fiber is well known for its high resistance to photo-darkening, and it exhibited negligible degradation of laser performance over a period of several months and numerous tests. We have conducted a long-term power stability experiment over ~60 hours with a single-pump configuration under the output power at ~75W (Figure 90). Apart from some power fluctuations in the few percent levels, most likely due to temperature changes in the lab, there was very little sign of photo-darkening. It is worth mentioning that the long term stability test was performed with only a single pump. This is because we wanted to be safe while running the laser continuously especially over several nights.

4. Conclusions

The project is to develop double-clad hollow-core Raman gas lasers (Thrust I) and 100 μ m ytterbium-doped leakage channel fibers (Thrust II), both for power scaling of fiber lasers to well beyond kW. In thrust I, we have made significant progress in the fabrication of hollow-core fibers. Fibers with loss of <0.05dB/m at 3 μ m has been demonstrated.

In thrust II, we have made significant breakthrough in demonstrating efficient flat-top mode in active LCF with effective area of 1900 μ m² and record quantum-limited efficiency of ~95%. Systematic design study of 100 μ m-core multiple-cladding-resonance leakage channel fibers have been conducted. The 3rd iteration ytterbium-doped glass with an index of $\sim 2.3 \times 10^{-4}$ has enabled the demonstration ytterbium-doped 30 μ m-core LMA fiber operating near single-mode regime, proving that LMA fibers with arbitrarily low NA can be reliably made. Using 50/400 ytterbium-doped leakage channel fiber, we have systematically studied fiber lasers between 1000nm-1020nm, achieving slope efficiency >70% with respect to the launched pump power at 1018nm in 400 μ m cladding. A study on thermal lensing is also conducted. More recently, we have demonstrated record single-mode power of 220W at 1018nm using a 50/400 ytterbium-doped all-solid photonic bandgap fiber.

We have completed the 4th iteration ytterbium-doped glass in this period, which has a higher than expected index of 3.8×10^{-4} with respect to that of silica. This clearly shows that composition is not the only factor in determining the refractive index; the fabrication process and residue stress also play a role. More work is necessary to understand this in details. The high refractive index of the doped core glass significantly detuned the cladding resonance necessary to suppress HOM. Multimode output was observed in the fabricated 100 μ m-core ytterbium-doped LCF, while single mode was observed at the output of a passive LCF with an identical design. With an amplifier arrangement, the mode can be improved for the ytterbium-doped LCF. We are working on making a long taper at the input end of an amplifier to make this more robust. In the long run, much improved ytterbium-doped glass is essential for making fiber core dimension in the order of 100 μ m.

We are currently planning for another Yb glass iteration in 2019. This is the key to reach our goal of single-mode Yb lasers in 100 μ m-core fibers. Current preform capacity is occupied by ongoing works especially thulium glass efforts for AFRL.

We also have demonstrated that the Yb 3-level system at ~978nm can be operated just like the well-established Yb 4-level system in achieving single-mode high-power laser output with comparable efficiency using a Yb-doped double-clad all-solid photonic bandgap fiber with its bandgap optimized to suppress the 4-level system in a practical monolithic setup. We have achieved record output power of 151.4W, M^2 of ~1.2 at full power, and laser efficiency of 63% with respect to the launched pump power in an all-fiber monolithic Yb-doped double-clad all-solid photonic bandgap fiber laser.

5. References

1. P.D. Dragic, "SBS suppressed, single mode Yb-doped fiber amplifiers", OFC, JThA10 (2009).
2. A. Kobyakov, S. Kumar, D.Q. Chowdhury, A.B. Ruffin, M. Sauer and S.R. Bickham, "Design concept for optical fibers with enhanced SBS threshold," Optics Express, vol.13, 5335-5346(2005).
3. V.I. Kovalev and R.G. Harrison, "Suppression of stimulated Brillouin scattering in high-power single-frequency fiber amplifiers," Optics Letters, **31**, 161-163(2006).
4. D. Engin, W Liu, M. Akbulut, B. McIntosh, H.R. Verdun, and S. Gupta, "1kW cw Yb-fiber amplifier with <0.5GHz linewidth and near diffraction limited beam quality," SPIE PhotonicsWest, paper 7914-06(2011).
5. C. Zeringue, I.A. Dajani, and G.T. Moore, "Suppression of stimulated Brillouin scattering in gain optical fibers through phase-modulation: a time dependent model," SPIE PhotonicsWest, paper 7914-08(2011).
6. C. Jauregui, T. Eidam, J. Limpert, and A. Tunnermann, "Impact of modal interference on the beam quality of high-power fiber amplifier," Optics Express, **19**, 3258-3271(2011).
7. A.V. Smith and J.J. Smith, "Mode instability in high power fiber amplifiers," Optics Express, **19**, 10180-10192(2011).
8. Benabid F., et al, "Stimulated Raman Scattering in Hydrogen-Filled Hollow-Core Photonic Crystal Fiber", Science, **298**, 399 (2002).
9. F. Couny, F. Benabid and P.S. Light, "Subwatt threshold cw Raman fiber-gas laser based on H₂-filled hollow-core photonic crystal fiber," Physics Review Letters, **99**, 143903(2007).
10. R.J. Heeman and H.P. Godfried, "Gain reduction measurements in transient stimulated Raman scattering," IEEE Journal of Quantum Electronics, **31**, 358-364(1995).
11. Yeh P. Yariv A. and Hong C.S., "Electromagnetic propagation in periodic stratified media, I general theory," J. Opt. Soc. Am., **67**, 423-438(1977).
12. Yeh P. and Yariv A., Theory of Bragg fiber, J. Opt. Soc. Am, **68**, 1196-1201(1978).
13. A. Argyros, T.A. Birks, S.G. Leon-Saval, C.M.B. Cordeiro and P.St.J. Russell, "Guidance properties of low-contrast photonic bandgap fibers," Optics Express, vol.13, 2503-2510(2005).
14. Aghaie K.Z., Dangui V., Dignonnet M.J.F., and Fan S., "Classification of the core modes of hollow-core photonic bandgap fibers," IEEE J. of Quan. Elect., **15**, 1192-1200(2009).
15. Alam M.S., Saitoh K., and Koshiba M., "High group birefringence in air-core photonic bandgap fibers," Opt. Lett., **30**, 824-826(2005).
16. Amezcua-Correa R., Boderick N.G.R., Petrovich M.N., Poletti F., and Richardson D.J., "Design of 7 and 19 cells core air-guiding photonic crystal fibers for low-loss, wide bandwidth and dispersion controlled operation," Opt. Express., **15**, 17577-17586(2007).
17. Amezcua-Correa R., Gerome F., Leon-Saval S.G., Boderick N.G.R., Birks T.A., and Knight J.C., "Control of surface modes in low loss hollow-core photonic bandgap fibers," Opt. Express. **16**, 1142-1149(2008).
18. Argyros A., Birks T.A., Leon-Saval S.G., Cordeiro C.M.B., Luan F., and Russell P.St.J., "Photonic bandgap with an index step of one percent," Opt. Express., **13**, 309-314(2005).
19. Argyros A. and Pla J., "Hollow-core polymer fibers with a Kagome lattice: potential for transmission in the infrared," Opt. Express., **15**, 7713-7719(2007).
20. Barkou S.E., Broeng J. and Bjarklev A., "Silica-air photonic crystal fiber design that permits waveguiding by a true photonic bandgap effect," Opt. Lett., **24**, 46-48(1999).
21. Bhagwat A.R. and Gaeta A.L., "Nonlinear optics in hollow-core photonic bandgap fibers," Opt. Express., **16**, 5035-5047(2008).
22. Birks T.A., Bird D.M., Hedley T.D., Pottage J.M. and Russell P.St.J., "Scaling laws and vector effects in bandgap guiding fibers," Opt. express., **12**, 69-74(2003).
23. Birks T.A., Pearce G.J. and Bird D.M., "Approximate band structure calculation for photonic bandgap fibers," Opt. Express. **14**, 9483-9490(2006).
24. Birks , T.A., Luan F., Pearce G.J., Wang A., Knight J.C., and Bird D.M., "Bend loss in all-solid bandgap fibers," Opt. Express., **14**, 5688-5698(2006).
25. Bouwmans G., Luan F., Knight J.C., Russell P.St.J., Farr L., Mangan B.J., and Sabert H., "Property of a hollow-core photonic bandgap fiber at 850nm wavelength," **11**, 1613-1620(2003).
26. Chen X.C., Li M.J., Venkataraman N., Gallagher M.T., Wood W.A., Crowley A.M., Carberry J.P., Zenteno L.A., and Koch K.W., "Highly birefringent hollow-core photonic bandgap fiber," Opt. Express., **12**, 3888-3893(2004).
27. Couny F., Sabert H., Roberts P.J., Williams D.P., Tomlinson A., Mangan B.J., Farr L., Knight J.C., Birks T.A., and Russell P.St.J., "Visualizing the photonic band gap in hollow core photonic crystal fibers," **13**, 558-563(2005).
28. Couny F., Benabid F., and Light P.S., "Large-pitch kagome-structured hollow-core photonic crystal fiber," Opt. Lett., **31**, 3574-3576(2006).
29. Couny F., Benabid F., Roberts P.J., Burnett and Maier S.A., "Identification of Bloch-modes in hollow-core photonic crystal fiber cladding," Opt. Express. **15**, 325-338(2007).

30. Couny, Benabid F., Roberts P.J., Light P.S. and Raymer M.G., "Generation and photonic guidance of multi-octave optical frequency combs," *Science*, **318**, 1118-1121(2007).
31. Couny F., Roberts P.J., Birks T.A. and Benabid F., "Square-lattice large-pitch hollow-core photonic crystal fiber," *Opt. Express*, **16**, 20626-20636(2008).
32. Couny F. and Benabid F., "Optical frequency comb generation in gas-filled hollow core photonic crystal fibers," *J. Opt. A: Pure Appl. Opt.* **11** 103002(2009).
33. Cregan R.F., Mangan B.J., Knight J.C., Birks T.A., Russell P.St.J., Roberts P.J., and Allan D.C., "Single-mode, photonic band gap guidance of light in air," *Science*, **285**, 1537-1539(1999).
34. Dangui V., Kim H.Y., Digonnet M.J.F., and Kino G.S., "Phase sensitivity to temperature of the fundamental mode in air-guiding photonic bandgap fibers," *Opt. Express*, **13**, 6669-6684(2005).
35. Digonnet M.J.F., Kim H.K., Shin J., Fan S. and Kino G.S., "Simple geometric criterion to predict the existence of surface modes in air-core photonic bandgap fibers," *Opt. Express*, **12**, 1864-1872(2004).
36. Digonnet M.J.F., Kim H.K., Kino G.S. and Fan S., "Understanding air-core photonic bandgap fibers: analogy to conventional fibers," *IEEE J. Lightwave Technol.* **23**, 4169-4177(2005).
37. Duguay M.A., Kukubun Y., Koch T.L., and Pfeiffer L., "Anti-resonant reflecting optical waveguides in SiO₂-Si multiplayer structures," *Appl. Phys. Lett.* **49**, 13-15(1986).
38. Dupriez P., Gerome F., Knight J.C., Clowes J. and Wadsworth W.J., "Tunable high energy femtosecond soliton fiber laser based on hollow-core photonic bandgap fiber," *Conference on Lasers and Electro-Optics*, San Jose, paper CTuV2(2008).
39. Galea A.D., Couny F., Coupland S., Roberts P.J., Sabert H., Knight J.C., Birks T.A., and Russell P.St.J., "Selective mode excitation in hollow-core photonic crystal fiber," *Opt. Lett.*, **30**, 717-719(2005).
40. Jérôme F., Cook K., George A.K., Wadsworth W.J. and Knight J.C., "Delivery of sub-100fs pulses through 8m of hollow-core fiber using soliton compression," *Opt. Express*, **15**, 7126-7131(2007).
41. Hansen T.P., Broeng J., Jakobsen C., Vienne G., Simonsen H.R., Nielsen M.D., Skovgaard P.M.W., Folkens J.R., and Bjarklev A., "Air-guiding photonic bandgap fibers: spectral properties, macrobending loss, and practical handling," *J. Lightwave Technol.*, **22**, 11-15(2004).
42. Jasapara J., Her T.H., Bise R., Windeler R., and DiGiovanni D.J., "Group-velocity dispersion measurements in a photonic bandgap fiber," *J. Opt. Soc. Am. B*, **20**, 1611-1615(2003).
43. Kim H.K., Shin J., Fan S. and Digonnet J.F., "Designing air-core photonic bandgap fibers free of surface modes," *IEEE J. of Quantum Electronics*, **40**, 551-556(2004).
44. Humbert G., Knight J.C., Bouwmans G., Russell P.St.J., Williams D.P., Roberts P.J., and Mangan B.J., "Hollow core photonic crystal fibers for beam delivery," *Opt. Express*, **12**, 1477-1484(2004).
45. Lægsgaard J., Mortensen N.A., Riishede J. and Bjarklev A., "Material effect in air-guiding photonic bandgap fibers," *J. Opt. Soc. Am. B*, **20**, 2046-2051(2003).
46. Litchinitser N.M., Abeeluck A.K., Headley C. and Eggleton B.J., "Anti-resonant reflecting photonic crystal optical waveguides," *Opt. Lett.* **27**, 1592-1594(2002).
47. Litchinitser N.M., Dunn S.C., Usner B., Eggleton B.J., White T.P., McPhedran R.C., and Sterke C.M. de, "Resonance in micro-structured optical waveguides," *Opt. Express*, **11**, 1243-1251(2003).
48. Luan F., George A.K., Hedley T.D., Pearce G.J., Bird D.M., Knight J.C. and Russell P.St.J., "All-solid photonic bandgap fibers," *Opt. Lett.*, **29**, 2369-2371(2004).
49. Murao T., Saitoh K., Florous N.J., and Koshiba M., "Design of effectively single mode air-core photonic bandgap fiber with improved transmission characteristics for the realization of ultimate low loss waveguide," *Opt. Express*, **15**, 4628-4280(2007).
50. Ouzounov D.G., Ahmad F.R., Muller D., Venkataraman N., Gallagher M.T., Thomas M.G., Silcox J., Koch K.W. and Gaeta A.L., "Generation of megawatt optical soliton in hollow-core photonic band-gap fiber," *Science*, **310**, 1702-1704(2003).
51. Pearce G.J., Wiederhecker, Poulton C.G., Burger S. and Russell P.St.J., "Models for guidance in Kagome-structured hollow-core photonic crystal fibers," *Opt. Express*, **15**, 12680-12685(2007).
52. Poletti F. and Richardson D.J., "Hollow-core photonic bandgap fibers based on a square lattice cladding," *Opt. Lett.* **32**, 2282-2284(2007).
53. Poli F., Foroni M., Bottacini M., Fuochi M., Burani N., Rosa L., Cucinotta A., and Selleri S., "Single mode regime of square lattice photonic crystal fibers," *J. Opt. Soc. Am. A*, **22**, 1655-1661(2005).
54. Pottage J.M., Bird D.M., Hedley T.D., Birks T.A., Knight J.C., and Russell P.St.J., "Robust photonic bandgaps for hollow core guidance in PCF made from high index glass," *Opt. Express*, **11**, 2854-2861(2003).
55. Roberts P.J., Couny F., Sabert H., Mangan B.J., Williams D.P., Farr L., Mason M.W., Tomlinson A., Birks T.A., Knight J.C., and Russell P.St.J., "Ultimate low loss of hollow-core crystal fibers," *Opt. Express*, **13**, 236-244(2004).
56. Roberts P.J., Williams D.P., Mangan B.J., Sabert H., Couny F., Wadsworth W.J., Birks T.A., Knight J.C. and Russell P.St.J., "Realizing low loss air-core photonic crystal fibers by exploiting an anti-resonant core surround," *Opt. Express*, **13**, 8277-8285(2005).
57. Roberts P.J., Williams D.P., Sabert H., Mangan B.J., Bird D.M., Birks T.A., Knight J.C., and Russell P.St.J., "Design of low-loss and highly birefringent hollow-core photonic crystal fiber," *Opt. Express*, **14**, 7329-7341(2006).
58. Russell P.St.J., "Photonic crystal fibers," *Science*, **299**, 358-362(2003).
59. Saitoh K. and Koshiba M., "Photonic bandgap fibers with high birefringence," **14**, 1291-1293(2002).
60. Saitoh K. and Koshiba M., "Leakage loss and group velocity dispersion in air-core photonic bandgap fibers," *Opt. Express*, **11**, 3100-3109(2003).
61. Saitoh K. and Koshiba M., "Confinement losses in air-guiding photonic crystal bandgap fibers," *IEEE Photonics Technology Letters*, **15**, 236-238(2003).
62. Saitoh K., Mortensen N.A., and Koshiba M., "Air-core photonic bandgap fibers: the impact of surface modes," *Opt. Express*, **12**, 394-400(2004).

63. Shephard J. D., MacPherson W. N., Maier R. R. J., Jones J. D. C. and Hand D. P., "Single-mode mid-IR guidance in a hollow-core photonic crystal fiber," *Opt. Express.*, **13**, 7139-7144(2005).
64. Shepherd J.D., Jones J.D.C., Hnad D.P., Bouwmans G., Knight J.C., Russell P.St.J., and Mangan B.J., "High energy nanosecond laser pulses delivered single-mode through hollow-core PBG fibers," *Opt. Express.*, **12**, 717-723(2004).
65. Shirakawa A., Tanisho M., and Ueda K., "Polarization-maintaining fiber compressor by birefringent hollow-core photonic bandgap fiber," *Opt. Express.*, **14**, 12039-12048(2006).
66. Smith C.M., Venkataraman N., Gallagher M.T., Muller D., West J.A., Borelli N.F., Allen D.C., and Koch K.W., "Low-loss hollow core silica/sir photonic bandgap fiber," *Nature*, **424**, 657-659(2003).
67. Stone J.M., Pearce G.J., Luan F., Birks T.A., Knight J.C., George , A.K. and Bird D.M., "An improved photonic bandgap fiber based on an array of rings," *Opt. Express.*, **14**, 6291-6296(2006).
68. Thapa R., Knabe K., Corwin K.L. and Washburn B.R., "Arc fusion splicing of hollow-core photonic bandgap fibers for gas filled fiber cells," *Opt. Express.*, **14**, 9576-9583(2006).
69. Wegmuller M., Legre M. Gusin N., Hansen T.P., Jakobsen C., and Broeng J., "Experimental investigation of the polarization properties of a hollow core photonic bandgap fiber for 1550nm," *Opt. Express.*, **13**, 1457-1467(2005).
70. Welch M.G., Cook K., Amezcuca-Correa R., Germe F., Wadsworth W.J., Gorbach A.V., Skryabin D.V., and Knight J.C., "Solitons in hollow core photonic crystal fiber: engineering nonlinearity and compressing pulses," *J. Lightwave. Technol.*, **27**, 1644-1652(2009).
71. West J.A., Smith C.M., Borrelli N.F., Alan D.C., and Koch K.W., "Surface modes in air-core photonic bandgap fibers," *Opt. Express.* **12**, 1485-1496(2004).
72. White T.P., McPhedran R.C., Botten L.C., Smith G.H., and Streke C.M. de, "Calculation of air-guiding modes in photonic crystal fibers using multipole method," *Opt. Express.*, **9**, 721-732(2001).
73. White T.P., McPhedran R.C., Sterke C.M. De, Litchinitser N.M., and Eggleton B.J., "Resonance and scattering in micro-structured optical fibers," *Opt. Lett.* **27**, 1977-1979(2002).
74. L. Dong, B.K. Thomas, S. Suzuki and L. Fu, "Extending transmission bandwidth of air-core photonic bandgap fibers," *Optical Fiber Technology*, invited paper, **16**, 442-448(2010).
75. W.S. Wong, X. Peng, J.M. McLaughlin and L. Dong: "Breaking the limit of maximum effective area for robust single-mode propagation in optical fibers", *Optics Letters*, **30**, 2855-2857(2005).
76. L. Dong, X. Peng and J. Li: "Leakage channel optical fibers with large effective area", *Journal of Optical Society of America B*, **24**, 1689-1697(2007).
77. T. Wu, L. Dong and H. Winful, "Bend performance of leakage channel fibers," *Optics Express*, **16**, 4278-4285(2008).
78. L. Dong, T.W. Wu, H.A. McKay, L. Fu, J. Li and H.G. Winful, "All-glass large core leakage channel fibers," *IEEE Journal of Selected Topics in Quantum Electronics*, **14**, invited paper, 47-53(2009).
79. L. Dong, H.A. Mckay, A. Marcinkevicius, L. Fu, J. Li, B.K. Thomas, and M.E. Fermann, " Extending Effective Area of Fundamental Mode in Optical Fibers, " *IEEE Journal of Lightwave Technology*, **27**, invited paper, 1565-1570(2009).
80. L. Dong, "A vector boundary matching technique for efficient and accurate determination of photonic bandgaps in photonic bandgap fibers " *Optics Express*, **19**, 12582-12593(2011).
81. M.E. Fermann, "Single mode excitation of multimode fibers with ultra-short pulses," *Optics Letters*, pp.52-54, 1988.
82. J.P. koplw, D.A.V. Kliner and L. Goldberg, "Single-mode operation of a coiled multimode fiber amplifier," *Optics Letters*, vol.25, 442-444(2000).
83. M.J. Li, X. Chen, A. Liu, S. Gray, J. Wang, D.T. Donnell and L.A. Zenteno, "Limit of effective area for single-mode operation in step-index large mode area laser fibers, " *Journal of Lightwave Technology*, **27**, 3010-3016(2009).
84. D. Guertin, N. Jacobsen, K. Tankala, and A. Galvanauskas, "33 μ m core effectively single-mode chirally-coupled-core fiber laser at 1064nm, " *Optical Fiber Communications Conference*, paper OWU2(2008).
85. A. Siegman, "gain-guided, index-anti-guided fiber lasers," *Journal of Optical Society of America B*, **24**, 1677-1682(2007).
86. C.D. Brooks and F. Teodoro, "Multi-MW peak-power, single-transverse-mode operation of a 100 μ m core diameter, Yb-doped rodlike photonic crystal fiber amplifier," *Applied Physics*, **89**, 111119(2006).
87. J. Limpert, O. Schmidt, J. Rothhardt, F. Röser, T. Schreiber, and A. Tünnermann, "Extended single-mode photonic crystal fiber, " *Optics Express*, **14**, 2715-2720(2006).
88. S. Ramachandra, J.W. Nicholson, S. Ghalmi, M.F. Yan, P. Wisk, E. Monberg, and F.V. Dimarcello, "Light propagation with ultra-large modal areas in optical fibers, " *Optics Letters*, **31**, 1797-1799(2006).
89. D. Taverner, D.J. Richardson, L. Dong, J.E. Caplen, K. Williams, R.V. Pentyl: "158 μ J pulses from a single transverse mode, large mode-area EDFA, " *Optics Letters*, **22**, 378-380(1997).
90. P. Laperle, C. Paré, H. Zheng, A. Croteau and Y. Taillon, "Yb-doped LMA triple-clad fiber laser, " *Proceeding of SPIE*, vol.6343, pp.63430, 2006.
91. J.M. Fini, "Design of solid and microstructured fibers for suppression of higher order modes, " *Optics Express*, **13**, 3477-3490(2005).
92. S. Ramachandran, J.W. Nicholson, S. Ghalmi, M.F. Yan, P. Wisk, E. Monberg, and F.V. Dimarcello, "Light propagation with ultra large modal areas in optical fibers, " *Optics Letters*, **31**, 1797-1799(2006).
93. J.M. Fini and S. Ramachandran, "Natural bend-distortion immunity of higher-order-mode large-mode-area fibers," *Optics Letters*, **32**, 748-750(2007).
94. J. Nicholson, "Higher-order-mode fiber amplifiers," *Application of Lasers for Sensing and Free Space Communications*, paper LSWD1(2010).

95. X. Peng and L. Dong: "Fundamental mode operation in polarization-maintaining ytterbium-doped fiber with an effective area of $1400\mu\text{m}^2$ ", *Optics Letters*, **32**, 358-360(2006).
96. L. Dong, J. Li and X. Peng: "Bend resistant fundamental mode operation in ytterbium-doped leakage channel fibers with effective areas up to $3160\mu\text{m}^2$ ", *Optics Express*, **14**, 11512-11519(2006).
97. L. Dong, H.A. McKay, L. Fu, M. Ohta, A. Marcinkevicius, S. Suzuki, and M.E. Fermann, "Ytterbium-doped all glass leakage channel fibers with highly fluorine-doped silica pump cladding, " *Optical Express*, **17**, 8962-8969(2009).
98. J.M. Fini, "Bend-resistant design of conventional and microstructured fibers with very large mode area, " *Optics express*, **14**, 69-81(2006).
99. S. Suzuki, H.A. McKay, X. Peng, L. Fu, L. Dong, "Highly ytterbium-doped silica fibers with low photo-darkening, " *Optical Express*, **17**, 9924-9932(2009).
100. J. Nilsson, J.K. Sahu, J.N. Jang, R. Selvas and D.C. Hanna, "Cladding-pumped Raman fiber amplifier," OSA Topical Meetings on Optical Amplifiers and Applications, paper PD2-1, 2002.
101. C.A. Codemard, J.K. Sahu and J. Nilsson, "Cladding-pumped Raman fiber amplifier for high-gain, high energy single-stage amplification", *Optical Fiber Communications Conference*, paper OTuF5, 2005.
102. C.A. Codemard, P. Dupriez, Y. Jeong, J.K. Sahu, M. Ibsen, and J. Nilsson, "High-power continuous-wave cladding-pumped Raman fiber laser, ", *Optics Letters*, **31**, 2290-2292(2006).
103. J. W. Nicholson, A. D. Yablon, J. M. Fini, and M. D. Mermelstein, "Measuring the Modal Content of Large-Mode-Area Fibers," *IEEE J. Sel. Topics Quantum Electron.* 15, no. 1, pp. 61–70, Jan. 2009.
- 104.** D. N. Schimpf, R. A. Barankov, and S. Ramachandran, "Cross-correlated (C2) imaging of fiber and waveguide modes," *Opt. Express* 19, 13008-13019 (2011).